NASA-TM-81336 19830025574

NASA Technical Memorandum 81336

FOR REFERENCE

NOT TO BE TAKEN FROM THIS ROOM

An Experimental Study of Transonic Flow About a Supercritical Airfoil

Frank W. Spaid,
John A. Dahlin,
William D. Bachalo,
and Louis S. Stivers, Jr.

LIBRARY COPY

LANGLEY RESEARCH CENTER
LIBRARY, NASA
HAMPTON, VIRGINIA

August 1983

25th Anniversary
1958-1983

NASA

NASA Technical Memorandum 81336

An Experimental Study of Transonic Flow About a Supercritical Airfoil

Frank W. Spaid
McDonnell Douglas Research Laboratories
St. Louis, Missouri

John A. Dahlin
Douglas Aircraft Company
Long Beach, California

William D. Bachalo
Aerometrics, Inc.
Mountain View, California

Louis S. Stivers, Jr.
Ames Research Center
Moffett Field, California

National Aeronautics
and Space Administration

Scientific and Technical
Information Branch

1983

NOMENCLATURE

a	function of M_e, γ, and r in van Driest transformation, equation (4)
C_F	total skin-friction coefficient of one side of a flat plate
C_f	local skin-friction coefficient, τ/q_e
C_p	pressure coefficient, $(p - p_\infty)/q_\infty$
C_f^*	skin-friction coefficient computed from transformed velocity profile, u^*
c	airfoil chord
c_d	airfoil section drag coefficient
c_l	airfoil section lift coefficient
d	probe tip height
H	boundary-layer shape factor, δ^*/θ
K_{G-D}	Gladstone-Dale constant
k	boundary-layer trip roughness height
k_{cr}	minimum value of k that will cause transition to occur at the trip
L_{eff}	effective optical path length
ℓ	characteristic length
M	Mach number
p	pressure
q	dynamic pressure, $1/2\ \rho u^2$
Re_c	Reynolds number based on chord
Re_ℓ	Reynolds number based on length, ℓ
r	recovery factor
u	velocity
u^*	velocity transformed by van Driest transformation, equation (3)
u_τ	shear velocity, $\sqrt{\tau_w/\rho_w}$
u^+	transformed velocity normalized by shear velocity, u^*/u_τ
w	empirical wake function, equation (6)

x	coordinate measured parallel to free-stream direction
z	coordinate normal to airfoil plane
z^+	law-of-the-wall coordinate, $(zu_\tau)/\nu_w$
α_{geom}	angle of attack measured with respect to the tunnel test-section centerline
γ	specific heat ratio
δ	boundary-layer thickness
δ^*	boundary-layer displacement thickness, $\int_0^\delta \left(1 - \frac{\rho u}{\rho_e u_e}\right) dz$
θ	boundary-layer momentum thickness, $\int_0^\delta \frac{\rho u}{\rho_e u_e}\left(1 - \frac{u}{u_e}\right) dz$
λ	laser wavelength
ν	kinematic viscosity
Π	wake coefficient for transformed boundary-layer profile, equation (5)
ρ	density
τ	shear stress

Subscripts:

c	based on airfoil chord
e	conditions at edge of boundary layer
t	stagnation conditions
w	conditions at the wall (airfoil surface)
∞	free-stream conditions

AN EXPERIMENTAL STUDY OF TRANSONIC FLOW ABOUT A SUPERCRITICAL AIRFOIL

Frank W. Spaid,* John A Dahlin,† William D. Bachalo,‡ and Louis S. Stivers, Jr.

Ames Research Center

SUMMARY

A series of experiments was conducted on flow fields about two airfoil models whose sections are slight modifications of the original Whitcomb supercritical airfoil section. Data obtained include surface static-pressure distributions, far-wake surveys, oil-flow photographs, pitot-pressure surveys in the viscous regions, and holographic interferograms. These data were obtained for different combinations of lift coefficient and free-stream Mach number, which included both subcritical cases and flows with upper-surface shock waves. The availability of both pitot-pressure data and density data from interferograms allowed determination of flow field properties in the vicinity of the trailing edge and in the wake, without recourse to any assumptions about the local static pressure. The data show that significant static-pressure gradients normal to viscous layers exist in this region, and that they persist to approximately 10% chord downstream of the trailing edge. Comparisons are made between measured boundary-layer properties and results from boundary-layer computations that employed measured static-pressure distributions, as well as comparisons between data and results of airfoil flow field computations.

INTRODUCTION

An experimental study of the flow about a supercritical airfoil was reported in references 1-3. That study utilized two models of essentially the original NASA Whitcomb integral (unslotted) airfoil section and was conducted as a cooperative program by McDonnell Douglas Research Laboratories (MDRL), Douglas Aircraft Company (DAC), and Ames Research Center (ARC). The investigation was intended to provide detailed flow field survey data that would contribute to a better understanding of mechanisms associated with transonic drag rise. This report presents results from a continuation of that cooperative program. A portion of this material is presented in references 4 and 5.

This investigation was motivated in part by the increased importance of viscous-inviscid interactions in transonic flows about aft-loaded, supercritical airfoils, relative to earlier designs having little or no aft camber. The flow field about a supercritical airfoil operating at its design Mach number and lift coefficient is

---

*Principal Scientist, McDonnell Douglas Research Laboratories, St. Louis, Missouri.

†Senior Engineer/Scientist, Douglas Aircraft Company, Long Beach, California.

‡Senior Scientist, Aerometrics, Inc., Mountain View, California.

Note: This research was supported in part under the McDonnell Douglas Independent Research and Development Program.

characterized by regions of strong viscous-inviscid interaction, primarily the interaction of the upper-surface boundary layer with a shock wave, and in the trailing-edge region. These interactions are coupled because the properties of the upper-surface boundary layer as it approaches the trailing edge, and its subsequent response to the adverse pressure gradient resulting from the pronounced aft camber, are significantly influenced by its interaction with the shock wave farther upstream. The aft loading is associated with a large static-pressure difference between the upper and lower surfaces just upstream of the trailing edge, remnants of which persist into the near wake. The coupling between the external inviscid flow and the viscous boundary layer and wake complicates the numerical computation of these flow fields. An inviscid, subcritical computation of the flow about a conventional airfoil having little aft camber often produces a static-pressure distribution that is a good approximation to the experimental distribution; as a result, flow field properties can be predicted adequately by iteration between an inviscid program and a boundary-layer program in the conventional manner. However, the straightforward application of this procedure to an aft-loaded airfoil often fails because the initial inviscid calculation may be so different from the actual flow field that convergence to a physically realistic solution does not occur.

A variety of techniques, incorporating various levels of empiricism and complexity, have been used to overcome these difficulties. Numerous unpublished empirical fixes have been used in the computation of transonic flow fields about aft-loaded airfoils. Two examples are (1) the addition of an estimated displacement-thickness distribution to the airfoil coordinates before the initial inviscid calculation, which is later replaced by results of boundary-layer calculations, and (2) the extrapolation of the calculated boundary-layer displacement thickness distribution near the trailing edge in a manner that is known to facilitate agreement between the computed and experimental pressure distributions. A systematic, semiempirical method for treatment of the trailing-edge region for both supercritical and other types of airfoils was proposed by Bavitz (ref. 6). Results of a detailed analysis of the trailing-edge region were incorporated into a procedure for airfoil flow field calculation developed by Melnik et al. (ref. 7). Analyses of the shock-wave/boundary-layer interaction region (refs. 8 and 9) have the potential for being incorporated into an airfoil computation method. Several investigators (refs. 10-12) applied the Reynolds-averaged Navier-Stokes equations to the computation of airfoil flow fields.

Experimental data are required for the evaluation and further development of these prediction methods. The present data are intended to support the development of methods for computation of transonic flow fields about airfoils by allowing more detailed comparisons with experimental data than are possible when only the usual surface static-pressure (lift) and far-wake survey (drag) data are obtained. Test conditions include cases having significant viscous-inviscid interaction effects; situations dominated by extensive separation were excluded. In some instances, surface static-pressure and pitot-pressure measurements are combined with density data obtained from holographic interferograms, resulting in an unusually complete description of the time-mean flow fields.

The primary data and associated data analysis are presented in this report. Additional reduced data are presented in a separate publication, the Supplement to NASA TM-81336, which is available upon request. A request form is provided following the list of references.

APPARATUS AND TEST PROCEDURE

Wind Tunnel

The experiments were conducted in the 2- by 2-Foot Transonic Wind Tunnel at Ames Research Center. This tunnel is a variable-speed, continuous-flow, ventilated-wall, variable-pressure facility, which was reengineered for occasional two-dimensional research testing by adding rotating, model-supporting, glass side windows mounted in unventilated, plane sidewalls. A maximum unit Reynolds number of 26.3×10^6/m generally can be maintained, and a high subsonic Mach number is held to within ±0.002. A spark Schlieren system and an 82-tube drag rake, programmed to provide total-pressure readings at 1.3 mm intervals and static pressure readings at 25.4 mm intervals across the wake of a model, are available.

Models and Traversing Rig

The test-section arrangement for these experiments is shown in figures 1 and 2. Airfoil models were mounted between the sidewall windows, and either the traversing rig or drag rake was mounted on the tunnel sting. Two 15.24-cm chord models of the airfoil were used during these experiments. One model has a nominally sharp trailing edge, and the other has a blunt trailing edge equal to 1% chord, formed by downward rotation of the aft lower-surface contour from 65% chord to the trailing edge. This method of modifying the geometry to produce the additional trailing-edge thickness also has the effect of increasing the aft camber slightly. The sharp-trailing-edge model has an aerodynamically smooth, porous leading-edge segment for dispensing oil mixed with fluorescent dye, which is used for flow visualization. The centerline static-pressure-orifice layout is shown in figure 3 for both models; table 1 gives the airfoil coordinates.

Boundary-layer and near-wake surveys were obtained with the aid of a two-degree-of-freedom traversing rig and probe assembly which allowed both remote streamwise and vertical movement of the probe. Continuous potentiometer strips were used to determine probe position. Calibration of the high-resolution vertical-position output was checked frequently with a machinist's height gage. Contact with the height gage (and with the airfoil during the experiments) was determined by an electrical fouling circuit. Uncertainty in measurement of a 25.4 mm distance with the gage is about ±0.04 mm, resulting in a ±0.15% uncertainty in the distance between points in a survey from this source. The data system resolution was 394 counts/mm. The measurement of distance from a survey point to the airfoil surface was limited in accuracy by tunnel-induced vibration. It was necessary to locate the airfoil surface with the probe while the tunnel was running in order to minimize errors caused by aerodynamically induced deflections of the model and the traversing rig. As the probe was moved toward the airfoil surface, the vertical probe-position readout typically indicated 0.05 mm of travel between the first indication by the fouling circuit and the point at which continuous contact was established. Calibration of the horizontal-position readout was performed with a scale, resulting in an accuracy of ±0.5 mm.

Probe tips, of the type described in references 1-3, were made from 0.25 mm o.d. stainless steel tubing, flattened and ground at the end to a height of 0.10 mm, and aligned with the horizontal plane. A portion of the data was obtained with a tip made from 0.8 mm o.d. stainless steel tubing, also flattened and ground at the end to a height of 0.10 mm.

Holographic Interferometer

Holographic interferograms were obtained with a system which utilized the existing tunnel Schlieren mirrors, a pulsed ruby laser for creating the holograms, and a helium-neon laser for hologram reconstruction. Holograms were obtained showing the entire field of view of the test section windows, both with and without flow in the test section. After processing, the no-flow plate and one of the plates taken at test conditions were positioned in a reconstruction plate holder, illuminated with the reference beam, and aligned for infinite-fringe interferograms. This dual-plate method (ref. 13) allows the fringe orientation to be chosen during reconstruction. Since the method involves interference between waves that follow the same optical path but are separated in time, imperfections in optical elements are cancelled.

A possible disadvantage of the dual-plate method is that wavefronts throughout the field of view will be distorted by density gradients if the field of view does not include a region of uniform flow. In that case, there is no direct means to verify that the system is in the alignment required for infinite-fringe interferometry. In the present instance, the good overall agreement between surface static-pressure distributions obtained from the interferograms and those obtained from the static-pressure orifices (the comparison shown later in this paper) provides indirect verification of infinite fringe alignment.

If the flow is adequately two-dimensional, fringes on an infinite-fringe interferogram correspond to density contours in the flow, with a constant-density increment between fringes given by

$$\rho_1 - \rho_2 = \frac{\lambda}{L_{eff} K_{G-D}} \tag{1}$$

where ρ_1 and ρ_2 are the densities at two adjacent fringes; L_{eff} is the effective optical path length, including the effect of the sidewall boundary layers (for the present case, $L_{eff} = 0.599$ m); λ is the laser wavelength; and K_{G-D} is the Gladstone-Dale constant. The value of density at one fringe must be determined by independent means. The method used in this investigation was to choose the density level at a reference fringe to give the best overall agreement between surface static-pressures derived from interferograms and those measured at static-pressure orifices.

More information concerning the application of holography to airfoil testing is given in reference 14.

INFLUENCE OF BOUNDARY-LAYER TRIP CONFIGURATION ON AIRFOIL PERFORMANCE

The experiments described in references 1-3 were conducted with leading-edge boundary-layer trips. If such a trip is effective in causing transition to occur near the leading edge, complications associated with interaction between a shock wave and a laminar, or transitional, boundary layer are avoided, as are effects of interaction between an aft-located roughness strip and a turbulent boundary layer originating near a leading-edge suction peak. However, at relatively low Reynolds number, locating the transition strips farther aft can result in a displacement-thickness distribution near the trailing edge that provides a better simulation of viscous-inviscid interaction effects occurring at full-scale Reynolds number. During the

present investigation, emphasis was on aft-located boundary-layer trips in an attempt to take advantage of this potential for full-scale Reynolds number simulation. The recommendations of Braslow et al. (ref. 15) were used as guidelines in selecting trip configurations.

The roughness elements used for the boundary-layer trips were spherical glass beads which had been sieved to obtain a size variation of approximately ±5% of the nominal diameter. The trips were 1.6 to 2.2 mm in width. The value of x/c used in identifying a trip is the downstream edge. The trips were applied by masking the desired region with cellophane tape, coating the region with adhesive from a wiper of the type formerly supplied with Polaroid black-and-white print film, spraying the glass beads on with an airbrush, and immediately removing the tape while the adhesive was still wet. The tape was removed as soon as possible to avoid the formation of ridges in the adhesive at the edges of the trip. It was difficult to spray the beads such that the desired uniform, sparse distribution of roughness was achieved; it was often necessary to apply the trip several times before the result was acceptable. Data obtained with trips having closely spaced elements (spacing of the order of a few bead diameters) usually show disturbances in the surface static-pressure distribution near the trip and anomalously large boundary-layer thicknesses downstream of the trip.

A series of experiments was conducted during 1975 to evaluate the usefulness of testing at relatively low Reynolds number with aft-located boundary-layer trips and to select appropriate test conditions for more detailed study. (The data of this investigation were obtained from several tunnel-occupancy periods over a period of several years; the tabulated data and the data presented in the appendix are identified by run number and year.)

The effectiveness of each trip configuration tested in the 1975 tunnel-occupancy period was verified by the sublimation flow-visualization technique. Fluorene (alphadiphenylenemethane) was dissolved in a volatile solvent and sprayed on the model. The tunnel was started, and test conditions were held constant until the characteristic sublimation pattern was observed, that is, a thin coating of fluorene remaining on the model forward of the trip and essentially a clean model-surface downstream. Interpretation of sublimation patterns was sometimes complicated by nonuniformity of the original coating, but in each case it was concluded that the trip had been effective in causing boundary-layer transition.

This study was motivated in part by the comparison shown in figure 4. Data corresponding to two boundary-layer trip configurations obtained from the 2- by 2-ft tunnel at $Re_c = 3\times10^6$ and 4×10^6 are compared with data obtained at $Re_c = 14.6\times10^6$ from the 0.38- by 1.52-m test section of a transonic wind tunnel operated by the National Research Council (NRC) of Canada. The NRC data correspond to natural transition. The data from the 2- by 2-ft tunnel were limited to $Re_c = 3\times10^6$ for $M_\infty > 0.76$ because a tendency of the tunnel drive system to overheat limited the run rate at higher Reynolds numbers in this Mach number range. The difference in drag levels at the lower Mach numbers is in good agreement with scaling laws for turbulent skin-friction drag (see ref. 16). The differences between the two sets of data in the region of rapid drag rise implied a need for further study. Since the NRC data were obtained at a Reynolds number much closer to that for which the airfoil was designed and are in reasonable agreement with drag data for this airfoil obtained from other facilities, the data from the 2- by 2-ft tunnel were initially regarded as questionable.

Drag polars for $M_\infty = 0.76$, $Re_c = 4\times10^6$, and for $M_\infty = 0.80$, $Re_c = 3\times10^6$ from a subsequent investigation are shown in figures 5 and 6. Data were obtained with the sharp-trailing-edge model with several trip configurations. Also included are fairings of high-Reynolds-number data obtained from the NRC tunnel, presented both as measured and shifted in an attempt to compensate for the Reynolds number difference. The shifting of drag data presented in this section for facilitating comparisons between data obtained at different Reynolds numbers was accomplished as follows: Reynolds number scaling is assumed to follow the Schultz-Grunow flat-plate total skin-friction law (ref. 16):

$$C_F = \frac{0.427}{(\log Re_\ell - 0.407)^{2.64}} \tag{2}$$

The variation of skin-friction drag with Reynolds number is assumed to be independent of Mach number and angle of attack. A drag increment is computed at $M_\infty = 0.5$ and is applied throughout the Mach number and angle-of-attack range, using $c_d = 0.0105$ at $M_\infty = 0.5$, $Re_c = 4\times10^6$, and $c_l = 0.6$ as a reference level. Values of k/k_{cr} corresponding to each trip configuration and chord Reynolds number are given. The quantity k_{cr} is the roughness height corresponding to a roughness Reynolds number of 600, the value indicated in reference 15 to be the minimum roughness height that causes transition to occur at the trip if the Reynolds number based on distance from the leading edge to the trip is greater than 10^5. Data presented in reference 15 indicate that roughness sizes greater than $2k_{cr}$ produce additional roughness drag.

The data of figures 5 and 6 were obtained with the same upper-surface boundary-layer trip. Figure 5 gives data corresponding to three lower-surface trip locations having approximately minimum-size roughness for the lower Reynolds number. The results are comparable for lower-surface trip x/c values of 0.06 and 0.18 at the higher lift coefficients. The lower-surface trip at $x/c = 0.35$ produces slightly higher drag at $M_\infty = 0.76$ throughout most of the c_l range. At $M_\infty = 0.8$, the polar obtained with this trip has a different shape from the others, with high drag levels in the intermediate c_l range. Similar data shown in figure 6 for constant lower-surface trip location and a range of roughness heights show that the optimum height for this chordwise location is approximately the upper limit of allowable roughness, according to the criterion of reference 15.

Examples of static-pressure distributions at $M_\infty = 0.8$ at two angles of attack are shown in figure 7. Data obtained with trips giving the best and poorest drag performance in the intermediate c_l range have been chosen for comparison. The static-pressure distribution obtained at $\alpha_{geom} = 1.0°$, near the minimum of each drag polar, are similar, even though the corresponding drag difference is large. At $\alpha_{geom} = 3.0°$, the drag is apparently dominated by shock losses, and both the static-pressure distributions and the drag levels are similar.

Figure 8 consists of a series of fluorescent oil-flow photographs of the lower surface of the sharp-trailing-edge model. The boundary-layer trip and the circular patches of epoxy filler covering heads of machine screws can be seen in the photographs. These photographs show that at some test conditions the flow was separated in the lower-surface concavity. Figure 8(a) corresponding to $M_\infty = 0.6$, $\alpha_{geom} = 2.6°$, shows the flow to be attached in the concavity. This test condition is the only one in which the flow was attached in the concavity for which extensive boundary-layer and wake-survey data were obtained. Figures 8(b) through 8(e) correspond to the test conditions of the static-pressure comparison, figure 7. At $\alpha_{geom} = 1.0°$, the chordwise extent of separation is approximately the same for both trip configurations. At

the higher angle of attack, the flow corresponding to the lower-surface trip at $x/c = 0.35$ is attached, but it is separated with the trip at $x/c = 0.18$.

A series of lower-surface boundary-layer surveys was obtained with the sharp-trailing-edge model during a test conducted in 1977 to obtain more detailed data to support interpretation of the drag data previously presented. Data were obtained at $M_\infty = 0.8$, $Re_c = 3\times10^6$, and $\alpha_{geom} \cong 1.0°$. Four of the lower-surface trip configurations of the 1975 test series were chosen for study. The upper-surface trip was the same in all experiments, $x/c = 0.35$, $k = 0.08$ mm.

Two sets of profile data are presented in figure 9 corresponding to the trips giving the best and the poorest drag performance. (Details of the boundary-layer data-reduction process will be presented later.) The profiles of figure 9(a), corresponding to the best trip, show attached flow at $x/c = 0.5$ and 0.6, forward of the concavity. The profile at $x/c = 0.75$ is near separation, and the profile at $x/c = 0.91$ is separated, although the layer of reversed flow is thin relative to the boundary-layer thickness. Since a pitot-probe is incapable of measuring reverse velocities, data for which the measured pitot pressure is less than or equal to the local static pressure have been omitted from the plots. The shape of the trailing-edge profile shows the effect of the lower-surface expansion in the last few percent chord. The profiles of figure 9(b), although similar to those of figure 9(a) at $x/c = 0.5$ and 0.6, show a larger separated region and a correspondingly thicker trailing-edge boundary layer.

Both oil-flow photographs corresponding to $M_\infty = 0.8$, $\alpha_{geom} = 1.0°$ (figs. 8(b) and 8(c)) show a similar chordwise extent of separation. However, the boundary-layer and drag data show that in one case the separated region was thin, and its influence on the primary flow field characteristics was small; in the other case it was thick and apparently caused an increase in drag. At $M_\infty = 0.8$, $\alpha_{geom} = 3.0°$ (figs. 7(b) 8(d), and 8(e)), separation had a negligible influence on drag, implying a thin separated region.

Displacement-thickness distributions corresponding to the data of the previous figure are presented in figure 10, which also includes data corresponding to trip configurations resulting in intermediate drag performance. Accurate values of displacement thickness cannot be determined for profiles having significant regions of reverse flow; for these profiles, flow velocities were set equal to zero in the reverse-flow region, and the data were plotted with an arrow indicating that the values represent lower limits. Boundary-layer properties in the region approaching the concavity, $x/c = 0.5$ and 0.6, are plotted in figure 11 for the same test conditions as the data of the previous figure. Displacement thickness, shape factor ($H = \delta^*/\theta$), and skin-friction coefficient are presented. The skin-friction coefficient was determined by a least-squares fit to the law-of-the wall logarithmic profile.

There is no consistent trend linking development of the time-mean profile immediately upstream of the concavity, such as increasing H or decreasing C_f, with increasing separation in the concavity and correspondingly increasing drag. Apparently differences in the turbulence flow properties associated with the differences in trip configuration are responsible for the observed variations in response to the adverse pressure gradient in the upstream portion of the concavity. If attached flow is to be maintained in the concavity (or the extent of separation minimized), the beginning of transition must be sufficiently far upstream of the region of adverse pressure gradient. The poor performance observed with the lower-surface trip at $x/c = 0.35$ is probably a result of insufficient distance between the trip and

the beginning of the concavity. The influence of lower-surface bead size at a fixed chordwise location on drag may be associated with the ability of the larger bead sizes to accelerate the transition process. Although drag was not measured during the 1977 test series, the trend in lower-surface viscous drag is believed to follow the trend in lower-surface trailing-edge boundary-layer thickness.

A summary of drag data for several values of c_l is presented in figure 12. Data obtained with the sharp-trailing-edge model are shown for two boundary-layer-trip configurations. Limited data obtained with the blunt-trailing-edge model are included, together with a fairing of high-Reynolds-number data from a test in the NRC tunnel. All data obtained at $Re_c \neq 4\times10^6$ have been shifted to that Reynolds number by the method described previously. The drag-rise characteristics of the sharp-trailing-edge model corresponding to the lower-surface trip configuration $x/c = 0.18$, $k = 0.12$ mm, are consistent with the high-Reynolds-number data for $c_l < 0.8$ and are clearly superior to data obtained with the alternative trip configuration chosen earlier in this study. Data obtained with the blunt-trailing-edge model at $Re_c = 2\times10^6$ and 4×10^6 are in reasonable agreement with data obtained with the other model, although some discrepancies are present in the drag-rise region.

Results of this study imply that particular care should be taken in testing and interpreting data associated with high-aspect-ratio wings employing supercritical, aft-loaded airfoil sections, if local Reynolds numbers based on chord are in the range of the present study. Separation in the lower-surface concavity can lead to high values of drag, which are probably not representative of performance at flight Reynolds numbers. Although the present results indicate that a thin separated region in the concavity may not degrade performance, separation should be avoided. Oil-flow visualization studies should be conducted if this type of separation is likely.

AIRFOIL FLOW FIELD MEASUREMENTS

Static-Pressure Distributions

Plots of those static-pressure distributions for which boundary-layer data also were obtained are presented in figures 13(a)-13(g), and the corresponding tabulated data are given in table 2.

A comparison of static-pressure data obtained with the two airfoil models at $M_\infty = 0.6$ is shown in figure 13(e). The increased aft camber of the blunt-trailing-edge model is at least partially responsible for the observed differences in the static-pressure distributions. Some of the differences, such as those for $x/c < 0.3$ on the lower surface, may be caused by deviations of the actual airfoils from the theoretical coordinates.

Data obtained with the blunt-trailing-edge model at $M_\infty = 0.83$ are presented in figure 13(g). Data from the present study with aft-located boundary-layer trips are compared in this figure with data obtained with a leading-edge trip from reference 1. Although the Reynolds number and angle of attack are not matched precisely, these discrepancies are not sufficient to cause the difference in shock location; this variance is believed to be associated with the difference in upper-surface displacement-thickness distribution.

Probe interference effects observed during this study are similar to, but smaller than, those reported by Cook (ref. 17). Static-pressure distributions obtained

upstream of the probe location, with the probe near the surface in position for a survey, are superimposed in figures 13(a) and 13(d) on the corresponding distribution obtained with the probe retracted. Where interference effects are present, they always take the form of an additional adverse static-pressure gradient superimposed on the undisturbed static-pressure distribution. The magnitude of the effect decreases as the probe tip approaches the trailing edge. At the trailing edge and slightly forward of the trailing edge on the lower surface, probe interference effects on the static-pressure distribution were always negligible (less than the run-to-run data repeatability).

Results of an attempt to determine the effects of these static-pressure perturbations on boundary-layer properties are summarized in table 3. In the first two columns, calculated values of displacement thickness, momentum thickness, shape factor, and skin-friction coefficients are presented for upper-surface locations and for the test conditions of figure 13(a). Calculations were performed using the Cebeci-Smith finite-difference method (ref. 18), both for the undisturbed static-pressure distribution and for the distributions obtained with the probe tip at the survey station. Use of the perturbed pressure distribution in a two-dimensional calculation almost certainly overestimates the influence of the perturbation, because the actual perturbation is a three-dimensional effect (ref. 17). The experimental boundary-layer data were reduced using both the pressure coefficient obtained in the presence of the probe and the interference-free value. The former values were then corrected by ratios of the computed quantities (column 5, table 3), and percent differences were computed using the corrected values of column 5 as a reference. The measured data, reduced using the noninterference C_p, differ little, in most cases, from the data reduced using the C_p measured in the presence of the probe and corrected using the calculated values. A similar set of computations was performed in which data were first reduced using the C_p values containing interference effects and then expanded isentropically to the noninterference C_p, accounting for stream-tube area change. These boundary-layer properties differed only slightly from those calculated using the noninterference C_p. Although a completely satisfactory evaluation of interference effects is not possible without a set of interference-free experimental data, the use of the noninterference C_p directly is believed to give results that are at least as accurate as any of the more complex alternatives.

The influence of interference effects on the measured distribution of boundary-layer properties is minimized by the decreasing magnitude of the static-pressure perturbations with increasing x/c of the survey station. As a result, the full profiles forward on the airfoil are relatively resistant to the increased adverse pressure gradient, and the profiles nearer the trailing edge having larger shape factors are subjected to a smaller incremental pressure gradient.

Interferograms

Examples of interferograms obtained with the sharp-trailing-edge model and with an uncambered NACA 64A010 airfoil (ref. 14) are presented in figure 14. Figure 14(a) shows a predominantly subcritical case. A close-up of the trailing-edge region is shown in figure 14(b). Two supercritical cases with upper-surface shocks corresponding to two different angles of attack are shown in figures 14(c) and 14(d). Differences in the fringe patterns between the two airfoils near the trailing edge result from the stronger viscous interaction in this region associated with the supercritical airfoil. Fringe patterns in the viscous and inviscid regions are distinctly different. As a result, the approximate boundaries of the viscous regions are visible. Within the viscous regions, the static pressure varies only in the streamwise

direction, except near the shock and the trailing edge, but the fringe patterns show density gradients to be approximately parallel to streamlines. Static temperature variations associated with adiabatic deceleration therefore must be the predominant mechanism for production of density variations in the boundary layers and wakes. For the NACA 64A010 airfoil, the closed contours in the primarily inviscid flow are located symmetrically above and below the trailing edge. By contrast, for the supercritical airfoil, the closed contours are displaced streamwise in the interferograms, indicating local density maxima in the lower-surface concavity and downstream of the trailing edge on the upper surface of the near wake. The fringe pattern in the lower-surface boundary layer near the trailing edge is a composite of the viscous and inviscid patterns, indicating that adiabatic deceleration and static-pressure gradients are of comparable importance in producing density variations in this region.

Data from static-pressure orifices and pressures determined from the interferograms using the assumption of constant stagnation pressure and temperature are compared in figure 15. A comparison of 1977 and 1978 data showed that an apparent 0.4° increase in angle of attack in the 1978 data was required to achieve agreement with a corresponding static pressure distribution obtained in 1977. Values of angle of attack associated with the 1978 data have been decreased by 0.4° throughout this report, except in table 2, and in the appendix. Pitot-pressure data obtained for the test conditions of figure 15(b) show the stagnation pressure at the boundary-layer edge downstream of the shock to be equal to the free-stream value within experimental uncertainty. As a result, no corrections for shock losses were made in the computation of static pressure from the interferogram data for the cases of figures 15(b) and 15(c). Agreement is generally good between the two types of data, implying that a close approximation to infinite-fringe alignment was achieved. Oil-flow visualization photographs show that upper-surface shocks on the supercritical airfoil sweep forward near the sidewalls, causing an apparent smearing of the shock compression in the interferogram data. The comparison of figure 15(d) for the NACA 64A010 airfoil indicates that the flow near the shock is more nearly two-dimensional. Apparently the greater upper-surface curvature of this airfoil causes the shock to remain at a more nearly constant chordwise location than it does on the supercritical section.

The interferogram data give static-pressure distributions at the edges of the boundary layer and near wake, which are difficult to measure by other techniques. Significant static-pressure gradients normal to streamlines are present in the near-wake data for the supercritical airfoil and extend approximately 10% chord downstream in figures 15(a) and 15(b). The effect is less pronounced in figure 15(c) and for the NACA 6-series airfoil. Pressure variations across the lower-surface boundary layer near the trailing edge are present in the data for the supercritical airfoil. The flow is attached in the lower-surface concavity at the test conditions of figure 15(a), $M_\infty = 0.6$; the static pressure varies across the boundary layer throughout most of the lower-surface concavity in this situation. On the other hand, little or no static-pressure variation normal to the surface is indicated in the data of figure 15(b) for $M_\infty = 0.8$, $c_l = 0.61$ where the flow was separated in the concavity. The flow in the concavity at $M_\infty = 0.8$, $c_l = 0.44$ was also separated, and the data of figure 15(c) also indicate little static-pressure variation across the separated boundary layer.

Boundary-Layer and Wake-Profile Data

Two sets of boundary-layer data derived from pitot-pressure measurements have been chosen for presentation in detail; both were obtained with the sharp-trailing-edge model. Data were reduced, using the compressible Bernoulli equation in subsonic

flow and the Rayleigh pitot formula in supersonic flow, assuming constant stagnation temperature. The first data set corresponds to the case at $M_\infty = 0.6$, $Re_c = 4\times10^6$ (fig. 13(e)). The second corresponds to $M_\infty = 0.8$, $Re_c = 3\times10^6$, $\alpha_{geom} = 2.4°$ (fig. 13(f)) and is characterized by a shock located relatively far aft of the trip, so that effects of the trip on the shock-wave/boundary-layer interaction are minimized, but sufficiently far forward to permit the existence of a region of nearly constant static pressure immediately downstream of the shock, thus allowing recovery of the boundary-layer profile before encountering the adverse pressure gradient near the trailing edge. The boundary-layer profiles are presented in figures 16 and 17; velocities are normalized by the free-stream value, and a common length scale is used to facilitate direct comparison. The profiles of figure 16(a) show features typical of attached turbulent boundary layers, except at the trailing edge where the upper-surface profile appears to be approaching separation and the lower-surface profile shows the effects of the sudden expansion in the final few percent chord.

The laminar boundary layer at $x/c = 0.3$ on the upper surface is shown in figure 17(a). This boundary layer is approximately at the lower limit of resolution of the measuring technique. Values of overall boundary-layer thickness, displacement thickness, and momentum thickness, at this station all normalized by the chord, are tabulated and compared with values calculated by the Cebeci-Smith method (ref. 18), using the experimental pressure distribution. Agreement between measured and computed thicknesses is good. Subsequent thickening of the boundary layer by the shock located at $x/c \cong 0.55$ is apparent. Although no reverse flow is indicated by the lower-surface boundary-layer profile at $x/c = 0.91$, oil-flow data indicate that a separation bubble was present in the lower-surface concavity under these conditions. Instances where measured pitot pressures were slightly in excess of the local static pressure in regions where the flow was known to be reversed have been reported by others (refs. 19 and 20).

Figure 18 presents boundary-layer profiles derived independently from pitot-pressure and interferometry data. These data were reduced employing the usual assumption that the static pressure does not vary in the direction normal to the surface. This comparison serves primarily as a check on both types of data, since the techniques are subject to different error sources, and as a demonstration of repeatability, since the data were obtained during different tunnel entries. Other comparisons of this type show similar trends: the profiles obtained by the two methods at $M_\infty = 0.8$ were always in better agreement than those obtained at $M_\infty = 0.6$.

Trailing-edge profiles of density, pitot pressure, velocity, and static pressure are presented in figure 19. The velocity and static-pressure data were derived from the density and pitot-pressure measurements with the assumption of constant stagnation temperature. Integral properties for these profiles were calculated as described in reference 1, with the modifications for static-pressure variation across the boundary layers proposed by Zwaaneveld (ref. 21). The key feature of this modification is the definition of a reference inviscid flow having the experimentally determined static-pressure distribution and the free-stream stagnation pressure. The data of figure 19 show a decreasing static-pressure level with increasing z/c. A major portion of the waviness in the derived C_p distributions is undoubtedly associated with the fact that the density and pitot-pressure data were obtained in separate experiments. Errors in the location of the z-axis origin relative to the measured profiles also may have contributed to errors in calculated static pressure. These data show a static-pressure variation throughout the upper-surface boundary layer, especially for the lower Mach number, $M_\infty = 0.6$. Most of the variations in C_p within the lower-surface profiles are confined to the region near the surface. The average C_p levels in the lower-surface profiles are significantly higher than the

trailing-edge surface C_p's. The surface measurements were made with aft-facing orifices in the trailing edge, a technique which would be expected to give an average static-pressure level for the entire trailing-edge region.

The use of the surface trailing-edge C_p in computing velocities and integral properties for the lower-surface trailing-edge boundary layers leads to large errors. Lower-surface trailing-edge velocities were computed using the present method in the cases for which interferograms were available; C_p increments between the trailing-edge static-pressure orifice and the average value for the lower-surface profile derived from interferograms were used for the remaining cases.

Examples of near-wake profile data presented in figure 20 correspond to the test conditions of figures 15(a) and 15(b). Comparisons of wake-velocity profiles similar to those presented in figure 18 for boundary-layer data, in which the interferogram and pitot-pressure data were reduced independently, show reasonable agreement, except near the wake centerline; near the centerline, the minimum velocities derived from the interferograms are greater than those computed from the pitot-pressure measurements. Although the cause of this discrepancy is not completely understood, the fact that the interferogram represents an average of the density field over the test-section width is believed to be a contributing factor. The near-wake velocities of figure 20 were computed from the pitot-pressure data, using static-pressure levels determined from the interferogram at the edges of the wake and assuming a linear variation in static pressure across the wake.

Boundary-layer velocity profiles corresponding to attached flow were transformed to equivalent incompressible profiles, using the van Driest transformation (ref. 22):

$$u^* = \frac{u_e}{a} \sin^{-1}\left(a \frac{u}{u_e}\right) \tag{3}$$

where

$$a = \left(\frac{r \frac{\gamma - 1}{2} M_e^2}{1 + r \frac{\gamma - 1}{2} M_e^2}\right)^{1/2} \tag{4}$$

The subscript e refers to edge conditions, and r is the recovery factor, taken to be 0.89. The transformed profiles were fitted by an iterative least-squares technique to Coles' wall-wake formula (ref. 23):

$$u^+ = \frac{1}{0.41} \ln z^+ + 5.0 + \frac{\Pi}{0.41} w \tag{5}$$

$$w = 2 \sin^2\left(\frac{\pi z}{2\delta}\right) \tag{6}$$

where $u^+ = u^*/u_\tau$; $z = (zu_\tau)/\nu_w$; u_τ is the shear velocity $\sqrt{\tau_w/\rho_w}$; τ is the shear stress, and the subscript w refers to conditions at the surface. The quantities u_τ, Π (wake coefficient), and δ (boundary-layer thickness) were determined by the fitting process. Additional details pertaining to the transformation and fitting process are given in references 1 and 2. Apparently because of the abrupt expansion on the lower surface near the trailing edge, the lower-surface trailing-edge profiles did not conform to the wall-wake family and have been excluded from this presentation.

Most upper-surface trailing-edge profiles did not exhibit a distinct logarithmic region, implying a state of incipient separation.

The data of figures 16 and 17 are presented in wall-wake coordinates in figures 21-24. In most cases a well-defined logarithmic region is present near the wall. Some data for which the wake component of the profile was negligible have been omitted from figures 22 and 24. Boundary-layer and wake integral properties are summarized in table 4, and velocity and density profiles are presented in table 5.

A representative sample of the upper-surface trailing-edge profiles is compared with Stratford's separation profile (ref. 24) in figure 25. Stratford's analysis for an incompressible turbulent boundary layer at separation predicts the following velocity profile near the surface:

$$u = \left(\frac{4}{\rho k^2}\frac{dp}{dx}\right)^{1/2} z^{1/2} \tag{7}$$

where $k = 0.41$. This can be written,

$$\frac{u}{u_\infty} = \left[\frac{2}{k^2}\frac{\rho_\infty}{\rho_w}\frac{dC_p}{d(x/c)}\right]^{1/2}\left(\frac{z}{c}\right)^{1/2} \tag{8}$$

Values of the static-pressure gradient used in determining the predicted profiles of figure 25 were estimated from the data of figure 13. Figure 25(a) is clearly a separated profile. Since the points near the surface for figure 25(b) also lie below the predicted profile, it is probably separated too. Cases (c) and (d) are in reasonable agreement with the predicted profile, indicating a state of incipient separation. The experimental profile of figure 25(e) is probably attached, since it lies above the incipient separation profile and since a small logarithmic region exists near the surface (fig. 23(a)).

COMPARISONS WITH COMPUTATIONS

Boundary-Layer Computations

Comparisons between measured and calculated boundary-layer properties are presented in figure 26 for the case shown in figure 13(e), the sharp-trailing-edge model at $M_\infty = 0.6$. This case is probably the one for which the best overall agreement would be expected between measured and calculated boundary layers. First, the flow is almost completely subcritical, with only a small supersonic region at the leading edge, so that complications caused by shock-wave/boundary-layer interactions are absent. Second, both pitot-pressure measurements and oil-flow results indicate that the flow remained attached in the lower-surface concavity.

Experimental momentum and displacement thicknesses for the upper surface are compared in figure 26(a) with results of computations obtained from three boundary-layer computation methods, using the measured static-pressure distribution. Corresponding values of skin friction and shape factor are compared in figure 26(b). The boundary-layer computation methods used for this purpose are the Cebeci-Smith method (ref. 18), a finite-difference method which is among the most accurate and generally

applicable methods available, and two integral methods (refs. 25 and 26). The Nash-Macdonald method was developed specifically for computation of boundary layers on airfoils having flat-rooftop-type pressure distributions; it has been used in combination with programs for computation of transonic airfoil flow fields (refs. 27 and 28). Initial conditions for the Nash-Macdonald method for this and all subsequent cases were obtained from the Cebeci-Smith results, just downstream of transition. Agreement between measured and calculated properties is reasonably good for $x/c < 0.8$.

Discrepancies in C_f and H shown by Bower's method (ref. 25) for $0.3 < x/c < 0.4$ are caused by the use of an experimental profile for starting the calculation; it is remarkable how for $x/c > 0.4$, the predictions of this scheme are insensitive to the perturbation in initial conditions. The close agreement between the Cebeci-Smith computations and those of Bower's method is consistent with results from numerous similar comparisons between predictions of the Cebeci-Smith method and results from the methods of Reeves (ref. 29) and Bradshaw and Unsworth (ref. 30), even though each of these methods is substantially different from the others. Near the trailing edge, the Nash-Macdonald predictions depart drastically from those of the other schemes; the computed displacement thicknesses exceed measured values. Since the computed momentum thickness is underpredicted, this situation corresponds to a computed shape-factor distribution that is much larger than the experimental distribution. Only the Nash-Macdonald method predicts separation just upstream of the trailing edge, as indicated by the computed skin-friction distribution. Although the pitot-pressure measurements indicated that the flow was attached at the trailing edge, the presence of a small region of reverse flow may not have been detected by the probe. These data correspond to case (c) of figure 25, indicating incipient separation at the trailing edge.

The Nash-Macdonald method contains a direct dependence of a boundary-layer shape-factor parameter on the local static-pressure gradient; the latter was derived from a correlation of airfoil boundary-layer data restricted to adverse pressure gradients. Apparently this correlation causes the resulting prediction of displacement-thickness development near the trailing edge to differ from that of the other methods and to agree better with the experimental data in this region. Since the boundary-layer formulation is invalid in the immediate vicinity of the trailing edge, this agreement is partially fortuitous.

A similar set of comparisons for the lower surface is presented in figures 26(c) and 26(d). The calculations include the Cebeci-Smith and Nash-Macdonald methods. Agreement between both sets of calculations and the data is reasonably good upstream of the concavity. Both methods underpredict the growth of displacement thickness, and the skin-friction predictions of the Cebeci-Smith method are in better agreement with the experimental data. The discrepancies between measured and calculated skin friction upstream of the concavity may be due in part to inadequate correction for probe interference effects. This static-pressure distribution is considerably different from those used to determine the shape-factor correlation in the Nash-Macdonald method. Although the Nash-Macdonald method does not adequately treat flows in which the static-pressure gradient changes from adverse to favorable, it is marginally suitable for the flow type under consideration, in which a steep adverse pressure gradient is followed by one less severe.

Comparisons involving both upper and lower surfaces are shown in figure 27 for the case of the blunt-trailing-edge model at $M_\infty = 0.75$. This flow field was characterized by an upper-surface shock at about 18% chord.

In this and all subsequent cases involving a shock-wave/boundary-layer interaction, care was taken in the definition of the static-pressure distribution used for boundary-layer calculations. In a study reported by Lynch (ref. 31), boundary-layer properties computed by the Cebeci-Smith method downstream of a shock-induced pressure rise showed sensitivity to the extent of streamwise smoothing of the static-pressure distribution. Since static-pressure orifices on the models used in the present study are spaced at intervals of 5% chord, except at the leading edge, details of the surface static-pressure distribution in regions of shock-wave/boundary-layer interaction were not resolved. The calculations presented here utilized static-pressure distributions in which the shock-induced pressure rise was smoothed over a streamwise distance of 8-10 times the upstream value of δ, which was the most abrupt pressure rise that could be treated by the Cebeci-Smith program for the present set of experimental data. This distance is difficult to define precisely because of difficulty in defining both δ and the extent of the interaction region. Examination of a summary of experimental shock-wave/boundary-layer interaction data presented by Inger (ref. 32) indicates that this degree of smoothing of the wall static-pressure distribution is of the correct order of magnitude.

The large shape factors indicated by the measured boundary-layer profiles in the lower-surface concavity imply that the flow was probably separated, even though the measured pitot pressures were always greater than the static pressure. The data of figures 27(a)-27(c) were obtained from the two tests involving separate model installations. These results indicate that data repeatability was reasonably good; the most important source of discrepancies is probably associated with unavoidable differences in the boundary-layer transition strips. Since the upper-surface boundary layer was slightly thicker in the 1976 test than in the 1977 test, it is not surprising that the observed difference in displacement thickness is maximum at the trailing edge. Both the Cebeci-Smith and the Nash-Macdonald methods are in good agreement with the measurements downstream of the shock. The relative behavior of the Cebeci-Smith and the Nash-Macdonald methods near the trailing edge is similar to that of the earlier comparison. Note, however, that the Nash-Macdonald skin friction decreased to zero at $x/c = 0.91$. Downstream of this point, the calculation proceeds, using a constant value of shape-factor parameter which has little physical significance.

The comparisons of figure 27(c), involving lower-surface momentum and displacement thicknesses, are typical of the remaining lower-surface results. In this case, the Cebeci-Smith and the Nash-Macdonald predictions are in good agreement with the data at the first two stations, but the Cebeci-Smith predictions indicate separation at the third station, probably not far from the actual separation point. The Nash-Macdonald method predicted attached flow for this later station, as well as for all of the remaining lower-surface flows. Since neither formulation is valid for flow at or downstream of separation, comparisons downstream of a physical separation location are not meaningful.

Results obtained with the blunt-trailing-edge model nearer the design condition, $M_\infty = 0.8$, are shown in figure 28(a). In this case and in all of the following cases, the upper-surface boundary-layer trip was located at $x/c = 0.35$. Good agreement between measured and computed values of both momentum and displacement thicknesses is shown for the laminar boundary layer upstream of the trip. Agreement is fairly good between measured and computed properties at $x/c = 0.4$, but the shape-factor discrepancy and the proximity to the boundary-layer trip indicate that the experimental boundary layer was probably transitional at this station. Agreement of all calculated quantities with experiment from $0.5 \leq x/c \leq 0.85$ is good, a result not anticipated, because none of the details of the shock-wave/boundary-layer interaction are considered.

The sensitivity of the Nash-Macdonald method to local static-pressure gradients is manifested in a peak in the displacement thickness at the shock. Neither method is accurate near the trailing edge, where the Nash-Macdonald method again predicts early separation, based on computed C_f. The Nash-Macdonald method continues to proceed downstream of the point where zero skin friction is first predicted, using the previously mentioned arbitrary maximum value of shape-factor parameter. The lower-surface results of figure 28(c) are similar to those of figure 27(c).

Four sets of upper-surface data are presented in figure 29 for both blunt- and sharp-trailing-edge models at $M_\infty = 0.80$ and for the blunt-trailing-edge model at $M_\infty = 0.83$. Agreement between measured and calculated boundary layers on the forward portion of the airfoil is reasonably good, except in figure 29(a). These cases correspond to stronger, more-aft-located shock waves on the upper surface than those shown in figure 28, and the increases in boundary-layer thicknesses caused by the interactions are correspondingly greater. Predictions of these increases also are good.

Analyses proposed by Inger and Mason (ref. 8) and by Bohning and Zierep (ref. 9) predict separation at the shock for all cases of the present study. It is possible that separation bubbles were present in the interaction region but were too small to be detected by the techniques of this investigation.

The Cebeci-Smith predictions of displacement and momentum thickness fail at $0.90 < x/c < 0.95$. Further study is needed to determine whether the boundary-layer calculations are accurate throughout the entire region where the formulation is valid; if a special treatment of the trailing-edge region is employed, such as that proposed by Melnik et al. (ref. 7), the upstream boundary conditions provided by the conventional calculation must be accurate.

A typical example of a Nash-Macdonald prediction for this type of case is included in figure 29(c), in which a large overshoot in displacement thickness occurs at the shock and the predicted displacement thicknesses near the trailing edge are too large.

The data of figure 29(d) correspond to the case described in detail in references 1 and 2, except for the previously mentioned difference in boundary-layer trip location (see fig. 13(g)). The present data show the expected thinner boundary layer over the aft portion of the airfoil, relative to the data of references 1 and 2, associated with aft movement of transition, and also better agreement between measured and computed increases in momentum and displacement thicknesses caused by the shock.

Airfoil Flow Field Computations

Comparisons between measured and computed static-pressure distributions are presented in figure 30 for the test condition at $M_\infty = 0.6$, sharp-trailing-edge model (see figs. 14(a), 14(b), and 15(a)). The computation technique, developed by Garabedian and Korn (ref. 33) and extended by Tranen (ref. 34), uses the full potential equation for two-dimensional, steady, inviscid transonic flow, in conjunction with a quasi-conservative, rotated differencing scheme. The region exterior to the airfoil is mapped to the interior of a circle. The effective airfoil shape used for the calculation of figure 30(a) was obtained by adding a displacement thickness distribution faired through the measured values for this case to the airfoil coordinates, resulting in a profile having an open trailing edge. The calculation of the potential field uses only the airfoil surface-slope distribution. When the results

are transformed to the physical plane, the computed flow field includes a source within the airfoil whose strength is determined by the trailing-edge thickness. Agreement between the experimental and computed distribution is generally good, although the measured C_p levels were shifted by -0.03 for this comparison (see the appendix for a discussion of discrepancies in C_p levels). Discrepancies on the lower surface near the leading edge are believed to be caused by deviations of the airfoil model contour from the prescribed coordinates. Pressure levels in the concavity are affected strongly by the displacement-thickness distribution. Since the experimental values are used here, the difference between the measured and computed static pressure distribution in this region is greater than expected. Static-pressure levels in the concavity derived from the interferogram are even lower than the pressure-orifice data on figure 30(a).

The experimental data of figure 15(a) are compared with predictions of viscous-inviscid computations in figure 30(b). The method of reference 34 is a conventional iteration between inviscid and boundary-layer computation procedures that uses extrapolation of the computed displacement-thickness distribution near the trailing edge for $x/c > 0.997$. The method proposed by Melnik et al. (ref. 7) includes a detailed treatment of the trailing-edge and near-wake flow field. In both cases the computed aft loading is greater than that shown by the data.

Momentum and displacement-thickness distributions for the boundary layers and the near-wake obtained from the computations of figure 30(b) are compared with experimental data in figure 31. The comparison for the upper-surface boundary layer is given in figure 31(a). Both of the computed boundary-layer thickness distributions lie somewhat below the data, particularly for $x/c > 0.9$. Considerably better agreement would have been obtained if the computed shape factor, δ^*/θ, were closer to the measured value at $x/c \cong 0.8$, which is approximately at the beginning of the region of adverse pressure gradient. The computed response of a turbulent boundary layer to an adverse pressure gradient is sensitive to upstream conditions, particularly if the initial shape factor is greater than that corresponding to zero static-pressure gradient. Better agreement was obtained between the experimental lower-surface boundary-layer properties and the predictions of reference 7, as shown in figure 31(b). Since the special treatment of the trailing-edge region of Melnik et al. (ref. 7) extends upstream for only a distance of the order of a boundary-layer thickness, differences in computed boundary-layer properties shown in figure 31(b) are probably the result of differences in the boundary-layer computation methods and not the trailing-edge treatemnt. The computed static-pressure distributions differ from the experimental distribution in the concavity. Boundary-layer computations using the experimental static-pressure distribution would result in significantly smaller computed displacement thicknesses in the concavity than the distributions of figure 31(b).

Near-wake displacement and momentum thicknesses computed by the method of Melnik et al. (ref. 7) for the $M_\infty = 0.6$ case are in good agreement with experimental data, as shown in figure 31(c). The interferograms show that elevated static-pressure levels persist relatively far downstream of the trailing edge. Since momentum and displacement thicknesses determined from pitot-pressure surveys are relatively sensitive to the static pressure used in data reduction, interferometry is valuable in obtaining an accurate description of this type of wake.

Comparisons between the experimental static-pressure distribution and static-pressure distributions computed by the method of reference 34 for the supercritical case shown in figure 14(c) are presented in figure 32. Inviscid computations were performed for an effective airfoil shape obtained by adding a displacement-thickness

distribution faired through the measured values. The dashed line represents results of a nonconservative calculation performed at $M_\infty = 0.78$, with the angle of attack chosen to give reasonable agreement with the static pressure levels on the forward portion of the airfoil. Similar calculations performed at higher Mach numbers, and those performed using quasi-conservative differencing, tended to form strong shocks near the trailing edge and failed to converge. Viscous-inviscid calculations, using the method of reference 7, were similarly unsuccessful. The inverse feature developed by Tranen (ref. 34) was used to determine an effective airfoil shape which would yield approximately the experimental pressure distribution. The resulting static-pressure distribution is indicated by the solid line, also computed for $M_\infty = 0.78$, but using quasi-conservative differencing. The required modification to the effective airfoil shape, shown in the insert in figure 32, consists of an upward deflection of the upper surface, beginning at $x/c = 0.94$, and corresponds to a displacement thickness 50% greater than the measured value at the trailing edge. Preliminary calculations in which the effective airfoil shape was extended downstream of the trailing edge using a fairing of the measured displacement-thickness distribution gave similar results; the initial analysis calculation leads to shock waves that are too strong and too far aft, and unreasonably large wake displacement-thickness distributions are required to move the shock forward.

Additional comparisons between measured and computed results are presented in figure 33 in the form of Mach number contours. The measured Mach number contours were obtained from infinite-fringe interferograms. The edges of the boundary layers and wakes obtained from the interferograms also are shown. Agreement between measured and computed contours is reasonably good near the airfoil but becomes poorer with increasing distance from the airfoil. The experimental contours show a more rapid approach to free-stream conditions with distance from the airfoil, normal to the chord line, than the computed contours. If the behavior of the computed contours at some distance from the airfoil is representative of flow in an unbounded medium, then the behavior of the measured contours implies a situation more like that of flow in a free jet. In a free-jet flow, a constant static-pressure level equal to the free-stream value is imposed at the jet boundary, thereby forcing the disturbance field produced by the airfoil to vanish more rapidly with distance from the airfoil than it would in free air. Interpretation of the comparison of figure 33(b) is complicated because the computation was performed at $M_\infty = 0.78$, but Mach numbers assigned to the fringes were determined assuming $M_\infty = 0.8$. Alternative methods of comparison, such as assuming the experimental M_∞ to be lower or selecting experimental fringes to match the density ratio of the computed contours, resulted in poorer agreement than that shown in figure 33(b).

It is also possible that the interferometer was not set exactly in the infinite-fringe mode. As discussed previously, there was no means available to verify that the setting was in infinite-fringe mode when the wavefronts in the entire field of view were disturbed by the flow about the airfoil.

Comparisons of measured and calculated density contours, using data obtained from the same wind tunnel, were presented by Rose and Seginer (ref. 11). These comparisons imply that the effective angle of attack in the tunnel is a function of streamwise location. The conclusions of Rose and Seginer are based in part on discrepancies between computed and measured contours upstream of the leading edge in which the angle of attack of the computation was chosen to give best overall agreement with the experimental surface static pressures. The trend of disagreement between measured and computed contours for variation in the streamwise direction in reference 11 is the reverse of that shown in figure 33. In reference 11, the computed contours approach the free-stream conditions more rapidly than the experimental contours, as

the distance upstream of the leading edge is increased. The same comparison also shows that the experimental contours approach the free-stream conditions more rapidly than the computed contours as the distance from the airfoil, normal to the chord line, increases. This trend for the cross-stream direction is consistent with the present results.

CONCLUDING REMARKS

Data were obtained on the flow about a supercritical airfoil, including surface static-pressure distributions, far-wake surveys (drag measurements), oil-flow visualizations, pitot-pressure surveys in the viscous regions, and holographic interferograms. For cases characterized by upper-surface shock waves near midchord, upper-surface boundary-layer transition was fixed at 35% chord to achieve a boundary-layer thickness distribution near the trailing edge representative of a Reynolds number range higher than that at which the experiments were conducted.

Airfoil drag performance is sensitive to the lower-surface boundary-layer trip configuration, apparently because of the influence of boundary-layer trip configuration on the extent of separation in the concavity.

Combining surface static-pressure, pitot-pressure, and interferogram data provides detailed descriptions of time-mean flow fields about the airfoil. The average static-pressure level in the lower-surface boundary layer at the trailing edge is substantially higher than the pressure measured by the trailing-edge orifice. Static-pressure differences across the wake extend approximately 10% chord downstream of the trailing edge.

Attached boundary-layer profiles, transformed by the van Driest transformation, are in good agreement with Coles' profile family.

Comparisons made between measured flow field properties and results from computations show the following features:

1. The upper-surface boundary-layer predictions of the Cebeci-Smith method are reasonably good except near the trailing edge where the discrepancies may be partially a result of the breakdown of the boundary-layer approximations. The generally good agreement between theory and experiment downstream of the shock-wave/boundary-layer interactions supports the suggestion of Melnik et al. (ref. 7) that special treatment of such interactions may not be necessary for engineering calculations when the flow remains attached.

2. The Nash-Macdonald method predicts thicker boundary layers near the trailing edge, but the predicted displacement thicknesses are often considerably greater than the measured values. The sensitivity of this method to the local pressure gradient produces peaks in the displacement-thickness distributions at the shock; special treatment would be required if the method were coupled with an inviscid program.

3. Both methods give fairly accurate results on the lower surface when the flow remains attached.

Computations of the surface static-pressure distribution, employing both measured and calculated displacement-thickness distributions, are in fairly good agreement with experiment at $M_\infty = 0.6$. Good agreement between measured lower-surface

boundary-layer and near-wake properties and predictions of a viscous-inviscid interaction method is shown at $M_\infty = 0.6$. Growth of the upper-surface boundary layer near the trailing edge is underpredicted for that case. Reasonable agreement between a measured static-pressure distribution and one computed by an inviscid transonic computer program for a case at $M_\infty = 0.8$ characterized by an upper-surface shock at midchord, requires a reduction in the Mach number of the computation to 0.78 and modification of the effective upper-surface contour near the trailing edge; the latter modification is equivalent to adding a trailing-edge displacement thickness 50% greater than the experimental value. Comparisons of computed Mach number contours with contours derived from interferograms show differences that could be interpreted as wall-interference effects.

Ames Research Center
National Aeronautics and Space Administration
Moffett Field, Calif. 94035,

APPENDIX

REPEATABILITY OF STATIC-PRESSURE DISTRIBUTIONS

The experiments described in this report were conducted in a sequence of four tunnel-occupancy periods, one per year from 1975 through 1978. Some discrepancies were noted between static-pressure data obtained during different occupancy periods at the same nominal test conditions and also between data obtained during this series and those published in references 1 and 2. The purpose of this appendix is to illustrate the degree of repeatability achieved during this investigation and to discuss possible sources of the observed discrepancies.

Some of these variations are clearly the result of real differences in the flow fields from which the data were obtained. For example, differences in static-pressure distributions in the lower-surface concavity are almost certainly caused by differences in the extent of separation in the concavity. The inability to reproduce a boundary-layer trip configuration precisely is believed to be at least partially responsible for differences of this type. Other differences seem just as clearly to be associated with the data acquisition process and not with any significant differences in the flow fields. Discrepancies of this type include apparent shifts in the angle of attack or C_p level required to achieve a particular static-pressure distribution. Data obtained for a range of Mach number and angle of attack during a single occupancy period support the conclusion that when two static-pressure distributions corresponding to the same nominal Mach and Reynolds numbers were essentially identical, except possibly for a shift in C_p level, then the airfoil flow fields were also identical to the same level of approximation; no two different combinations of Mach number and angle of attack produce the same static-pressure distribution.

Data obtained in 1973 (refs. 1 and 2) and 1975 with the blunt-trailing-edge model and a leading-edge boundary-layer trip are presented in figure 34. The earlier data show higher static-pressure levels in the lower-surface concavity throughout the Mach number range, implying that the separation bubble was consistently thinner in 1973 than in 1975. The comparison of figure 34(a) for $M_\infty = 0.75$ shows an apparent shift in the overall static-pressure level between the two sets of data; the 1975 level is lower (more negative). This trend is also present in the higher-Mach-number data, figures 34(b) and 34(c).

Comparisons involving the blunt-trailing-edge model with aft-located boundary-layer trips are shown in figure 35. Some interpolation is necessary in interpreting figure 35(a), in which data from 1975 and 1976 are compared at $M_\infty = 0.6$ because data for the same angle of attack are not available. However, it is clear that the apparent static-pressure level of the 1975 data is lower than that of the 1976 data and that the upper-surface static-pressure distributions near the trailing edge are different. Data at $M_\infty = 0.6$ shown in figure 35(b) from 1976 to 1977 are in reasonable agreement, except for a small difference in C_p level. The two sets of data from the 1977 series were obtained several weeks apart, with an intervening period during which testing was discontinued but the model installation was not disturbed. These data show an apparent shift of 0.2° in angle of attack. The comparison between the data from the 1975 series at $M_\infty = 0.8$, shown in figure 35(c), shows a second supersonic region terminated by a shock on the upper surface, and relatively low static-pressure levels in the lower-surface concavity. Similar trends are apparent at $M_\infty = 0.83$, figure 35(d). The data of figures 35(c) and 35(d) show an apparent shift in both angle of attack and C_p level.

Comparisons of data obtained with the sharp-trailing-edge model are shown in figures 36 and 37. The data of figure 36(a) show good agreement between results of the 1977 and 1978 tests at $M_\infty = 0.6$, except for a small apparent shift in C_p level and an apparent angle-of-attack discrepancy of 0.4°. Data obtained at $M_\infty = 0.8$ from the 1975, 1977, and 1978 tests are compared in figures 36(b)-36(d). These data show the previously noted discrepancies in apparent angle of attack and C_p level. The 1975 data show the lowest apparent C_p levels and more aft-located shock waves than data obtained in 1977 or 1978.

Almost all of the boundary-layer and wake pitot-pressure surveys of this investigation were obtained during 1977, and interferograms were obtained in 1978 with the sharp-trailing-edge model. Static-pressure distributions obtained from these two tunnel-occupancy periods are in good agreement when a small C_p shift ($\Delta C_p = .03$) is incorporated and the 0.4° shift in apparent angle of attack is compensated for. Examples corresponding to $M_\infty = 0.8$ are given in figure 37 (see also fig. 36(a)).

REFERENCES

1. Hurley, F. X.; Spaid, F. W.; Roos, F. W.; Stivers, L. S. Jr.; and Bandettini, A.: Detailed Transonic Flow Field Measurements about a Supercritical Airfoil Section. NASA TM X-3244, 1975.

2. Hurley, F. X.; Spaid, F. W.; Roos, F. W.; Stivers, L. S. Jr.; and Bandettini, A.: Supercritical Airfoil Flowfield Measurements. J. Aircraft, vol. 12, no. 9, Sept. 1975, pp. 737-744.

3. Spaid, F. W.; Hurley, F. X.; and Hellman, T. H.: Miniature Probe for Transonic Flow Direction Measurements. AIAA J., vol. 13, no. 2, Feb. 1975, pp. 253-255.

4. Spaid, F. W.; and Stivers, L. S. Jr.: Supercritical Airfoil Boundary Layer Measurements. AIAA Paper 79-1501, July 1979.

5. Spaid, F. W.; and Bachalo, W. D.: Experiments on the Flow About a Supercritical Airfoil, Including Holographic Interferometry. AIAA Paper 80-0343, Jan. 1980.

6. Bavitz, P. C.: An Analysis Method for Two-Dimensional Transonic Viscous Flow. NASA TN D-7718, 1975.

7. Melnik, R. E.; Chow, R.; and Mead, H. R.: Theory of Viscous Transonic Flow Over Airfoils at High Reynolds Number. AIAA Paper 77-680, June 1977.

8. Mason, W. H.; and Inger, G. R.: Analytical Theory of Transonic Normal Shock-Boundary Layer Interaction. AIAA Paper 75-831, June 1975.

9. Bohning, R.; and Zierep, J.: Condition for the Onset of Separation of the Turbulent Boundary Layer on a Curved Wall with a Normal Shock Wave. Translated from Zeitschrift für angewandte Mathematik und Physik, vol. 29, 1978.

10. Deiwert, G. S.: Numerical Simulation of High Reynolds Number Transonic Flows. AIAA J., vol. 13, no. 10, Oct. 1975, pp. 1354-1359.

11. Rose, W. C.; and Seginer, A.: Calculation of Transonic Flow over Supercritical Airfoil Sections. J. Aircraft, vol. 15, no. 8, Aug. 1978, pp. 514-519.

12. Walitt, L.; King, L. S.; and Liu, C. Y.: Computation of Viscous Transonic Flow About a Lifting Airfoil. AIAA J., vol. 16, no. 8, Aug. 1978, pp. 775-776.

13. Trolinger, J. D.; Bogdonoff, S. M.; and Smith, J. A.: Laser Instrumentation for Flow Field Diagnostics. AGARDograph 186, 1974.

14. Johnson, D. A.; and Bachalo, W. D.: Transonic Flow About a Two-Dimensional Airfoil — Inviscid and Turbulent Flow Properties. AIAA Paper 78-1117, July 1978.

15. Braslow, A. L.; Hicks, R. M.; and Harris, R. V., Jr.: Use of Grit-Type Boundary-Layer Transition Trips on Wind-Tunnel Models. NASA TN D-3579, 1966.

16. Hoerner, S. F.: Fluid-Dynamic Drag. Published by the author, 2 King Lane, Greenbriar, Brick Town, N.J., 1965, pp. 2-1 to 2-10.

17. Cook, T. A.: Measurements of the Boundary-Layer and Wake of Two Aerofoil Sections at High Reynolds Numbers and High-Subsonic Mach Numbers. R. & M. No. 3722, British R.A.E., 1973.

18. Cebeci, T.; and Smith, A. M. O.: Analysis of Turbulent Boundary Layers. Academic Press, 1974, pp. 258-384.

19. Vidal, R. J.; Wittliff, C. E.; Catlin, P. A.; and Sheen, B. H.: Reynolds Number Effects on the Shock Wave-Turbulent Boundary Layer Interaction at Transonic Speeds. AIAA Paper 73-661, July 1973.

20. Kooi, J. W.: Experiment on Transonic Shock-Wave Boundary Layer Interaction. Flow Separation. AGARD CP-168, Nov. 1975.

21. Zwaaneveld, J.: Comparison of Various Methods for Calculating Profile Drag from Pressure Measurements in the Near Wake at Subcritical Speeds. Aerodynamic Drag. AGARD-CP-124, 1973.

22. van Driest, E. R.: Turbulent Boundary Layer in Compressible Fluids. J. Aeronaut. Sci., vol. 18, no. 3, Mar. 1951, pp. 145-160.

23. Coles, D. E.: The Young Person's Guide to the Data. In Proceedings: Computation of Turbulent Boundary Layers. 1968 AFOSR-IFP-Stanford Conference, Vol. II, Compiled Data, D. E. Coles and E. A. Hirst, eds., Stanford University, 1969.

24. Stratford, B. S.: The Prediction of Separation of the Turbulent Boundary Layer. J. Fluid Mech., vol. 5, part 1, Jan. 1959, pp. 1-16.

25. Bower, W. W.: Analytical Procedure for Calculation of Attached and Separated Subsonic Diffuser Flows. J. Aircraft, vol. 13, no. 1, Jan. 1976, pp. 49-56.

26. Nash, J. F.; and Macdonald, A. G. J.: The Calculation of Momentum Thickness in a Turbulent Boundary Layer at Mach Numbers up to Unity. C.P. no. 963, British Aeronautical Research Council, 1967.

27. Garabedian, P. R.: Computational Transonics. Aerodynamic Analyses Requiring Advanced Computers, Part II, Paper no. 44, NASA SP-347, 1975, pp. 1269-1280.

28. Carlson, L. A.; and Rocholl, B. M.: Application of Direct-Inverse Techniques to Airfoil Analysis and Design. Advanced Technology Airfoil Research, vol. 1, NASA CP-2045, 1978, pp. 55-72.

29. Reeves, B. L.: Two-Layer Model of Turbulent Boundary Layers. AIAA J., vol. 12, no. 7, July 1974, pp. 932-939.

30. Bradshaw, P.; and Unsworth, K.: An Improved FORTRAN Program for the Bradshaw-Ferris-Atwell Method of Calculating Turbulent Shear Layers. Aero Report no. 74-02, Imperial College of Science and Technology, London, 1974.

31. Lynch, F. T.: Recent Applications of Advanced Computational Methods in the Aerodynamic Design of Transport Aircraft Configurations. Douglas Paper 6639, 11th Congress of ICAS, Lisbon, Portugal, 1978.

32. Inger, G. R.: Analysis of Transonic Normal Shock-Boundary Layer Interaction and Comparison with Experiment. AIAA Paper 76-331, July 1976.

33. Garabedian, P. R.; and Korn, D. G.: Analysis of Transonic Airfoils. Commun. Pure Appl. Math., vol. 24, no. 11, Nov. 1971, pp. 841-851.

34. Tranen, T. L.: A Rapid Computer Aided Transonic Airfoil Design Method. AIAA Paper 74-501, June 1974.

Copies of "Supplement to NASA TM-81336" will be furnished upon request. The supplement consists of additional reduced data obtained from tests of two slightly modified versions of the original NASA Whitcomb airfoil section and a model of the NACA 0012 airfoil section.

Requests for "Supplement to NASA TM-81136" should be addressed to:

NASA Scientific and Technical Information Facility
Attn: Distribution Control Department
P.O. Box 8757
Baltimore/Washington International Airport, MD 21240

CUT

Date _____

Please forward "Supplement to NASA TM-81336" to

_____
Name of organization

_____
Street number

_____
City and State Zip code

Attention: Mr. _____

Title _____

TABLE 1. — DSMA 523 AIRFOIL COORDINATES, SHARP AND BLUNT TRAILING EDGES

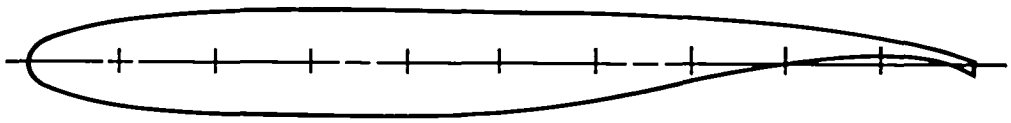

x/c	z_{upper}/c	z_{lower}/c
0.000500	0.005069	−0.005096
0.001000	0.007096	−0.007128
0.002500	0.011063	−0.011078
0.005000	0.015320	−0.015320
0.007500	0.018417	−0.018417
0.010000	0.020716	−0.020671
0.012500	0.022651	−0.022548
0.015000	0.024267	−0.024135
0.020000	0.026918	−0.026744
0.030000	0.030729	−0.030667
0.040000	0.033459	−0.033607
0.060000	0.037407	−0.038087
0.080000	0.040367	−0.041739
0.100000	0.042987	−0.044648
0.120000	0.045198	−0.046796
0.140000	0.047017	−0.048616
0.160000	0.048543	−0.050114
0.180000	0.049828	−0.051348
0.200000	0.050902	−0.052370
0.220000	0.051802	−0.053207
0.240000	0.052563	−0.053890
0.260000	0.053199	−0.054423
0.280000	0.053729	−0.054808
0.300000	0.054161	−0.055056
0.320000	0.054513	−0.055163
0.340000	0.054788	−0.055137
0.360000	0.054998	−0.054978
0.380000	0.055149	−0.054701
0.400000	0.055240	−0.054283
0.420000	0.055272	−0.053719

x/c	z_{upper}/c	z_{lower}/c (sharp TE)	z_{lower}/c (blunt (TE)
0.440000	0.055247	−0.053009	
0.460000	0.055146	−0.052143	
0.480000	0.054973	−0.051136	
0.500000	0.054723	−0.049915	
0.520000	0.054390	−0.048483	
0.540000	0.053976	−0.046780	
0.560000	0.053486	−0.044613	
0.580000	0.052917	−0.052006	
0.600000	0.052269	−0.038885	
0.620000	0.051540	−0.035181	
0.640000	0.050726	−0.030940	
0.660000	0.049826	−0.026087	−0.026390
0.680000	0.048832	−0.020633	−0.021541
0.700000	0.047725	−0.015445	−0.016958
0.720000	0.046494	−0.010574	−0.012692
0.740000	0.045130	−0.006027	−0.008750
0.760000	0.043625	−0.001872	−0.005200
0.780000	0.041942	0.001892	−0.002041
0.800000	0.040043	0.005224	0.000686
0.820000	0.037907	0.008108	0.002965
0.840000	0.035502	0.010505	0.004757
0.860000	0.032780	0.012374	0.006021
0.880000	0.029666	0.013645	0.006687
0.900000	0.026155	0.014169	0.006606
0.920000	0.022185	0.013798	0.005630
0.950000	0.017708	0.012338	0.003565
0.960000	0.012642	0.009726	0.000348
0.980000	0.006842	0.005773	−0.004210
1.000000	0.000308	0.000498	−0.010109
Leading-edge radius/c = 0.023			

GP11-0232-35

TABLE 2. — STATIC-PRESSURE DISTRIBUTIONS, CASES FOR WHICH BOUNDARY-LAYER AND WAKE PROFILES WERE MEASURED

Trip - upper, x/c = 0.05, 0.09 mm
lower, x/c = 0.18, 0.13 mm

$M_\infty = 0.60$, $Re_c = 2 \times 10^6$,
$c_l = 0.58$, $\alpha_{geom} = 1.63^\circ$,
Run 22:1, fig. 13(a)

x/c	C_p	
	Upper	Lower
0.000	1.069	–
0.005	−1.324	0.447
0.015	−1.507	–
0.025	−1.601	–
0.050	−1.168	0.051
0.100	−0.802	−0.104
0.150	−0.687	−0.082
0.200	−0.619	−0.110
0.250	−0.546	−0.120
0.300	−0.499	−0.105
0.350	−0.472	−0.107
0.400	−0.452	−0.128
0.450	−0.443	−0.145
0.500	−0.441	−0.148
0.550	−0.440	−0.137
0.600	−0.430	−0.056
0.650	−0.420	0.119
0.700	−0.419	0.249
0.750	−0.405	0.332
0.800	−0.400	0.378
0.850	−0.375	0.413
0.900	−0.284	0.441
0.950	−0.092	0.426
0.975	–	0.384
1.000	0.038	–

$M_\infty = 0.75$, $Re_c = 2 \times 10^6$,
$c_l = 0.58$, $\alpha_{geom} = 1.23^\circ$,
Run 26:1, fig. 13(b)

x/c	C_p	
	Upper	Lower
0.000	1.154	–
0.005	−0.620	0.312
0.015	−0.925	–
0.025	−1.126	–
0.050	−1.155	−0.048
0.100	−1.138	−0.225
0.150	−1.100	−0.169
0.200	−1.047	−0.196
0.250	−0.505	−0.200
0.300	−0.455	−0.171
0.350	−0.447	−0.166
0.400	−0.440	−0.192
0.450	−0.450	−0.204
0.500	−0.459	−0.202
0.550	−0.473	−0.177
0.600	−0.458	−0.053
0.650	−0.439	0.141
0.700	−0.435	0.263
0.750	−0.416	0.331
0.800	−0.396	0.366
0.850	−0.340	0.406
0.900	−0.210	0.432
0.950	−0.029	0.438
0.975	–	0.406
1.000	0.058	–

(a) Blunt trailing edge, 1976.

GP11-0232-36

TABLE 2. — Continued.

Trip - upper, x/c = 0.05, 0.10 mm
lower, x/c = 0.18, 0.13 mm

$M_\infty = 0.60$, $Re_c = 2 \times 10^6$,
$c_l = 0.58$, $\alpha_{geom} = 1.4^\circ$,
Run 40:1

x/c	c_p Upper	c_p Lower
0.000	−0.038	–
0.005	−1.249	0.480
0.015	−1.669	–
0.025	−1.592	–
0.050	−1.287	0.098
0.100	−0.770	−0.087
0.150	−0.672	−0.071
0.200	–	−0.069
0.250	−0.521	−0.090
0.300	−0.481	−0.073
0.350	−0.454	−0.081
0.400	–	−0.101
0.450	−0.423	−0.122
0.500	−0.394	−0.121
0.550	−0.422	−0.111
0.600	−0.412	−0.039
0.650	−0.400	0.137
0.700	−0.394	0.269
0.750	−0.389	0.348
0.800	−0.378	0.400
0.850	−0.342	0.435
0.900	−0.265	0.459
0.950	−0.070	0.437
0.975	–	0.406
1.000	0.071	–

$M_\infty = 0.75$, $Re_c = 2 \times 10^6$,
$c_l = 0.58$, $\alpha_{geom} = 1.0^\circ$,
Run 45:1

x/c	c_p Upper	c_p Lower
0.000	−0.051	–
0.005	−0.532	0.349
0.015	−0.976	–
0.025	−1.099	–
0.050	−1.187	−0.005
0.100	−1.070	−0.189
0.150	−1.027	−0.154
0.200	–	−0.139
0.250	−0.433	−0.153
0.300	−0.424	−0.134
0.350	−0.426	0.037
0.400	–	−0.144
0.450	−0.426	−0.169
0.500	−0.406	−0.161
0.550	−0.443	−0.147
0.600	−0.439	0.037
0.650	−0.419	0.168
0.700	−0.409	0.287
0.750	−0.390	0.357
0.800	−0.373	0.391
0.850	−0.317	0.433
0.900	−0.198	0.452
0.950	−0.013	0.450
0.975	–	0.429
1.000	0.089	–

Trip - upper, x/c = 0.35, 0.13 mm
lower, x/c = 0.18, 0.13 mm

$M_\infty = 0.80$, $Re_c = 2 \times 10^6$,
$c_l = 0.63$, $\alpha_{geom} = 0.9^\circ$,
Run 80:2, fig. 13(c)

x/c	c_p Upper	c_p Lower
0.000	−0.084	–
0.005	−0.356	0.283
0.015	−0.788	–
0.025	−0.903	–
0.050	−1.000	−0.053
0.100	−0.963	−0.273
0.150	−0.945	−0.213
0.200	–	−0.188
0.250	−0.886	−0.201
0.300	−0.882	−0.162
0.350	–	−0.160
0.400	−0.833	−0.179
0.450	−0.662	−0.202
0.500	−0.324	−0.188
0.550	−0.353	−0.153
0.600	−0.382	−0.025
0.650	−0.404	0.180
0.700	−0.425	0.293
0.750	−0.433	0.348
0.800	−0.429	0.384
0.850	−0.358	0.421
0.900	−0.215	0.449
0.950	−0.001	0.469
0.975	–	0.436
1.000	0.113	–

$M_\infty = 0.80$, $Re_c = 2 \times 10^6$,
$c_l = 0.77$, $\alpha_{geom} = 1.6^\circ$,
Run 80:4, fig. 13(d)

x/c	c_p Upper	c_p Lower
0.000	−0.086	–
0.005	−0.449	0.424
0.015	−0.869	–
0.025	−0.984	–
0.050	−1.084	0.065
0.100	−1.050	−0.140
0.150	−1.034	−0.112
0.200	–	−0.097
0.250	−0.987	−0.116
0.300	−0.986	−0.090
0.350	–	−0.094
0.400	−0.936	−0.114
0.450	−0.924	−0.139
0.500	−0.854	−0.134
0.550	−0.912	−0.109
0.600	−0.414	0.006
0.650	−0.291	0.207
0.700	−0.287	0.325
0.750	−0.306	0.387
0.800	−0.331	0.426
0.850	−0.297	0.464
0.900	−0.184	0.489
0.950	0.010	0.501
0.975	–	0.462
1.000	0.117	–

$M_\infty = 0.83$, $Re_c = 2 \times 10^6$,
$c_l = 0.61$, $\alpha_{geom} = 0.78^\circ$,
Run 79:2, fig. 13(g)

x/c	c_p Upper	c_p Lower
0.000	−0.069	–
0.005	−0.219	0.253
0.015	−0.636	–
0.025	−0.741	–
0.050	−0.849	−0.080
0.100	−0.814	−0.339
0.150	−0.808	−0.256
0.200	–	−0.233
0.250	−0.772	−0.231
0.300	−0.779	−0.181
0.350	–	−0.175
0.400	−0.761	−0.195
0.450	−0.740	−0.219
0.500	−0.688	−0.198
0.550	−0.754	−0.150
0.600	−0.778	−0.003
0.650	−0.781	0.201
0.700	−0.436	0.297
0.750	−0.260	0.349
0.800	−0.246	0.380
0.850	−0.211	0.418
0.900	−0.096	0.443
0.950	0.054	0.470
0.975	–	0.448
1.000	0.130	–

(b) Blunt trailing edge, 1977.

GP11-0232-43

TABLE 2. — Continued.

Trip - upper, x/c = 0.05, 0.05 mm
lower, x/c = 0.18, 0.13 mm

$M_\infty = 0.6$, $Re_c = 4 \times 10^6$,
$c_l = 0.58$, $\alpha_{geom} = 2.6^\circ$,
Run 84:3, fig. 13(e)

x/c	c_p Upper	c_p Lower
0.000	0.987	–
0.002	0.155	1.068
0.005	−0.488	0.969
0.010	–	0.677
0.025	–	0.223
0.050	−1.371	0.073
0.075	−0.904	0.037
0.100	−0.829	−0.030
0.150	–	−0.003
0.200	−0.622	−0.033
0.250	−0.549	−0.063
0.300	−0.483	−0.080
0.350	−0.476	−0.104
0.400	−0.435	−0.119
0.450	−0.429	−0.119
0.500	−0.412	−0.153
0.550	−0.402	−0.134
0.600	−0.388	−0.087
0.650	−0.404	0.066
0.700	−0.367	0.243
0.750	−0.348	0.339
0.800	−0.346	0.400
0.850	–	0.444
0.900	−0.178	–
0.950	–	0.466
1.000	0.104	–

Trip - upper, x/c = 0.35, 0.13 mm
lower, x/c = 0.18, 0.13 mm

$M_\infty = 0.80$, $Re_c = 2 \times 10^6$,
$c_l = 0.61$, $\alpha_{geom} = 1.8^\circ$,
Run 2:2, fig. 13(f)

x/c	c_p Upper	c_p Lower
0.000	1.170	–
0.002	0.713	1.045
0.005	0.276	0.868
0.010	–	0.478
0.025	−0.839	−0.013
0.050	−1.086	−0.092
0.075	−1.052	−0.143
0.100	−0.990	−0.193
0.150	–	−0.189
0.200	−0.987	−0.152
0.250	−0.976	−0.180
0.300	−0.942	−0.185
0.350	−0.896	−0.207
0.400	−0.911	−0.227
0.450	−0.904	−0.222
0.500	−0.831	−0.252
0.550	−0.345	−0.187
0.600	−0.246	−0.074
0.650	−0.274	0.134
0.700	−0.298	0.267
0.750	−0.300	0.312
0.800	−0.273	0.352
0.850	–	0.389
0.900	−0.084	–
0.950	–	0.463
1.000	0.178	–

Trip - upper, x/c = 0.35, 0.08 mm
lower, x/c = 0.18, 0.13 mm

$M_\infty = 0.80$, $Re_c = 3 \times 10^6$,
$c_l = 0.71$, $\alpha_{geom} = 2.4^\circ$,
Run 121:1, fig. 13(f)

x/c	c_p Upper	c_p Lower
0.000	1.155	–
0.002	0.656	1.072
0.005	0.207	0.927
0.010	–	0.584
0.025	−0.913	0.109
0.050	−1.151	0.007
0.075	−1.117	−0.034
0.100	−1.061	−0.092
0.150	–	−0.086
0.200	−1.049	−0.096
0.250	−1.033	−0.123
0.300	−0.997	−0.127
0.350	−1.000	−0.147
0.400	−0.970	−0.153
0.450	−0.970	−0.149
0.500	−0.959	−0.186
0.550	−0.554	−0.150
0.600	−0.297	−0.054
0.650	−0.240	0.145
0.700	−0.251	0.294
0.750	−0.254	0.350
0.800	−0.249	0.394
0.850	–	0.436
0.900	−0.083	–
0.950	–	0.512
1.000	0.196	–

GP11-0232-44

(c) Sharp trailing edge, 1977.

TABLE 2. — Concluded.

Trip - upper, x/c = 0.05, 0.05 mm
lower, x/c = 0.18, 0.13 mm

$M_\infty = 0.60$, $Re_c = 4 \times 10^6$,
Run 36, $\alpha_{geom} = 3.0^o$,
Fig. 15(a)

x/c	C_p Upper	C_p Lower
0.000	1.0213	–
0.002	0.1919	1.0820
0.005	−0.4338	0.9772
0.010	−1.1744	0.6739
0.025	−1.8737	0.1936
0.050	−1.2471	−0.0090
0.075	−0.9114	–
0.100	−0.8062	−0.0651
0.150	−0.7377	−0.0351
0.200	−0.6242	−0.0703
0.250	−0.5671	−0.0934
0.300	−0.4911	−0.1044
0.350	−0.4853	−0.1278
0.400	−0.4561	−0.1423
0.450	−0.4380	−0.1498
0.500	−0.4296	−0.1933
0.550	−0.4213	−0.1852
0.500	−0.4118	−0.1118
0.650	−0.3998	0.0420
0.700	−0.4026	0.2296
0.750	−0.3978	0.3179
0.800	−0.3901	0.3782
0.850	−0.3320	0.4247
0.900	−0.2340	0.4543
0.950	−0.0215	0.4490
0.999	0.0707	–

Trip - upper, x/c = 0.35, 0.13 mm
lower, x/c = 0.18, 0.13 mm

$M_\infty = 0.80$, $Re_c = 3 \times 10^6$,
Run 46, $\alpha_{geom} = 1.4^o$,
Fig. 15(c)

x/c	C_p Upper	C_p Lower
0.000	1.1940	–
0.002	0.8194	0.9611
0.005	0.3952	0.7466
0.010	−0.1416	0.3193
0.025	−0.7119	−0.2400
0.050	−0.9796	–
0.075	−0.9219	−0.3565
0.100	−0.8335	−0.4331
0.150	−0.8473	−0.3408
0.200	−0.8485	−0.3393
0.250	−0.8185	−0.3534
0.300	−0.7635	−0.3421
0.350	−0.7532	−0.3656
0.400	−0.3554	−0.3672
0.450	−0.3309	−0.3653
0.500	−0.3879	−0.3911
0.550	−0.4000	−0.2909
0.600	−0.4243	−0.1449
0.650	–	0.0824
0.700	−0.4598	0.1868
0.750	−0.4319	0.2252
0.800	−0.3967	0.2462
0.850	−0.3087	0.2850
0.900	−0.1506	0.3358
0.950	0.0669	0.3866
0.999	0.1304	–

Trip - upper, x/c = 0.35, 0.13 mm
lower, x/c = 0.18, 0.13 mm

$M_\infty = 0.80$, $Re_c = 2 \times 10^6$,
Run 17, $\alpha_{geom} = 2.2^o$,
Fig. 15(b)

x/c	C_p Upper	C_p Lower
0.000	1.1803	–
0.002	0.7321	1.0445
0.005	0.2961	0.8518
0.010	−0.2415	0.4771
0.025	−0.8163	−0.0444
0.050	−1.0796	−0.0183
0.075	−1.0535	−0.1816
0.100	−0.9994	−0.2280
0.150	−0.9777	−0.1886
0.200	−0.9962	−0.1943
0.250	−0.9821	−0.2287
0.300	−0.9525	−0.2317
0.350	−0.9609	−0.2634
0.400	−0.9272	−0.2746
0.450	−0.9038	−0.2651
0.500	−0.9115	−0.3032
0.550	−0.5899	−0.2417
0.600	−0.2768	−0.1152
0.650	−0.2786	0.0971
0.700	−0.3241	0.2319
0.750	−0.3460	0.2749
0.800	−0.3298	0.3095
0.850	−0.2718	0.3431
0.900	−0.1438	0.3895
0.950	0.0724	0.4391
0.999	0.1460	–

$M_\infty = 0.80$, $Re_c = 3 \times 10^6$,
Run 41, $\alpha_{geom} = 2.8$

x/c	C_p Upper	C_p Lower
0.000	1.1715	–
0.002	0.6715	1.0611
0.005	0.2175	0.9230
0.010	−0.3274	0.5529
0.025	−0.9169	0.0802
0.050	−1.1475	−0.0182
0.075	−1.1441	−0.0869
0.100	−1.0582	−0.1449
0.150	−1.0723	−0.1143
0.200	−1.0774	−0.1225
0.250	−1.0411	−0.1702
0.300	−1.0217	−0.1590
0.350	−1.0318	−0.2077
0.400	−0.9851	−0.2217
0.450	−0.9802	−0.2117
0.500	−0.9602	−0.2655
0.550	−0.9696	−0.2094
0.600	−0.4935	−0.0996
0.650	−0.2565	0.1142
0.700	−0.2737	0.2574
0.750	−0.2928	0.3142
0.800	−0.2802	0.3423
0.850	−0.2357	0.3896
0.900	−0.1403	0.4353
0.950	0.0734	0.4671
0.999	0.1555	–

GP11-0232-45

(d) Sharp trailing edge, 1978.

TABLE 3. — EVALUATION OF PROBE INTERFERENCE

		Calculated boundary layers, ref. 18			Experimental and corrected quantities[a]			% Difference	
x/c		① No interference	② Interference	③ Ratio ①/②	④ C_p, with interference	⑤ Corrected ④ x ③	⑥ C_p, no interference	⑦ (④−⑤)/⑤	⑧ (⑥−⑤)/⑤
0.3	δ^*	0.001517	0.001627	0.9324	0.00181	0.00169	0.00173	7.1	2.4
	θ	0.000893	0.000956	0.9345	0.00101	0.00094	0.00097	7.4	3.2
	H	1.698	1.702	0.9977	1.786	1.782	1.774	0.2	−0.4
	C_f	0.00306	0.00286	1.0676	0.00305	0.00326	0.00320	−6.4	−1.8
0.7	δ^*	0.00261	0.00274	0.9537	0.00315	0.00300	0.00303	5.0	1.0
	θ	0.001617	0.001693	0.9551	0.00190	0.00181	0.00184	5.0	1.7
	H	1.616	1.619	0.9981	1.665	1.662	1.650	0.2	−0.7
	C_f	0.00283	0.00273	1.0362	0.00277	0.00287	0.00288	−3.5	0.3
0.8	δ^*	0.00289	0.00313	0.9237	0.00370	0.00342	0.00346	8.2	1.2
	θ	0.001797	0.001932	0.9301	0.00220	0.00205	0.00210	7.3	2.4
	H	1.610	1.621	0.9932	1.682	1.671	1.645	0.7	−1.6
	C_f	0.00276	0.00255	1.0821	0.00235	0.00254	0.00255	−7.5	0.4
0.9	δ^*	0.00369	0.00368	1.0035	0.00470	0.00472	0.00458	−0.4	−3.0
	θ	0.00225	0.00226	0.9956	0.00267	0.00266	0.00263	0.4	−1.1
	H	1.644	1.631	1.0080	1.759	1.773	1.739	−0.8	−1.9
	C_f	0.00212	0.00222	0.9527	0.00181	0.00172	0.00193	5.2	12.2

[a]Experimental case corresponding to fig. 13(a).

GP11-0232-37

TABLE 4. — BOUNDARY-LAYER AND WAKE INTEGRAL PROPERTIES

Trip - upper, x/c = 0.05, 0.09 mm,
lower, x/c = 0.18, 0.13 mm

$M_\infty = 0.60$, $Re_c = 2 \times 10^6$, $c_l = 0.58$, $\alpha_{geom} = 1.63^\circ$

x/c	C_p	δ^*/c	θ/c	H	C_f	Run
0.299U	−0.498	0.00173	0.00097	1.744	0.00320	16
0.699U	−0.418	0.00303	0.00184	1.650	0.00288	17
0.802U	−0.400	0.00346	0.00210	1.645	0.00255	18
0.899U	−0.286	0.00454	0.00261	1.738	0.00195	19
0.950U	−0.094	0.00689	0.00345	1.994	0.00100	20
1.000U	0.033	0.01154	0.00451	2.561	–	21-1
0.499L	−0.148	0.00159	0.00101	1.569	0.00357	14
0.650L	0.142	0.00349	0.00199	1.756	0.00174	28
0.750L	0.332	0.00762	0.00327	2.326	0.00072	29
1.000L	0.143	0.00442	0.00277	1.595	–	21-2
1.050	0.100	0.01790	0.00881	2.032	–	30
1.099	0.093	0.01552	0.00927	1.676	–	22

GP11-0232-38

Trip - upper, x/c = 0.05, 0.09 mm,
lower, x/c = 0.18, 0.13 mm

$M_\infty = 0.75$, $Re_c = 2 \times 10^6$, $c_l = 0.58$, $\alpha_{geom} = 1.23^\circ$

x/c	C_p	δ^*/c	θ/c	H	C_f	Run
0.300U	−0.457	0.00212	0.00107	1.987	0.00269	23
0.700U	−0.435	0.00350	0.00190	1.840	0.00266	24
0.900U	−0.210	0.00530	0.00273	1.943	0.00161	25
0.999U	0.057	0.01638	0.00498	3.289	–	26-1
0.499L	−0.205	0.00188	0.00103	1.823	0.00338	31
0.650L	0.142	0.00447	0.00216	2.073	0.00135	32
0.750L	0.332	0.00999	0.00412	2.421	0.00040	33
0.999L	0.157	0.00438	0.00280	1.567	–	26-2
1.100	0.093	0.01680	0.00959	1.753	–	27

GP11-0232-82

(a) Blunt trailing edge, 1976.

Trip - upper, x/c = 0.05, 0.10 mm,
lower, x/c = 0.18, 0.13 mm

$M_\infty = 0.60$, $Re_c = 2 \times 10^6$, $c_l = 0.58$, $\alpha_{geom} = 1.4^\circ$

x/c	C_p	δ^*/c	θ/c	H	C_f	Run
1.000U	0.050	0.00866	0.00378	2.291	–	39
0.500L	−0.119	0.00127	0.00081	1.569	0.00382	58
0.910L	0.458	0.00987	0.00455	2.168	–	68
0.985L	0.370	0.00399	0.00264	1.514	0.00284	70
1.000L	0.150	0.00411	0.00220	1.872	–	43
1.000L	0.150	0.00281	0.00187	1.498	–	56
1.050	0.120	0.01611	0.00856	1.882	–	40
1.100	0.113	0.01272	0.00785	1.621	–	41
1.200	0.099	0.00997	0.00695	1.434	–	42
1.500	0.060	0.01024	0.00809	1.265	–	5

GP11-0232-83

(b) Blunt trailing edge, 1977.

TABLE 4. — Continued.

Trip - upper, x/c = 0.05, 0.10 mm,
lower, x/c = 0.18, 0.13 mm

$M_\infty = 0.75$, $Re_c = 2 \times 10^6$, $c_l = 0.58$, $\alpha_{geom} = 1.0^\circ$

x/c	C_p	δ^*/c	θ/c	H	C_f	Run
0.300U	−0.425	0.00195	0.00104	1.886	0.00291	50
0.800U	−0.372	0.00343	0.00198	1.736	0.00286	49
0.950U	−0.013	0.00727	0.00344	2.116	0.00134	48
0.980U	0.050	0.01035	0.00419	2.467	0.00033	54
1.000U	0.090	0.01390	0.00437	3.180	–	47
0.500L	−0.162	0.00141	0.00084	1.680	0.00376	66
0.910L	0.453	0.01185	0.00495	2.396	–	74
0.945L	0.452	0.00821	0.00425	1.932	0.00153	76
0.985L	0.410	0.00528	0.00312	1.691	0.00238	72
1.000L	0.180	0.00389	0.00249	1.562	–	51
1.100	0.123	0.01511	0.00842	1.794	–	52
1.200	0.109	0.01223	0.00807	1.516	–	53
1.500	0.070	0.01071	0.00790	1.355	–	7

GP11-0232-84

Trip - upper, x/c = 0.35, 0.13 mm,
lower, x/c = 0.18, 0.13 mm

$M_\infty = 0.80$, $Re_c = 2 \times 10^6$, $c_l = 0.63$, $\alpha_{geom} = 0.90^\circ$

x/c	C_p	δ^*/c	θ/c	H	C_f	Run
0.300U	−0.882	0.00089	0.00027	3.288	–	104
0.400U	−0.837	0.00101	0.00034	3.027	–	106
0.550U	−0.352	0.00179	0.00080	2.233	0.00344	108
0.650U	−0.405	0.00201	0.00104	1.928	0.00338	112
0.750U	−0.435	0.00230	0.00122	1.882	0.00324	114
0.850U	−0.359	0.00252	0.00142	1.781	0.00313	116
0.900U	−0.217	0.00315	0.00174	1.812	0.00259	118
0.950U	0.005	0.00562	0.00268	2.097	0.00117	120
1.000U	0.115	0.01077	0.00373	2.890	0.00023	102
0.500L	−0.180	0.00147	0.00081	1.813	0.00374	164
0.750L	0.348	0.00948	0.00367	2.585	0.00053	166
0.910L	0.460	0.01381	0.00523	2.641	–	178
0.985L	0.410	0.00626	0.00355	1.766	–	180
1.000L	0.205	0.00409	0.00258	1.585	–	168
1.000L	0.205	0.00397	0.00253	1.569	–	122
1.050	0.150	0.01728	0.00840	2.058	–	125
1.100	0.143	0.01330	0.00785	1.693	–	124
1.200	0.129	0.01040	0.00704	1.477	–	123

GP11-0232-85

(b) Continued.

TABLE 4. — Continued.

Trip - upper, x/c = 0.35, 0.13 mm,
lower, x/c = 0.18, 0.13 mm

$M_\infty = 0.80$, $Re_c = 2 \times 10^6$, $c_l = 0.77$, $\alpha_{geom} = 1.6^o$

x/c	C_p	δ^*/c	θ/c	H	C_f	Run
0.300U	−1.021	0.00082	0.00024	3.485	–	129
0.500U	−0.892	0.00127	0.00060	2.116	0.00359	131
0.650U	−0.316	0.00288	0.00143	2.005	0.00214	133
0.800U	−0.310	0.00325	0.00179	1.812	0.00284	135
0.900U	−0.172	0.00402	0.00205	1.966	0.00240	137
0.950U	0.005	0.00621	0.00295	2.105	0.00127	139
1.000U	0.138	0.01113	0.00408	2.729	0.00025	127
0.300L	−0.082	0.00087	0.00050	1.728	0.00433	172
0.500L	−0.130	0.00133	0.00079	1.691	0.00391	154
0.600L	0.005	0.00219	0.00120	1.828	0.00302	156
0.650L	0.208	0.00326	0.00159	2.049	0.00198	158
0.750L	0.390	0.00850	0.00331	2.567	0.00055	160
0.910L	0.498	0.01244	0.00491	2.534	–	184
0.985L	0.425	0.00524	0.00326	1.660	0.00244	182
1.000L	0.228	0.00406	0.00264	1.540	–	141
1.050	0.170	0.01737	0.00869	1.999	–	142
1.100	0.163	0.01349	0.00797	1.694	–	143
1.200	0.149	0.01177	0.00795	1.481	–	144

GP11-0232-86

Trip - upper, x/c = 0.35, 0.13 mm,
lower, x/c = 0.18, 0.13 mm

$M_\infty = 0.83$, $Re_c = 2 \times 10^6$, $c_l = 0.61$, $\alpha_{geom} = 0.78^o$

x/c	C_p	δ^*/c	θ/c	H	C_f	Run
0.300U	−0.778	0.00101	0.00030	3.344	–	85
0.450U	−0.745	0.00090	0.00045	2.024	0.00376	87
0.700U	−0.430	0.00292	0.00141	2.077	0.00231	89
0.850U	−0.210	0.00371	0.00188	1.969	0.00222	91
0.900U	−0.092	0.00448	0.00217	2.065	0.00180	93
0.950U	0.055	0.00725	0.00308	2.350	0.00078	95
1.000U	0.130	0.01339	0.00416	3.220	–	83
0.500L	−0.198	0.00142	0.00081	1.745	0.00383	146
0.750L	0.347	0.01063	0.00379	2.803	0.00040	148
0.910L	0.452	0.01534	0.00538	2.849	–	176
0.985L	0.430	0.00723	0.00393	1.838	0.00202	174
1.000L	0.220	0.00420	0.00266	1.578	–	150
1.000L	0.220	0.00441	0.00272	1.621	–	97
1.100	0.194	0.01556	0.00873	1.781	–	98
1.200	0.170	0.01344	0.00896	1.500	–	100

GP11-0232-87

(b) Concluded.

TABLE 4. — Continued.

Trip - upper, x/c = 0.05, 0.05 mm,
lower, x/c = 0.18, 0.13 mm

$M_\infty = 0.60$, $Re_c = 4 \times 10^6$, $c_l = 0.58$, $\alpha_{geom} = 2.6^o$

x/c	C_p	δ^*/c	θ/c	H	C_f	Run
0.300U	−0.485	0.00135	0.00066	2.040	0.00331	102
0.500U	−0.417	0.00186	0.00115	1.622	0.00260	104
0.700U	−0.370	0.00270	0.00151	1.792	0.00254	106
0.800U	−0.345	0.00276	0.00173	1.594	0.00252	108
0.900U	−0.175	0.00381	0.00225	1.696	0.00211	110
0.950U	−0.015	0.00605	0.00326	1.854	0.00117	112
1.000U	0.110	0.01069	0.00435	2.460	–	114
0.300L	−0.080	0.00056	0.00038	1.487	0.00442	100
0.500L	−0.155	0.00103	0.00058	1.789	0.00370	88
0.600L	−0.085	0.00117	0.00077	1.525	0.00341	90
0.650L	0.059	0.00214	0.00106	2.012	0.00254	92
0.750L	0.335	0.00502	0.00242	2.073	0.00090	94
0.910L	0.461	0.00725	0.00383	1.892	0.00120	96
1.000L	0.180	0.00288	0.00191	1.505	–	98
1.000L	0.180	0.00271	0.00162	1.674	–	120
1.050	0.130	0.01162	0.00682	1.704	–	115
1.100	0.123	0.00993	0.00645	1.540	–	116
1.200	0.109	0.00885	0.00625	1.416	–	118

GP11-0232-88

Trip - upper, x/c = 0.35, 0.13 mm,
lower, x/c = 0.18, 0.13 mm

$M_\infty = 0.80$, $Re_c = 2 \times 10^6$, $c_l = 0.61$, $\alpha_{geom} = 1.8^o$

x/c	C_p	δ^*/c	θ/c	H	C_f	Run
0.300U	−0.941	0.00070	0.00022	3.228	–	4
0.400U	−0.910	0.00130	0.00052	2.499	0.00337	24
0.450U	−0.904	0.00144	0.00057	2.520	0.00355	6
0.600U	−0.243	0.00303	0.00153	1.984	0.00228	8
0.750U	−0.300	0.00300	0.00162	1.850	0.00300	10
0.850U	−0.195	0.00327	0.00194	1.688	0.00284	12
0.900U	−0.085	0.00430	0.00240	1.787	0.00231	14
0.950U	0.082	0.00663	0.00329	2.017	0.00130	16
1.000U	0.188	0.01133	0.00462	2.454	–	18
0.300L	−0.185	0.00092	0.00053	1.756	0.00418	26
0.500L	−0.235	0.00143	0.00073	1.968	0.00382	28
0.600L	−0.072	0.00176	0.00101	1.743	0.00327	30
0.650L	0.134	0.00306	0.00161	1.899	0.00184	32
0.750L	0.313	0.01086	0.00383	2.840	–	34
0.910L	0.438	0.01662	0.00535	3.106	–	36
1.000L	0.257	0.00535	0.00338	1.584	–	20
1.050	0.231	0.01487	0.00856	1.737	–	21
1.100	0.225	0.01279	0.00798	1.602	–	22
1.200	0.185	0.01124	0.00756	1.486	–	37

GP11-0232-89

(c) Sharp trailing edge, 1977.

TABLE 4. — Continued.

Trip - upper, x/c = 0.35, 0.08 mm,
lower, x/c = 0.18, 0.13 mm

$M_\infty = 0.80$, $Re_c = 3 \times 10^6$, $c_l = 0.71$, $\alpha_{geom} = 2.4^\circ$

x/c	C_p	δ^*/c	θ/c	H	C_f	Run
0.300U	−0.998	0.00079	0.00023	3.527	–	125
0.450U	−0.965	0.00122	0.00041	2.968	0.00354	123
0.650U	−0.242	0.00360	0.00170	2.114	0.00157	127
0.800U	−0.248	0.00311	0.00175	1.780	0.00256	129
0.900U	−0.081	0.00412	0.00233	1.769	0.00228	131
0.950U	−0.005	0.00539	0.00299	1.803	0.00186	133
1.000U	0.197	0.01007	0.00447	2.252	0.00066	135
0.300L	−0.129	0.00099	0.00056	1.768	0.00347	150
0.500L	−0.185	0.00113	0.00061	1.839	0.00374	144
0.600L	−0.055	0.00176	0.00092	1.915	0.00297	146
0.750L	0.350	0.00891	0.00322	2.770	0.00037	148
0.910L	0.483	0.01301	0.00522	2.491	–	142
1.000L	0.250	0.00444	0.00282	1.572	–	137
1.100	0.235	0.01246	0.00781	1.596	–	140
1.200	0.195	0.01053	0.00718	1.467	–	138

GP11-0232-90

(c) Concluded.

Trip - upper, x/c = 0.35, 0.08 mm,
lower, x/c = 0.06, 0.05 mm

$M_\infty = 0.80$, $Re_c = 3 \times 10^6$, $c_l = 0.435$, $\alpha_{geom} = 1.05^\circ$

x/c	C_p	δ^*/c	θ/c	H	C_f	Run
0.500L	−0.295	0.00164	0.00093	1.757	0.00321	40
0.600L	−0.091	0.00226	0.00121	1.870	0.00262	43
0.750L	0.256	0.01332	0.00403	3.302	–	45
0.910L	0.387	0.02057	0.00523	3.933	–	47
1.000L	0.270	0.00625	0.00384	1.627	–	49

GP11-0232-91

Trip - upper, x/c = 0.35, 0.08 mm,
lower, x/c = 0.18, 0.08 mm

$M_\infty = 0.80$, $Re_c = 3 \times 10^6$, $c_l = 0.432$, $\alpha_{geom} = 0.98^\circ$

x/c	C_p	δ^*/c	θ/c	H	C_f	Run
0.500L	−0.298	0.00130	0.00075	1.728	0.00353	52
0.600L	−0.099	0.00228	0.00121	1.879	0.00255	54
0.750L	0.280	0.01425	0.00362	3.936	–	56
0.910L	0.406	0.02480	0.00525	4.724	–	58
1.000L	0.255	0.00817	0.00495	1.650	–	60

GP11-0232-92

(d) Sharp trailing edge, 1977,
boundary-layer trip study.

TABLE 4. — Concluded.

Trip - upper, x/c = 0.35, 0.08 mm,
lower, x/c = 0.35, 0.10 mm

$M_\infty = 0.80$, $Re_c = 3 \times 10^6$, c_l 0.452, $\alpha_{geom} = 0.94^o$

x/c	C_p	δ^*/c	θ/c	H	C_f	Run
0.500L	−0.296	0.00135	0.00078	1.741	0.00341	63
0.600L	−0.120	0.00209	0.00118	1.770	0.00267	65
0.750L	0.322	0.01900	0.00302	6.296	–	67
0.910L	0.450	0.03336	0.00612	5.453	–	69
1.000L	0.245	0.01244	0.00759	1.639	–	71

GP11-0232-93

Trip - upper, x/c = 0.35, 0.08 mm,
lower, x/c = 0.18, 0.13 mm

$M_\infty = 0.80$, $Re_c = 3 \times 10^6$, $c_l = 0.440$, $\alpha_{geom} = 0.99^o$

x/c	C_p	δ^*/c	θ/c	H	C_f	Run
0.500L	−0.301	0.00123	0.00071	1.738	0.00356	74
0.600L	−0.095	0.00169	0.00098	1.724	0.00295	76
0.750L	0.272	0.01131	0.00365	3.098	–	78
0.910L	0.425	0.01752	0.00501	3.498	–	80
1.000L	0.257	0.00520	0.00328	1.582	–	82

GP11-0232-94

(d) Concluded.

TABLE 5. — BOUNDARY-LAYER VELOCITY AND DENSITY PROFILES

X/C = .299U RUN 16			X/C = .699U RUN 17			X/C = .802U RUN 18			X/C = .899U RUN 19			X/C = .950U RUN 20		
z/c	u/u_∞	ρ/ρ_∞	z/c	u/u_∞	ρ/ρ_∞	z/c	u/u_∞	ρ/ρ_∞	z/c	u/u_∞	ρ/ρ_∞	z/c	u/u_∞	ρ/ρ_∞
.0193	1.2399	.9097	.0269	1.2026	.9244	.0275	1.1836	.9264	.0303	1.1367	.9479	.0424	1.0463	.9830
.0159	1.2363	.9091	.0228	1.2016	.9242	.0237	1.1865	.9269	.0257	1.1374	.9480	.0379	1.0463	.9830
.0129	1.2391	.9096	.0202	1.2029	.9244	.0216	1.1888	.9273	.0232	1.1360	.9478	.0350	1.0463	.9830
.0114	1.2383	.9094	.0174	1.1984	.9237	.0194	1.1885	.9272	.0206	1.1331	.9473	.0317	1.0463	.9830
.0098	1.2362	.9091	.0160	1.1920	.9226	.0177	1.1831	.9263	.0188	1.1195	.9452	.0288	1.0463	.9830
.0086	1.2323	.9084	.0143	1.1792	.9206	.0154	1.1611	.9229	.0162	1.0836	.9387	.0264	1.0423	.9824
.0076	1.2176	.9060	.0125	1.1461	.9153	.0135	1.1267	.9175	.0142	1.0441	.9340	.0239	1.0337	.9811
.0066	1.1873	.9011	.0107	1.1018	.9087	.0121	1.1009	.9137	.0124	1.0053	.9286	.0228	1.0340	.9811
.0049	1.1289	.8914	.0094	1.0694	.9040	.0103	1.0623	.9082	.0104	.9563	.9222	.0204	1.0069	.9772
.0035	1.1290	.8921	.0080	1.0248	.8979	.0085	1.0100	.9012	.0093	.9286	.9186	.0184	.9698	.9721
.0049	1.0969	.8875	.0067	.9782	.8919	.0070	.9042	.8954	.0080	.8858	.9138	.0163	.9268	.9664
.0046	1.0756	.8845	.0057	.9526	.8887	.0059	.9290	.8911	.0066	.8416	.9088	.0141	.8785	.9604
.0041	1.0501	.8810	.0049	.9248	.8854	.0048	.8882	.8862	.0052	.7967	.9042	.0125	.8263	.9544
.0037	1.0307	.8785	.0040	.8939	.8819	.0040	.8637	.8838	.0043	.7605	.9006	.0107	.7758	.9489
.0033	1.0097	.8757	.0034	.8759	.8799	.0032	.8345	.8807	.0036	.7237	.8972	.0091	.7306	.9444
.0029	.9721	.8711	.0030	.8531	.8775	.0026	.7995	.8772	.0029	.6886	.8941	.0077	.6728	.9391
.0027	.9467	.8680	.0027	.8346	.8755	.0021	.7681	.8742	.0025	.6714	.8926	.0066	.6347	.9358
.0024	.9362	.8668	.0023	.8207	.8741	.0017	.7384	.8715	.0021	.6412	.8902	.0055	.5845	.9319
.0020	.9148	.8644	.0019	.7861	.8707	.0014	.7153	.8695	.0016	.6105	.8878	.0047	.5468	.9292
.0017	.8815	.8607	.0015	.7716	.8693	.0012	.6984	.8681	.0014	.5824	.8858	.0043	.5295	.9280
.0016	.8734	.8598	.0014	.7495	.8673	.0011	.6536	.8645	.0011	.5621	.8844	.0038	.4979	.9259
.0013	.8441	.8568	.0010	.7280	.8654	.0009	.6383	.8633	.0009	.5353	.8826	.0033	.4037	.9250
.0011	.8123	.8536	.0009	.7148	.8642	.0006	.6054	.8609	.0008	.5165	.8814	.0030	.4510	.9231
.0009	.7855	.8510	.0007	.6627	.8599	.0005	.5932	.8600	.0006	.5086	.8809	.0023	.4094	.9209
.0007	.7622	.8489							.0006	.5008	.8804	.0018	.3792	.9194
												.0014	.3494	.9180
												.0012	.3389	.9176
												.0008	.3250	.9170
												.0006	.3012	.9161

GP11-0232-39

X/C = 1.000U RUN 21-1			X/C = .499L RUN 14			X/C = .650L RUN 28			X/C - .750L RUN 29			X/C = 1.000L RUN 21-2		
z/c	u/u_∞	ρ/ρ_∞	z/c	u/u_∞	ρ/ρ_∞	z/c	u/u_∞	ρ/ρ_∞	z/c	u/u_∞	ρ/ρ_∞	z/c	u/u_∞	ρ/ρ_∞
.0426	.9802	1.0055	.0201	1.0779	.9742	.0223	.9136	1.0238	.0278	.8166	1.0583	.0391	.9110	1.0236
.0366	.9788	1.0053	.0172	1.0777	.9742	.0191	.9134	1.0238	.0246	.8134	1.0579	.0338	.9114	1.0236
.0328	.9833	1.0060	.0134	1.0781	.9743	.0169	.9145	1.0240	.0225	.8141	1.0580	.0289	.9176	1.0245
.0313	.9814	1.0057	.0114	1.0770	.9741	.0146	.9108	1.0235	.0205	.8101	1.0575	.0254	.9139	1.0240
.0293	.9669	1.0036	.0095	1.0659	.9724	.0126	.8954	1.0214	.0187	.7940	1.0556	.0232	.9114	1.0236
.0277	.9509	1.0014	.0077	1.0464	.9695	.0110	.8693	1.0181	.0173	.7688	1.0527	.0213	.9034	1.0226
.0249	.9190	.9971	.0066	1.0146	.9650	.0096	.8295	1.0132	.0159	.7329	1.0487	.0193	.8866	1.0204
.0224	.8696	.9909	.0048	.9509	.9564	.0079	.7673	1.0061	.0141	.6839	1.0437	.0164	.8239	1.0163
.0202	.8202	.9850	.0037	.9056	.9507	.0063	.7075	.9998	.0125	.6241	1.0380	.0178	.8702	1.0183
.0178	.7654	.9790	.0030	.8724	.9468	.0056	.6764	.9968	.0114	.5787	1.0341	.0149	.8390	1.0145
.0157	.6986	.9723	.0027	.8573	.9450	.0046	.6215	.9919	.0102	.5383	1.0309	.0126	.8014	1.0101
.0132	.6736	.9648	.0022	.8306	.9421	.0038	.5829	.9887	.0096	.5098	1.0288	.0106	.7652	1.0060
.0105	.5164	.9575	.0017	.8073	.9395	.0035	.5603	.9869	.0077	.4426	1.0244	.0092	.7505	1.0045
.0080	.4119	.9511	.0015	.7845	.9372	.0034	.5436	.9856	.0064	.3833	1.0210	.0078	.7332	1.0027
.0067	.3405	.9476	.0013	.7631	.9350	.0027	.5170	.9837	.0057	.3546	1.0195	.0067	.7117	1.0005
.0059	.3420	.9477	.0011	.7445	.9332	.0025	.4991	.9825	.0042	.2966	1.0169	.0057	.7035	.9987
.0051	.2821	.9453	.0009	.7384	.9326	.0021	.4623	.9801	.0029	.2440	1.0149	.0049	.7016	.9989
.0047	.2670	.9448	.0007	.7118	.9301	.0019	.4549	.9796	.0016	.2128	1.0140	.0044	.6883	.9982
.0040	.2305	.9436	.0006	.6927	.9284	.0018	.4532	.9795	.0014	.2185	1.0141	.0039	.6879	.9982
.0037	.2372	.9437	.0005	.6744	.9268	.0016	.4351	.9785	.0011	.1841	1.0132	.0033	.6915	.9985
.0028	.2084	.9430				.0015	.4311	.9782				.0029	.6809	.9984
.0018	.1809	.9423				.0013	.4106	.9771				.0026	.6823	.9976
.0011	.1579	.9418				.0013	.4148	.9773				.0023	.6773	.9972
						.0010	.3883	.9759				.0021	.6709	.9966
						.0006	.3638	.9746				.0019	.6783	.9973
						.0005	.3638	.9746				.0015	.6723	.9967
												.0010	.6627	.9958
												.0008	.6330	.9932
												.0008	.5867	.9893
												.0005	.3126	.9728

GP11-0232-47

TABLE 5. — Continued.

X/C = 1.050 RUN 30			X/C = 1.099 RUN 22			X/C =.300U RUN 23			X/C = .700U RUN 24			X/C = .900U RUN 25		
z/c	u/u_∞	ρ/ρ_∞	z/c	u/u_∞	ρ/ρ_∞	z/c	u/u_∞	ρ/ρ_∞	z/c	u/u_∞	ρ/ρ_∞	z/c	u/u_∞	ρ/ρ_∞
.0342	.9489	1.0179	.0297	.9360	1.0144	.0139	1.2157	.8655	.0264	1.2076	.8738	.0317	1.1010	.9401
.0297	.9492	1.0179	.0231	.9342	1.0141	.0115	1.2149	.8653	.0235	1.2085	.8740	.0270	1.1005	.9400
.0291	.9481	1.0178	.0188	.9368	1.0145	.0100	1.2156	.8655	.0215	1.2066	.8735	.0250	1.1029	.9405
.0228	.9458	1.0175	.0159	.9351	1.0143	.0090	1.2150	.8654	.0185	1.2060	.8734	.0231	1.1005	.9400
.0199	.9360	1.0161	.0135	.9345	1.0142	.0084	1.2085	.8637	.0179	1.2013	.8722	.0214	1.0979	.9389
.0167	.9059	1.0121	.0110	.9147	1.0115	.0081	1.2066	.8632	.0162	1.1863	.8685	.0190	1.0937	.9360
.0140	.8623	1.0066	.0088	.8706	1.0059	.0078	1.2079	.8636	.0145	1.1685	.8643	.0166	1.0375	.9297
.0113	.8124	1.0007	.0070	.8451	1.0028	.0074	1.1885	.8588	.0128	1.1413	.8579	.0151	1.0147	.9212
.0090	.7605	.9950	.0055	.8204	.9999	.0070	1.1819	.8572	.0111	1.1075	.8504	.0135	.9844	.9146
.0065	.6947	.9884	.0035	.7824	.9956	.0063	1.1409	.8476	.0093	1.0668	.8418	.0119	.9464	.9072
.0042	.6278	.9824	.0018	.7366	.9908	.0057	1.1135	.8415	.0080	1.0227	.8330	.0101	.8967	.8981
.0018	.5590	.9768	.0001	.6869	.9859	.0052	1.0873	.8359	.0066	.9880	.8263	.0085	.8472	.8896
.0001	.5061	.9731	-.0018	.6339	.9812	.0047	1.0366	.8256	.0056	.9578	.8211	.0069	.8017	.8825
-.0019	.4387	.9689	-.0035	.6053	.9788	.0043	.9804	.8150	.0049	.9268	.8158	.0057	.7477	.8746
-.0036	.3810	.9658	-.0041	.5854	.9772	.0038	.9629	.8119	.0041	.9004	.8114	.0045	.6998	.8682
-.0043	.3750	.9655	-.0048	.5704	.9760	.0034	.9337	.8069	.0036	.8760	.8076	.0036	.6349	.8626
-.0056	.3419	.9648	-.0054	.5436	.9740	.0029	.8785	.7980	.0030	.8463	.8031	.0030	.6209	.8587
-.0060	.3386	.9638	-.0074	.5217	.9729	.0026	.8599	.7951	.0026	.8310	.8008	.0024	.5917	.8555
-.0077	.2939	.9619	-.0082	.5118	.9718	.0023	.8301	.7907	.0022	.8073	.7975	.0021	.6019	.8566
-.0079	.2948	.9620	-.0093	.4982	.9709	.0019	.7878	.7848	.0019	.7948	.7959	.0017	.5477	.8511
-.0100	.2965	.9620	-.0102	.4965	.9708	.0019	.8124	.7882	.0015	.7854	.7958	.0015	.5119	.8477
-.0122	.3482	.9642	-.0113	.4852	.9700	.0016	.7775	.7835	.0014	.7461	.7893	.0012	.4887	.8457
-.0150	.4777	.9712	-.0127	.4922	.9705	.0014	.7756	.7832	.0012	.7149	.7855	.0009	.4709	.8449
-.0173	.5938	.9795	-.0136	.4852	.9700	.0013	.7438	.7791	.0009	.6751	.7809	.0008	.4531	.8428
-.0197	.6937	.9883	-.0146	.5041	.9713	.0012	.7492	.7798	.0008	.6697	.7803	.0006	.4399	.8418
-.0218	.7475	.9936	-.0150	.5075	.9715	.0011	.6816	.7717	.0006	.6492	.7781			
-.0247	.7982	.9991	-.0163	.5194	.9723	.0009	.7034	.7743						
-.0282	.8414	1.0041	-.0172	.5418	.9739									
-.0310	.8786	1.0086	-.0179	.5498	.9745									
-.0345	.9154	1.0134	-.0196	.5817	.9769									
-.0380	.9385	1.0165	-.0208	.6049	.9788									
-.0415	.9464	1.0176	-.0224	.6723	.9864									
-.0453	.9500	1.0181	-.0299	.7868	.9972									
			-.0339	.8560	1.0041									
			-.0357	.8766	1.0067									
			-.0373	.8949	1.0090									
			-.0394	.9111	1.0111									
			-.0410	.9253	1.0129									
			-.0427	.9347	1.0142									
			-.0444	.9422	1.0152									
			-.0473	.9471	1.0159									
			-.0524	.9555	1.0171									
			-.0588	.9561	1.0171									

GP11-0232-48

X/C = .999U RUN 26-1			X/C = .499L RUN 31			X/C - .650L RUN 32			X/C = .750L RUN 33			X/C = .999L RUN 26-2		
z/c	u/u_∞	ρ/ρ_∞	z/c	u/u_∞	ρ/ρ_∞	z/c	u/u_∞	ρ/ρ_∞	z/c	u/u_∞	ρ/ρ_∞	z/c	u/u_∞	ρ/ρ_∞
.0452	.9589	1.0133	.0162	1.0973	.9406	.0250	.9220	1.0383	.0322	.8206	1.0904	.0388	.9200	1.0438
.0420	.9636	1.0143	.0141	1.1009	.9414	.0218	.9210	1.0381	.0283	.8226	1.0908	.0318	.9193	1.0436
.0396	.9611	1.0137	.0136	1.1008	.9414	.0214	.9231	1.0383	.0250	.8211	1.0905	.0279	.9190	1.0436
.0369	.9528	1.0120	.0118	1.0987	.9409	.0193	.9207	1.0380	.0239	.8174	1.0898	.0254	.9103	1.0417
.0345	.9473	1.0108	.0098	1.0925	.9394	.0172	.9206	1.0380	.0219	.7992	1.0863	.0229	.8993	1.0395
.0318	.9220	1.0055	.0081	1.0657	.9332	.0154	.9166	1.0372	.0202	.7617	1.0795	.0200	.8818	1.0359
.0292	.8833	.9978	.0071	1.0392	.9272	.0135	.8976	1.0332	.0180	.7059	1.0701	.0173	.8580	1.0312
.0263	.8236	.9867	.0059	1.0019	.9192	.0117	.8618	1.0262	.0158	.6286	1.0585	.0152	.8260	1.0252
.0231	.7447	.9736	.0049	.9664	.9120	.0103	.8194	1.0182	.0154	.6117	1.0562	.0126	.7787	1.0168
.0204	.6626	.9618	.0039	.9279	.9046	.0084	.7531	1.0069	.0132	.5271	1.0457	.0104	.7485	1.0118
.0175	.5705	.9503	.0031	.8854	.8969	.0068	.6912	.9973	.0109	.4313	1.0358	.0083	.7286	1.0086
.0149	.4763	.9406	.0021	.8335	.8882	.0058	.6446	.9908	.0088	.3464	1.0288	.0070	.7049	1.0049
.0126	.3863	.9331	.0018	.8090	.8843	.0048	.5949	.9844	.0070	.2884	1.0249	.0057	.6943	1.0034
.0106	.3050	.9278	.0015	.7812	.8801	.0041	.5521	.9794	.0050	.2252	1.0216	.0048	.6876	1.0024
.0084	.2336	.9242	.0013	.7609	.8771	.0033	.4951	.9733	.0033	.1863	1.0199	.0040	.6739	1.0004
.0067	.1782	.9220	.0011	.7400	.8741	.0027	.4470	.9688	.0019	.1476	1.0186	.0034	.6704	.9999
.0050	.1307	.9206	.0008	.7132	.8705	.0022	.4168	.9662	.0018	.1535	1.0188	.0027	.6628	.9988
.0037	.1072	.9201				.0016	.3857	.9637				.0020	.6559	.9979
.0020	.1034	.9200				.0013	.3683	.9624				.0018	.6517	.9987
.0013	.1015	.9200				.0011	.3440	.9607				.0011	.6607	.9985
.0007	.1252	.9208				.0007	.3331	.9600				.0007	.6339	.9949
												.0005	.5626	.9860

GP11-0232-49

TABLE 5. — Continued.

X/C = 1.100 RUN 27		
z/c	u/u_∞	ρ/ρ_∞
.0643	.9476	1.0250
.0598	.9511	1.0257
.0547	.9475	1.0250
.0510	.9456	1.0245
.0475	.9479	1.0250
.0434	.9376	1.0228
.0395	.9215	1.0194
.0363	.8856	1.0121
.0333	.8628	1.0077
.0304	.8330	1.0021
.0268	.7832	.9934
.0235	.7303	.9848
.0207	.6739	.9765
.0170	.6059	.9676
.0141	.5542	.9615
.0122	.5288	.9587
.0091	.4957	.9553
.0062	.4978	.9555
.0034	.5191	.9577
.0007	.5367	.9617
-.0018	.6079	.9678
-.0054	.6972	.9799
-.0080	.7405	.9878
-.0108	.8084	.9977
-.0139	.8742	1.0099
-.0174	.9142	1.0179
-.0197	.9291	1.0210
-.0239	.9401	1.0234
-.0292	.9412	1.0236
-.0324	.9342	1.0221
-.0382	.9343	1.0221

GP11-0232-50

X/C = 1.000U RUN 39			X/C = .500L RUN 58			X/C = .910L RUN 68			X/C = .985L RUN 70			X/C = 1.000L RUN 43		
z/c	u/u_∞	ρ/ρ_∞	z/c	u/u_∞	ρ/ρ_∞	z/c	u/u_∞	ρ/ρ_∞	z/c	u/u_∞	ρ/ρ_∞	z/c	u/u_∞	ρ/ρ_∞
.0418	.9714	1.0086	.0175	1.0487	.9771	.0410	.7478	1.0803	.0478	.7967	1.0650	.0510	.9195	1.0262
.0385	.9718	1.0087	.0133	1.0485	.9771	.0368	.7469	1.0802	.0349	.7988	1.0653	.0332	.9189	1.0261
.0347	.9708	1.0086	.0106	1.0483	.9770	.0318	.7480	1.0803	.0281	.8010	1.0655	.0289	.9197	1.0262
.0319	.9706	1.0085	.0090	1.0473	.9769	.0301	.7449	1.0800	.0244	.8010	1.0655	.0268	.9180	1.0260
.0295	.9732	1.0089	.0080	1.0433	.9763	.0284	.7476	1.0803	.0229	.8003	1.0654	.0246	.9184	1.0261
.0274	.9669	1.0080	.0073	1.0329	.9748	.0268	.7446	1.0800	.0218	.8010	1.0655	.0230	.9144	1.0255
.0254	.9595	1.0070	.0063	1.0168	.9725	.0251	.7316	1.0785	.0205	.7964	1.0650	.0205	.9089	1.0248
.0241	.9481	1.0054	.0054	.9913	.9689	.0226	.7133	1.0765	.0193	.7957	1.0649	.0190	.8960	1.0231
.0222	.9212	1.0017	.0044	.9590	.9646	.0217	.6786	1.0730	.0178	.7711	1.0620	.0175	.8860	1.0218
.0208	.8965	.9985	.0036	.9195	.9595	.0184	.6535	1.0705	.0170	.7834	1.0635	.0156	.8640	1.0191
.0189	.8650	.9945	.0029	.8843	.9552	.0192	.6220	1.0676	.0156	.7478	1.0594	.0136	.8309	1.0151
.0173	.8239	.9895	.0024	.8614	.9525	.0171	.5952	1.0652	.0150	.7597	1.0607	.0121	.8178	1.0130
.0162	.7944	.9862	.0023	.8442	.9506	.0163	.5504	1.0615	.0133	.7350	1.0580	.0112	.7899	1.0113
.0147	.7579	.9822	.0019	.8229	.9482	.0147	.5210	1.0593	.0123	.6826	1.0526	.0099	.7799	1.0093
.0130	.7126	.9776	.0017	.8031	.9460	.0137	.4892	1.0570	.0118	.7120	1.0556	.0084	.7556	1.0067
.0112	.6519	.9719	.0015	.7917	.9448	.0118	.4480	1.0542	.0106	.6856	1.0529	.0074	.7447	1.0055
.0097	.6006	.9675	.0013	.7620	.9418	.0093	.3969	1.0511	.0097	.6380	1.0483	.0062	.7305	1.0041
.0077	.5219	.9616	.0011	.7490	.9405	.0079	.3026	1.0493	.0091	.6495	1.0494	.0054	.7132	1.0023
.0062	.4674	.9580	.0009	.7339	.9390	.0065	.3150	1.0470	.0079	.6275	1.0474	.0040	.7030	1.0013
.0045	.3806	.9531	.0007	.7162	.9373	.0050	.2966	1.0462	.0067	.6031	1.0452	.0032	.6936	1.0004
.0033	.3343	.9510	.0006	.6792	.9340	.0036	.2671	1.0451	.0066	.6024	1.0455	.0024	.6783	.9990
.0023	.3079	.9499	.0005	.6546	.9319	.0026	.2591	1.0448	.0054	.5856	1.0437	.0019	.6678	.9980
.0015	.2771	.9487				.0017	.2576	1.0447	.0038	.5466	1.0406	.0015	.6528	.9966
						.0006	.2296	1.0438	.0036	.5490	1.0408	.0014	.6241	.9941
									.0024	.5310	1.0394	.0012	.5620	.9891
									.0023	.5258	1.0390	.0010	.3574	.9766
									.0016	.5194	1.0385	.0007	0.0000	.9683
									.0008	.5074	1.0376	.0005	0.0000	.9683

GP11-0232-51

TABLE 5. — Continued.

X/C = 1.000L RUN 56			X/C = 1.050 RUN 40			X/C = 1.100 RUN 41			X/C = 1.200 RUN 42			X/C = 1.500 RUN 5		
z/c	u/u_∞	ρ/ρ_∞	z/c	u/u_∞	ρ/ρ_∞	z/c	u/u_∞	ρ/ρ_∞	z/c	u/u_∞	ρ/ρ_∞	z/c	u/u_∞	ρ/ρ_∞
.0295	.9250	1.0272	.0496	.9365	1.0215	.0735	.9418	1.0201	.0470	.9452	1.0171	.0624	.9609	1.0097
.0250	.9252	1.0272	.0289	.9384	1.0218	.0265	.9413	1.0200	.0178	.9446	1.0171	.0325	.9611	1.0097
.0218	.9215	1.0267	.0261	.9375	1.0217	.0224	.9396	1.0198	.0137	.9448	1.0171	.0160	.9601	1.0096
.0202	.9174	1.0262	.0231	.9369	1.0216	.0177	.9411	1.0200	.0098	.9437	1.0169	.0059	.9607	1.0096
.0187	.9145	1.0258	.0203	.9392	1.0219	.0136	.9388	1.0197	.0059	.9382	1.0162	.0006	.9591	1.0094
.0171	.9039	1.0244	.0182	.9329	1.0210	.0103	.9238	1.0177	.0023	.9192	1.0136	-.0099	.9584	1.0093
.0157	.8931	1.0230	.0159	.9179	1.0189	.0070	.8901	1.0133	-.0007	.8900	1.0098	-.0135	.9566	1.0091
.0132	.8646	1.0193	.0138	.8946	1.0159	.0037	.8331	1.0063	-.0035	.8337	1.0056	-.0177	.9537	1.0087
.0113	.8347	1.0157	.0115	.8614	1.0116	.0009	.7717	.9994	-.0047	.8304	1.0033	-.0221	.9449	1.0074
.0086	.7975	1.0113	.0081	.8154	1.0061	-.0022	.6996	.9920	-.0075	.7880	.9988	-.0269	.9312	1.0056
.0072	.7706	1.0083	.0081	.7905	1.0032	-.0054	.6238	.9852	-.0112	.7407	.9927	-.0321	.9116	1.0030
.0060	.7543	1.0066	.0055	.7205	.9957	-.0079	.5626	.9803	-.0145	.6908	.9878	-.0370	.8849	.9995
.0048	.7366	1.0047	.0031	.6632	.9901	-.0103	.5262	.9776	-.0186	.6763	.9864	-.0410	.8644	.9969
.0040	.7237	1.0036	.0007	.5952	.9842	-.0129	.5020	.9774	-.0191	.6608	.9850	-.0467	.8312	.9927
.0031	.7118	1.0022	.0003	.5620	.9816	-.0152	.5276	.9777	-.0223	.6562	.9846	-.0468	.8323	.9931
.0023	.7023	1.0013	-.0017	.5049	.9774	-.0180	.5570	.9799	-.0260	.6692	.9858	-.0534	.7931	.9887
.0017	.6962	1.0007	-.0027	.4957	.9768	-.0202	.6097	.9840	-.0298	.7131	.9889	-.0569	.7958	.9889
.0012	.6871	.9998	-.0063	.3693	.9695	-.0226	.6601	.9884	-.0319	.7361	.9922	-.0623	.7892	.9881
.0009	.6802	.9991	-.0068	.3799	.9700	-.0252	.7188	.9939	-.0356	.7889	.9978	-.0687	.8029	.9897
.0007	.6677	.9980	-.0087	.3576	.9684	-.0272	.7602	.9981	-.0391	.8385	1.0035	-.0745	.8264	.9924
.0004	.6098	.9929	-.0106	.3534	.9687	-.0296	.7969	1.0021	-.0424	.8778	1.0083	-.0802	.8576	.9961
			-.0115	.3713	.9696	-.0312	.8243	1.0053	-.0466	.9117	1.0126	-.0849	.8830	.9993
			-.0137	.4345	.9730	-.0344	.8688	1.0106	-.0494	.9302	1.0151	-.0907	.9136	1.0032
			-.0151	.5010	.9772	-.0379	.9032	1.0150	-.0539	.9401	1.0164	-.0981	.9301	1.0057
			-.0172	.6042	.9850	-.0426	.9286	1.0183	-.0584	.9440	1.0170	-.1119	.9500	1.0093
			-.0195	.6853	.9922	-.0470	.9356	1.0193	-.0631	.9440	1.0170	-.1120	.9617	1.0098
			-.0207	.7187	.9955	-.0517	.9353	1.0192	-.0680	.9452	1.0171	-.1205	.9589	1.0094
			-.0227	.7670	1.0006	-.0564	.9360	1.0193				-.1304	.9615	1.0098
			-.0244	.7918	1.0033							-.1430	.9603	1.0096
			-.0263	.8154	1.0061									
			-.0296	.8583	1.0112									
			-.0324	.8894	1.0152									
			-.0361	.9148	1.0186									
			-.0391	.9246	1.0199									
			-.0432	.9301	1.0207									
			-.0474	.9288	1.0205									

GP11-0232-52

X/C = .300U RUN 50			X/C = .800U RUN 49			X/C = .950U RUN 48			X/C = .980U RUN 54			X/C = 1.000U RUN 47		
z/c	u/u_∞	ρ/ρ_∞	z/c	u/u_∞	ρ/ρ_∞	z/c	u/u_∞	ρ/ρ_∞	z/c	u/u_∞	ρ/ρ_∞	z/c	u/u_∞	ρ/ρ_∞
.0176	1.2019	.8765	.0334	1.1743	.8921	.0425	.9991	.9947	.0634	.9662	1.0121	.0518	.9468	1.0235
.0130	1.2032	.8768	.0329	1.1753	.8924	.0331	1.0015	.9953	.0423	.9684	1.0126	.0512	.9548	1.0252
.0114	1.2027	.8767	.0246	1.1763	.8926	.0300	1.0024	.9955	.0394	.9684	1.0126	.0453	.9488	1.0240
.0099	1.2027	.8767	.0226	1.1752	.8924	.0273	1.0013	.9952	.0368	.9696	1.0129	.0414	.9491	1.0240
.0088	1.1962	.8758	.0200	1.1746	.8922	.0250	.9997	.9949	.0335	.9709	1.0132	.0391	.9516	1.0245
.0077	1.1862	.8726	.0179	1.1655	.8900	.0230	.9859	.9918	.0315	.9701	1.0130	.0380	.9534	1.0250
.0072	1.1690	.8685	.0162	1.1509	.8865	.0206	.9595	.9862	.0292	.9670	1.0123	.0364	.9518	1.0246
.0066	1.1442	.8627	.0143	1.1277	.8811	.0189	.9403	.9822	.0275	.9581	1.0104	.0340	.9497	1.0241
.0063	1.1266	.8587	.0129	1.1038	.8751	.0176	.9080	.9760	.0254	.9425	1.0070	.0314	.9384	1.0211
.0058	1.1000	.8528	.0115	1.0739	.8662	.0158	.8733	.9692	.0236	.9145	1.0013	.0287	.9148	1.0148
.0053	1.0720	.8469	.0102	1.0513	.8645	.0144	.8432	.9638	.0222	.8913	.9966	.0269	.8879	1.0114
.0049	1.0530	.8430	.0093	1.0317	.8605	.0131	.8097	.9581	.0207	.8658	.9917	.0244	.8450	1.0032
.0044	1.0129	.8341	.0081	1.0020	.8533	.0118	.7786	.9530	.0193	.8340	.9859	.0228	.8134	.9975
.0039	.9854	.8269	.0071	.9792	.8504	.0108	.7459	.9480	.0179	.8020	.9803	.0211	.7752	.9909
.0036	.9558	.8246	.0060	.9502	.8491	.0096	.7117	.9430	.0164	.7669	.9745	.0192	.7227	.9826
.0034	.9378	.8215	.0054	.9288	.8414	.0084	.6719	.9375	.0151	.7291	.9686	.0171	.6662	.9745
.0030	.9175	.8181	.0045	.9010	.8347	.0074	.6317	.9324	.0134	.6777	.9611	.0151	.6034	.9663
.0026	.8780	.8117	.0038	.8762	.8327	.0061	.5769	.9260	.0121	.6352	.9544	.0138	.5575	.9609
.0024	.8711	.8107	.0032	.8562	.8295	.0051	.5346	.9215	.0107	.5886	.9497	.0121	.4964	.9545
.0021	.8481	.8072	.0028	.8361	.8265	.0042	.4825	.9165	.0092	.5232	.9425	.0106	.4385	.9492
.0019	.8330	.8049	.0023	.8082	.8224	.0041	.4836	.9167	.0080	.4834	.9386	.0094	.3788	.9444
.0017	.8257	.8039	.0019	.7923	.8201	.0029	.4156	.9108	.0073	.4507	.9356	.0078	.3210	.9405
.0014	.7900	.7980	.0015	.7750	.8178	.0023	.3808	.9083	.0062	.4045	.9318	.0065	.2607	.9372
.0012	.7691	.7961	.0011	.7500	.8144	.0016	.3408	.9056	.0055	.3702	.9293	.0055	.2126	.9350
.0010	.7598	.7949	.0010	.7347	.8125	.0013	.3254	.9047	.0047	.3352	.9269	.0043	.1579	.9331
.0009	.7435	.7928	.0008	.7251	.8113	.0010	.3033	.9034	.0038	.2914	.9243	.0033	.1075	.9318
.0006	.7289	.7910	.0006	.7087	.8092	.0007	.2780	.9020	.0030	.2517	.9223	.0026	0.0000	.9307
.0005	.7164	.7894	.0005	.6968	.8078	.0005	.2562	.9010	.0025	.2272	.9212	.0017	0.0000	.9307
.0004	.7087	.7885							.0021	.2085	.9204	.0010	0.0000	.9307
									.0017	.1955	.9199	.0008	0.0000	.9307
									.0016	.1904	.9198	.0005	0.0000	.9307
									.0014	.1797	.9194	.0004	0.0000	.9307
									.0012	.1730	.9192			
									.0010	.1611	.9188			
									.0007	.1482	.9184			
									.0006	.1385	.9182			

GP11-0232-53

TABLE 5. — Continued.

X/C = .500L RUN 66			X/C = .910L RUN 74			X/C = .945L RUN 76			X/C = .985L RUN 72			X/C = 1.000L RUN 51		
z/c	u/u_∞	ρ/ρ_∞	z/c	u/u_∞	ρ/ρ_∞	z/c	u/u_∞	ρ/ρ_∞	z/c	u/u_∞	ρ/ρ_∞	z/c	u/u_∞	ρ/ρ_∞
.0169	1.0791	.9536	.0477	.7566	1.1246	.0477	.7575	1.1238	.0419	.7793	1.1120	.0409	.9013	1.0487
.0134	1.0791	.9536	.0413	.7572	1.1247	.0401	.7566	1.1230	.0359	.7799	1.1121	.0326	.9028	1.0490
.0112	1.0791	.9538	.0368	.7572	1.1247	.0367	.7573	1.1237	.0317	.7820	1.1125	.0282	.8999	1.0484
.0101	1.0792	.9536	.0333	.7537	1.1244	.0322	.7577	1.1238	.0284	.7814	1.1124	.0264	.8993	1.0483
.0089	1.0788	.9535	.0260	.7451	1.1232	.0288	.7543	1.1232	.0260	.7808	1.1123	.0246	.8973	1.0479
.0081	1.0718	.9519	.0262	.7220	1.1185	.0251	.7416	1.1209	.0236	.7758	1.1114	.0223	.8910	1.0466
.0078	1.0685	.9511	.0240	.6667	1.1130	.0224	.7212	1.1173	.0209	.7657	1.1095	.0204	.8831	1.0450
.0069	1.0502	.9460	.0226	.6632	1.1088	.0209	.6948	1.1129	.0186	.7452	1.1058	.0172	.8552	1.0395
.0062	1.0303	.9424	.0207	.6105	1.1009	.0194	.6639	1.1080	.0166	.7174	1.1011	.0140	.8134	1.0320
.0057	1.0134	.9387	.0188	.5612	1.0943	.0176	.6338	1.1034	.0148	.6922	1.0969	.0117	.7833	1.0263
.0049	.9825	.9343	.0174	.5307	1.0905	.0160	.6085	1.0984	.0133	.6657	1.0927	.0098	.7562	1.0217
.0043	.9624	.9281	.0157	.4736	1.0840	.0146	.5720	1.0948	.0114	.6285	1.0872	.0082	.7358	1.0183
.0034	.9305	.9219	.0142	.4454	1.0811	.0132	.5431	1.0912	.0101	.6023	1.0835	.0068	.7162	1.0152
.0027	.8808	.9145	.0124	.3932	1.0762	.0114	.5044	1.0866	.0091	.5837	1.0810	.0058	.7036	1.0133
.0022	.8577	.9087	.0107	.3599	1.0734	.0096	.4770	1.0836	.0081	.5684	1.0791	.0049	.6940	1.0119
.0018	.8326	.9045	.0086	.3191	1.0704	.0085	.4522	1.0810	.0069	.5388	1.0754	.0040	.6865	1.0108
.0015	.8269	.9036	.0067	.2839	1.0681	.0070	.4162	1.0775	.0059	.5246	1.0737	.0030	.6754	1.0091
.0012	.8028	.8997	.0049	.2492	1.0661	.0057	.3790	1.0743	.0049	.5106	1.0721	.0023	.6673	1.0080
.0011	.7862	.8971	.0038	.2412	1.0656	.0048	.3816	1.0743	.0041	.4990	1.0708	.0020	.6607	1.0070
.0008	.7648	.8939	.0026	.2251	1.0648	.0033	.3596	1.0727	.0034	.4859	1.0694	.0015	.6473	1.0052
.0006	.7397	.8903	.0015	.2160	1.0645	.0023	.3434	1.0715	.0027	.4763	1.0683	.0012	.6433	1.0046
.0005	.7079	.8859	.0006	.2115	1.0642	.0014	.3431	1.0714	.0018	.4629	1.0669	.0009	.6334	1.0036
						.0008	.3174	1.0696	.0011	.4563	1.0663	.0008	.6202	1.0015
									.0007	.4426	1.0649	.0005	.5409	.9919

GP11-0232-54

X/C = 1.100 RUN 52			X/C = 1.200 RUN 53			X/C = 1.500 RUN 7			X/C = .300U RUN 104			X/C = .400U RUN 106		
z/c	u/u_∞	ρ/ρ_∞	z/c	u/u_∞	ρ/ρ_∞	z/c	u/u_∞	ρ/ρ_∞	z/c	u/u_∞	ρ/ρ_∞	z/c	u/u_∞	ρ/ρ_∞
.0370	.9266	1.0320	.0581	.9321	1.0277	.0647	.9515	1.0171	.0069	1.4230	.6979	.0131	1.4012	.7137
.0344	.9287	1.0325	.0323	.9336	1.0280	.0395	.9495	1.0166	.0059	1.4232	.6980	.0103	1.4021	.7140
.0297	.9307	1.0329	.0270	.9342	1.0281	.0215	.9492	1.0166	.0052	1.4228	.6979	.0095	1.4022	.7141
.0255	.9311	1.0330	.0227	.9340	1.0281	.0145	.9482	1.0163	.0048	1.4226	.6978	.0080	1.4012	.7137
.0220	.9298	1.0327	.0203	.9333	1.0279	.0080	.9464	1.0159	.0044	1.4220	.6979	.0074	1.4021	.7140
.0192	.9206	1.0307	.0163	.9296	1.0271	.0032	.9433	1.0153	.0040	1.4216	.6975	.0063	1.4010	.7137
.0171	.9038	1.0273	.0125	.9147	1.0240	-.0003	.9378	1.0141	.0036	1.4200	.6971	.0055	1.3999	.7134
.0150	.8813	1.0227	.0095	.8889	1.0188	-.0032	.9282	1.0120	.0033	1.4206	.6972	.0047	1.3964	.7124
.0123	.8334	1.0136	.0059	.8525	1.0118	-.0103	.9153	1.0093	.0030	1.4196	.6969	.0042	1.3953	.7118
.0102	.7918	1.0062	.0031	.8115	1.0043	-.0174	.8887	1.0039	.0028	1.4196	.6970	.0038	1.3852	.7091
.0082	.7505	.9993	-.0002	.7644	.9963	-.0234	.8572	.9978	.0026	1.4166	.6961	.0034	1.3747	.7062
.0062	.7052	.9923	-.0029	.7235	.9899	-.0294	.8342	.9939	.0024	1.4092	.6940	.0031	1.3697	.7048
.0041	.6363	.9833	-.0061	.6839	.9840	-.0364	.8052	.9883	.0022	1.3948	.6900	.0028	1.3473	.6987
.0023	.6080	.9790	-.0087	.6616	.9800	-.0417	.7932	.9862	.0019	1.3613	.6809	.0025	1.3428	.6975
.0004	.5665	.9740	-.0111	.6473	.9790	-.0465	.7919	.9859	.0018	1.3216	.6706	.0023	1.3017	.6869
-.0014	.5286	.9698	-.0120	.6468	.9789	-.0516	.7962	.9872	.0015	1.2817	.6609	.0020	1.2574	.6761
-.0036	.4954	.9664	-.0149	.6420	.9783	-.0558	.8086	.9888	.0014	1.1846	.6397	.0017	1.1856	.6601
-.0059	.4785	.9647	-.0182	.6518	.9796	-.0617	.8306	.9928	.0011	1.0526	.6153	.0014	1.1081	.6447
-.0084	.4733	.9643	-.0209	.6710	.9822	-.0662	.8500	.9964	.0009	.9011	.5926	.0012	1.0721	.6381
-.0093	.4777	.9647	-.0236	.6974	.9860	-.0710	.8755	1.0013	.0006	.7186	.5710	.0010	1.0263	.6302
-.0118	.4989	.9667	-.0269	.7346	.9914	-.0734	.8936	1.0049	.0004	.5966	.5608	.0008	.9378	.6165
-.0140	.5392	.9710	-.0303	.7769	.9984	-.0812	.9152	1.0093						
-.0171	.6099	.9792	-.0345	.8265	1.0070	-.0866	.9313	1.0127						
-.0195	.6636	.9863	-.0391	.8748	1.0160	-.0924	.9426	1.0151						
-.0222	.7214	.9948	-.0439	.9087	1.0228	-.0998	.9506	1.0168						
-.0252	.7766	1.0036	-.0485	.9269	1.0266	-.1091	.9529	1.0173						
-.0271	.8066	1.0088	-.0531	.9333	1.0279	-.1227	.9538	1.0176						
-.0302	.8466	1.0160	-.0571	.9347	1.0282									
-.0340	.8817	1.0228	-.0625	.9374	1.0288									
-.0372	.9061	1.0277												
-.0401	.9183	1.0303												
-.0432	.9238	1.0314												
-.0448	.9282	1.0323												
-.0469	.9294	1.0326												
-.0515	.9307	1.0329												
-.0555	.9311	1.0330												

GP11-0232-55

TABLE 5. — Continued.

X/C = .550U RUN 108			X/C = .650 RUN 112			X/C = .750U RUN 114			X/C = .850U RUN 116			X/C = .900U RUN 118		
z/c	u/u_∞	ρ/ρ_∞	z/c	u/u_∞	ρ/ρ_∞	z/c	u/u_∞	ρ/ρ_∞	z/c	u/u_∞	ρ/ρ_∞	z/c	u/u_∞	ρ/ρ_∞
.0183	1.1709	.8852	.0212	1.1976	.8671	.0235	1.2046	.8544	.0269	1.1695	.8825	.0264	1.1023	.9285
.0171	1.1714	.8853	.0146	1.1976	.8671	.0213	1.2050	.8546	.0230	1.1705	.8828	.0237	1.1027	.9286
.0138	1.1708	.8852	.0157	1.1976	.8671	.0195	1.2056	.8547	.0208	1.1705	.8828	.0220	1.1038	.9289
.0129	1.1714	.8853	.0142	1.1976	.8671	.0181	1.2056	.8547	.0190	1.1710	.8829	.0211	1.1044	.9291
.0118	1.1720	.8855	.0128	1.1976	.8671	.0172	1.2049	.8545	.0172	1.1711	.8829	.0191	1.1033	.9288
.0107	1.1705	.8851	.0117	1.1976	.8671	.0157	1.2054	.8547	.0158	1.1699	.8826	.0171	1.1013	.9283
.0096	1.1699	.8849	.0106	1.1929	.8658	.0140	1.2042	.8543	.0146	1.1674	.8819	.0148	1.0923	.9259
.0088	1.1678	.8843	.0088	1.1673	.8588	.0125	1.1986	.8528	.0136	1.1623	.8805	.0135	1.0823	.9232
.0075	1.1594	.8810	.0077	1.1382	.8511	.0113	1.1878	.8498	.0119	1.1444	.8756	.0117	1.0582	.9171
.0065	1.1253	.8730	.0067	1.1091	.8438	.0104	1.1740	.8461	.0101	1.1163	.8685	.0108	1.0349	.9113
.0059	1.1037	.8675	.0059	1.0892	.8375	.0091	1.1460	.8388	.0090	1.0889	.8617	.0096	1.0117	.9038
.0052	1.0773	.8610	.0051	1.0512	.8301	.0081	1.1231	.8330	.0084	1.0748	.8584	.0087	.9877	.9002
.0046	1.0399	.8523	.0046	1.0290	.8252	.0071	1.0960	.8264	.0073	1.0468	.8519	.0081	.9690	.8960
.0041	1.0151	.8468	.0038	.9961	.8182	.0063	1.0742	.8213	.0056	1.0022	.8420	.0074	.9503	.8920
.0037	.9850	.8424	.0037	.9885	.8166	.0057	1.0533	.8166	.0049	.9739	.8361	.0063	.9166	.8850
.0031	.9620	.8376	.0031	.9649	.8119	.0049	1.0260	.8106	.0038	.9347	.8284	.0062	.9090	.8834
.0025	.9276	.8278	.0026	.9357	.8062	.0036	.9832	.8017	.0028	.8866	.8195	.0054	.8830	.8783
.0020	.8981	.8232	.0022	.9125	.8019	.0028	.9398	.7933	.0024	.8723	.8169	.0050	.8601	.8740
.0016	.8530	.8153	.0012	.8524	.7914	.0022	.9057	.7870	.0018	.8322	.8102	.0044	.8398	.8703
.0012	.8307	.8115	.0010	.8235	.7867	.0016	.8928	.7847	.0015	.8114	.8068	.0041	.8244	.8675
.0009	.7845	.8042	.0007	.7775	.7796	.0016	.8688	.7806	.0012	.7801	.8020	.0034	.7846	.8608
						.0014	.8403	.7750	.0005	.6930	.7898	.0028	.7582	.8565
						.0010	.7958	.7690	.0004	.6817	.7884	.0024	.7441	.8543
						.0007	.7739	.7658				.0022	.7271	.8518
												.0019	.6952	.8471
												.0012	.6540	.8415
												.0006	.5983	.8346

GP11-0232-56

X/C = .950U RUN 120			X/C = 1.000U RUN 102			X/C = .500L RUN 164			X/C = .750L RUN 166			X/C = .910L RUN 178		
z/c	u/u_∞	ρ/ρ_∞	z/c	u/u_∞	ρ/ρ_∞	z/c	u/u_∞	ρ/ρ_∞	z/c	u/u_∞	ρ/ρ_∞	z/c	u/u_∞	ρ/ρ_∞
.0350	.9916	1.0001	.0494	.9364	1.0353	.0170	1.0884	.9420	.0360	.8148	1.1077	.0442	.7543	1.1423
.0315	.9925	1.0003	.0452	.9360	1.0352	.0146	1.0879	.9419	.0323	.8146	1.1077	.0410	.7546	1.1424
.0291	.9925	1.0003	.0389	.9388	1.0359	.0130	1.0887	.9421	.0289	.8131	1.1078	.0392	.7537	1.1422
.0270	.9932	1.0005	.0354	.9383	1.0358	.0116	1.0888	.9422	.0274	.8154	1.1079	.0371	.7551	1.1425
.0249	.9932	1.0005	.0322	.9309	1.0362	.0104	1.0879	.9419	.0259	.8158	1.1079	.0351	.7522	1.1419
.0232	.9942	1.0008	.0283	.9383	1.0358	.0091	1.0866	.9416	.0243	.8138	1.1075	.0328	.7492	1.1413
.0218	.9931	1.0005	.0255	.9310	1.0340	.0083	1.0818	.9403	.0231	.8087	1.1064	.0307	.7385	1.1391
.0201	.9904	.9998	.0240	.9201	1.0313	.0080	1.0776	.9392	.0211	.7898	1.1023	.0288	.7212	1.1356
.0184	.9832	.9980	.0226	.9006	1.0268	.0069	1.0630	.9354	.0195	.7588	.0959	.0266	.6934	1.1303
.0173	.9720	.9952	.0213	.8759	1.0211	.0062	1.0404	.9297	.0179	.7202	.0884	.0247	.6550	1.1234
.0163	.9609	.9925	.0186	.8117	1.0079	.0058	1.0298	.9271	.0163	.6764	.0805	.0232	.6149	1.1166
.0149	.9308	.9854	.0169	.7574	.9971	.0053	1.0130	.9230	.0145	.6162	.0705	.0218	.5007	1.1128
.0134	.8967	.9777	.0145	.7492	.9956	.0045	.9819	.9139	.0132	.5685	.0634	.0206	.5513	1.1069
.0124	.8713	.9723	.0141	.6769	.9833	.0038	.9593	.9107	.0123	.5280	.0580	.0191	.5104	1.1013
.0108	.8253	.9629	.0123	.6616	.9809	.0033	.9292	.9043	.0112	.4912	.0533	.0179	.4756	.0969
.0099	.7934	.9569	.0105	.5954	.9712	.0029	.9175	.9018	.0101	.4461	.0482	.0163	.4461	.0935
.0086	.7505	.9492	.0082	.5053	.9599	.0026	.8928	.8968	.0088	.4336	.0469	.0149	.4063	.0892
.0079	.7175	.9436	.0059	.4096	.9502	.0022	.8779	.8939	.0079	.3612	.0400	.0125	.3567	.0834
.0072	.6939	.9399	.0046	.3103	.9424	.0020	.8625	.8910	.0069	.3337	.0377	.0123	.3504	.0839
.0069	.6813	.9379	.0033	.2614	.9393	.0019	.8564	.8898	.0059	.2966	.0349	.0108	.3190	.0810
.0063	.6595	.9341	.0022	.2061	.9366	.0016	.8354	.8860	.0046	.2634	.0327	.0093	.2825	.0703
.0056	.6218	.9293	.0016	.1590	.9347	.0014	.8207	.8833	.0039	.2404	.0314	.0082	.2621	.0773
.0049	.5815	.9240	.0006	.1435	.9342	.0011	.8041	.8804	.0035	.2287	.0307	.0071	.2349	.0726
.0041	.5437	.9194		.1005	.9331	.0009	.7898	.8763	.0031	.2207	.0303	.0058	.2192	.0747
.0036	.5101	.9155				.0007	.7570	.8726	.0028	.2117	.0298	.0048	.2033	.0741
.0028	.4648	.9109							.0024	.2086	.0297	.0037	.1960	.0730
.0025	.4426	.9087							.0022	.2014	.0293	.0030	.1883	.0732
.0018	.4064	.9055							.0016	.1940	.0290	.0020	.1763	.0728
.0016	.3900	.9041							.0012	.1800	.0284	.0012	.1877	.0732
.0011	.3606	.9018							.0009	.1809	.0284			
.0009	.3385	.9002												
.0008	.3342	.8999												

GP11-0232-57

TABLE 5. — Continued.

X/C = .985L RUN 180

z/c	u/u_∞	ρ/ρ_∞
.0383	.7836	1.1270
.0352	.7837	1.1271
.0335	.7837	1.1271
.0311	.7853	1.1270
.0288	.7852	1.1267
.0270	.7775	1.1257
.0252	.7723	1.1246
.0231	.7629	1.1227
.0216	.7456	1.1192
.0192	.7233	1.1148
.0173	.6953	1.1095
.0160	.6780	1.1065
.0147	.6580	1.1029
.0132	.6242	1.0972
.0119	.5987	1.0932
.0110	.5864	1.0913
.0104	.5581	1.0872
.0086	.5356	1.0841
.0075	.5323	1.0836
.0068	.5137	1.0812
.0055	.5002	1.0785
.0046	.4920	1.0785
.0038	.4675	1.0779
.0025	.4675	1.0755
.0016	.4567	1.0743
.0007	.4424	1.0727

X/C = 1.000L RUN 168

z/c	u/u_∞	ρ/ρ_∞
.0372	.8866	1.0624
.0339	.8866	1.0624
.0310	.8865	1.0624
.0280	.8867	1.0620
.0255	.8826	1.0615
.0234	.8773	1.0603
.0209	.8656	1.0576
.0185	.8488	1.0539
.0161	.8221	1.0481
.0141	.7942	1.0424
.0119	.7605	1.0358
.0102	.7390	1.0317
.0085	.7130	1.0271
.0070	.6858	1.0241
.0054	.6772	1.0210
.0043	.6666	1.0193
.0037	.6577	1.0178
.0030	.6534	1.0171
.0026	.6488	1.0164
.0017	.6418	1.0153
.0015	.6344	1.0150
.0010	.6340	1.0141
.0008	.6310	1.0137
.0004	.5971	1.0087

X/C = 1.000L RUN 122

z/c	u/u_∞	ρ/ρ_∞
.0397	.8904	1.0635
.0348	.8899	1.0634
.0307	.8894	1.0632
.0278	.8881	1.0630
.0255	.8854	1.0623
.0227	.8772	1.0604
.0202	.8654	1.0577
.0182	.8503	1.0543
.0165	.8309	1.0501
.0147	.8076	1.0452
.0130	.7871	1.0410
.0115	.7631	1.0364
.0099	.7417	1.0323
.0080	.7193	1.0283
.0063	.6966	1.0243
.0049	.6807	1.0216
.0041	.6731	1.0204
.0034	.6658	1.0192
.0026	.6590	1.0181
.0025	.6573	1.0178
.0022	.6526	1.0171
.0018	.6494	1.0165
.0014	.6474	1.0162
.0009	.6390	1.0149
.0007	.6185	1.0118
.0004	.5098	1.0106

X/C = 1.050 RUN 125

z/c	u/u_∞	ρ/ρ_∞
.0396	.9163	1.0457
.0318	.9186	1.0463
.0297	.9180	1.0461
.0268	.9204	1.0467
.0240	.9214	1.0470
.0220	.9211	1.0469
.0202	.9200	1.0466
.0177	.9136	1.0451
.0158	.9019	1.0423
.0145	.8828	1.0379
.0129	.8585	1.0324
.0115	.8261	1.0255
.0107	.8065	1.0215
.0085	.7557	1.0117
.0066	.6989	1.0000
.0043	.6205	.9893
.0030	.5767	.9832
.0015	.5242	.9766
-.0005	.4505	.9684
-.0024	.4009	.9637
-.0039	.3639	.9605
-.0059	.3303	.9580
-.0081	.3230	.9574
-.0093	.3384	.9586
-.0110	.3770	.9616
-.0129	.4495	.9683
-.0134	.4667	.9701
-.0149	.5385	.9783
-.0171	.6196	.9892
-.0187	.6694	.9965
-.0204	.7098	1.0035
-.0225	.7565	1.0118
-.0237	.7808	1.0164
-.0277	.8041	1.0210
-.0296	.8231	1.0249
-.0316	.8495	1.0305
-.0338	.8662	1.0341
-.0366	.8875	1.0390
-.0391	.9004	1.0419
-.0418	.9059	1.0432
-.0444	.9133	1.0450
-.0473	.9161	1.0457
-.0507	.9170	1.0459

X/C = 1.100 RUN 124

z/c	u/u_∞	ρ/ρ_∞
.0003	0.0000	.9436
.0671	.9195	1.0432
.0506	.9202	1.0434
.0408	.9191	1.0433
.0299	.9238	1.0442
.0251	.9230	1.0441
.0220	.9234	1.0441
.0194	.9246	1.0444
.0167	.9241	1.0443
.0144	.9222	1.0439
.0125	.9166	1.0425
.0106	.9065	1.0401
.0089	.8880	1.0359
.0078	.8738	1.0326
.0062	.8468	1.0268
.0045	.8052	1.0181
.0033	.7791	1.0130
.0018	.7371	1.0053
-.0001	.6830	.9961
-.0018	.6451	.9901
-.0036	.5966	.9831
-.0057	.5689	.9794
-.0075	.5443	.9762
-.0091	.5307	.9746
-.0110	.5248	.9743
-.0125	.5342	.9750
-.0136	.5619	.9785
-.0178	.5955	.9824
-.0190	.6167	.9859
-.0213	.6532	.9914
-.0231	.6973	.9984
-.0250	.7273	1.0035
-.0275	.7685	1.0110
-.0295	.7965	1.0164
-.0316	.8238	1.0219
-.0343	.8496	1.0273
-.0369	.8738	1.0326
-.0390	.8868	1.0356
-.0420	.9034	1.0394
-.0446	.9119	1.0414
-.0478	.9171	1.0426
-.0510	.9200	1.0433
-.0542	.9222	1.0439

GP11-0232-58

X/C = 1.200 RUN 123

z/c	u/u_∞	ρ/ρ_∞
.0747	.9254	1.0385
.0603	.9247	1.0383
.0440	.9255	1.0385
.0337	.9253	1.0385
.0248	.9265	1.0388
.0186	.9267	1.0388
.0152	.9278	1.0391
.0120	.9263	1.0387
.0093	.9232	1.0380
.0068	.9159	1.0362
.0042	.9047	1.0336
.0018	.8874	1.0296
-.0010	.8612	1.0238
-.0043	.8213	1.0154
-.0063	.7936	1.0099
-.0083	.7661	1.0047
-.0101	.7418	1.0002
-.0128	.7167	.9958
-.0156	.6836	.9920
-.0184	.6825	.9901
-.0207	.6785	.9895
-.0229	.6829	.9902
-.0239	.6873	.9909
-.0260	.6983	.9927
-.0291	.7227	.9968
-.0315	.7445	1.0007
-.0350	.7817	1.0076
-.0382	.8154	1.0142
-.0412	.8473	1.0208
-.0443	.8728	1.0264
-.0470	.8925	1.0308
-.0503	.9075	1.0343
-.0531	.9166	1.0364
-.0563	.9238	1.0381
-.0597	.9263	1.0387
-.0633	.9285	1.0393
-.0671	.9294	1.0395
-.0721	.9294	1.0395
-.0780	.9296	1.0395

GP11-0232-59

TABLE 5. — Continued.

X/C = .300U RUN 129

z/c	u/u_∞	ρ/ρ_∞
.0065	1.4964	.6459
.0048	1.4973	.6462
.0044	1.4964	.6459
.0040	1.4960	.6458
.0036	1.4968	.6460
.0034	1.4959	.6458
.0032	1.4961	.6458
.0030	1.4950	.6455
.0027	1.4938	.6452
.0026	1.4929	.6449
.0023	1.4890	.6438
.0021	1.4776	.6405
.0018	1.4557	.6344
.0018	1.4362	.6291
.0016	1.3946	.6183
.0015	1.3519	.6080
.0014	1.3112	.5987
.0013	1.2727	.5905
.0011	1.0958	.5580
.0010	1.0390	.5523
.0008	.9669	.5393
.0007	.9041	.5313
.0006	.8188	.5218
.0004	.7417	.5142

X/C = .500U RUN 131

z/c	u/u_∞	ρ/ρ_∞
.0118	1.4222	.6917
.0097	1.4222	.6917
.0087	1.4223	.6917
.0082	1.4233	.6920
.0077	1.4233	.6920
.0076	1.4234	.6921
.0073	1.4236	.6921
.0070	1.4232	.6920
.0066	1.4198	.6910
.0063	1.4181	.6905
.0056	1.4094	.6880
.0053	1.4021	.6860
.0050	1.3895	.6825
.0047	1.3722	.6778
.0042	1.3479	.6699
.0040	1.3308	.6671
.0036	1.2982	.6590
.0033	1.2779	.6543
.0028	1.2466	.6472
.0026	1.2022	.6376
.0022	1.1760	.6323
.0019	1.1478	.6268
.0017	1.1348	.6243
.0015	1.1058	.6190
.0014	1.0857	.6154
.0011	1.0552	.6102
.0008	.9922	.6002
.0006	.9234	.5903

X/C = .650U RUN 133

z/c	u/u_∞	ρ/ρ_∞
.0195	1.1539	.8962
.0177	1.1543	.8963
.0158	1.1547	.8964
.0150	1.1548	.8964
.0142	1.1548	.8964
.0135	1.1547	.8964
.0125	1.1548	.8964
.0117	1.1548	.8963
.0107	1.1503	.8952
.0100	1.1375	.8917
.0095	1.1320	.8902
.0088	1.0993	.8817
.0082	1.0844	.8779
.0073	1.0307	.8630
.0070	1.0220	.8630
.0063	.9766	.8530
.0059	.9463	.8467
.0050	.8944	.8366
.0044	.8600	.8303
.0038	.8098	.8218
.0031	.7370	.8106
.0027	.7295	.8095
.0026	.7036	.8059
.0023	.6976	.8050
.0017	.6655	.8000
.0017	.6456	.7983
.0014	.6305	.7965
.0009	.5927	.7921
.0005	.5588	.7885

X/C = .800U RUN 135

z/c	u/u_∞	ρ/ρ_∞
.0257	1.1480	.8971
.0237	1.1484	.8972
.0223	1.1484	.8972
.0210	1.1481	.8971
.0201	1.1476	.8970
.0187	1.1485	.8973
.0178	1.1482	.8972
.0166	1.1482	.8972
.0152	1.1484	.8970
.0144	1.1314	.8926
.0132	1.1224	.8902
.0125	1.1024	.8849
.0116	1.0818	.8797
.0106	1.0587	.8743
.0101	1.0466	.8706
.0093	1.0283	.8658
.0080	.9849	.8571
.0078	.9782	.8557
.0074	.9678	.8535
.0072	.9600	.8518
.0068	.9477	.8493
.0062	.9234	.8444
.0058	.9131	.8424
.0054	.8942	.8388
.0049	.8889	.8378
.0047	.8749	.8352
.0040	.8607	.8327
.0037	.8473	.8303
.0036	.8501	.8308
.0035	.8268	.8268
.0034	.8346	.8281
.0028	.8126	.8244
.0022	.7826	.8200
.0016	.7508	.8159
.0013	.7391	.8130
.0008	.6790	.8046

X/C = .900U RUN 137

z/c	u/u_∞	ρ/ρ_∞
.0296	1.0781	.9428
.0258	1.0807	.9435
.0237	1.0817	.9438
.0220	1.0818	.9438
.0203	1.0821	.9439
.0189	1.0804	.9434
.0175	1.0775	.9427
.0164	1.0716	.9411
.0148	1.0583	.9377
.0134	1.0344	.9316
.0119	.9959	.9224
.0100	.9476	.9115
.0088	.9207	.9058
.0078	.8782	.8972
.0066	.8413	.8902
.0060	.8190	.8862
.0050	.7879	.8808
.0040	.7584	.8759
.0030	.7102	.8685
.0027	.6958	.8664
.0020	.6676	.8624
.0016	.6432	.8592
.0008	.5810	.8515

GP11-0232-60

X/C = .950U RUN 139

z/c	u/u_∞	ρ/ρ_∞
.0349	.9888	.9994
.0328	.9904	.9998
.0312	.9910	1.0000
.0293	.9927	1.0004
.0274	.9945	1.0008
.0257	.9943	1.0008
.0238	.9932	1.0005
.0217	.9881	.9992
.0201	.9798	.9972
.0189	.9678	.9942
.0171	.9433	.9884
.0161	.9192	.9828
.0150	.8952	.9775
.0135	.8556	.9692
.0119	.8093	.9600
.0106	.7716	.9531
.0093	.7332	.9465
.0083	.6972	.9407
.0073	.6754	.9373
.0067	.6533	.9340
.0061	.6212	.9295
.0051	.5853	.9248
.0045	.5616	.9219
.0038	.5261	.9172
.0033	.4970	.9145
.0027	.4732	.9121
.0019	.4296	.9079
.0014	.3955	.9050
.0007	.3520	.9016

X/C = 1.000U RUN 127

z/c	u/u_∞	ρ/ρ_∞
.0434	.9244	1.0423
.0393	.9239	1.0422
.0368	.9244	1.0423
.0349	.9263	1.0428
.0327	.9267	1.0429
.0305	.9262	1.0427
.0285	.9209	1.0415
.0270	.9142	1.0399
.0258	.9044	1.0375
.0242	.8879	1.0337
.0225	.8588	1.0272
.0210	.8187	1.0188
.0193	.7813	1.0114
.0175	.7286	1.0017
.0158	.6836	.9941
.0145	.6427	.9877
.0134	.6201	.9843
.0120	.5741	.9758
.0106	.4998	.9680
.0091	.4407	.9626
.0074	.3969	.9586
.0068	.3515	.9548
.0064	.3305	.9533
.0056	.3016	.9513
.0043	.2633	.9489
.0041	.2478	.9481
.0034	.2142	.9464
.0021	.1612	.9442
.0008	.1144	.9420
.0007	.0993	.9425

X/C = .300L RUN 172

z/c	u/u_∞	ρ/ρ_∞
.0097	1.0404	.9735
.0080	1.0407	.9736
.0069	1.0392	.9732
.0064	1.0390	.9731
.0059	1.0388	.9730
.0054	1.0347	.9720
.0048	1.0232	.9690
.0040	1.0044	.9643
.0037	.9923	.9613
.0033	.9781	.9578
.0031	.9671	.9552
.0028	.9526	.9518
.0025	.9331	.9474
.0021	.9024	.9408
.0018	.8804	.9361
.0015	.8582	.9317
.0013	.8425	.9286
.0011	.8121	.9229
.0007	.7819	.9174
.0005	.7388	.9101

X/C = .500L RUN 154

z/c	u/u_∞	ρ/ρ_∞
.0188	1.0642	.9581
.0168	1.0643	.9582
.0152	1.0637	.9580
.0133	1.0634	.9579
.0117	1.0640	.9581
.0100	1.0635	.9579
.0085	1.0608	.9572
.0073	1.0485	.9540
.0068	1.0397	.9517
.0063	1.0283	.9489
.0056	1.0113	.9446
.0051	.9889	.9393
.0045	.9703	.9349
.0039	.9508	.9305
.0033	.9284	.9256
.0030	.9086	.9214
.0026	.8934	.9185
.0024	.8760	.9147
.0021	.8633	.9122
.0017	.8327	.9064
.0012	.8061	.9016
.0010	.7887	.8985
.0007	.7635	.8943
.0004	.7199	.8873

X/C = .600L RUN 156

z/c	u/u_∞	ρ/ρ_∞
.0196	.9932	1.0005
.0170	.9930	1.0004
.0151	.9927	1.0004
.0137	.9942	1.0008
.0121	.9926	1.0004
.0106	.9879	.9992
.0092	.9715	.9951
.0082	.9527	.9906
.0074	.9321	.9858
.0066	.9052	.9798
.0054	.8653	.9713
.0048	.8393	.9660
.0042	.8138	.9611
.0037	.7899	.9566
.0034	.7740	.9538
.0030	.7518	.9499
.0023	.7075	.9426
.0020	.6924	.9402
.0017	.6734	.9373
.0016	.6619	.9356
.0011	.6379	.9322
.0007	.5869	.9254

GP11-0232-61

TABLE 5. — Continued.

X/C = .650L RUN 158			X/C = .750L RUN 160			X/C = .910L RUN 184			X/C = .985L RUN 182			X/C = 1.000L RUN 141		
z/c	u/u_∞	ρ/ρ_∞	z/c	u/u_∞	ρ/ρ_∞	z/c	u/u_∞	ρ/ρ_∞	z/c	u/u_∞	ρ/ρ_∞	z/c	u/u_∞	ρ/ρ_∞
.0266	.8876	1.0648	.0354	.7888	1.1200	.0430	.7330	1.1547	.0399	.7753	1.1335	.0409	.8805	1.0725
.0239	.8884	1.0649	.0324	.7901	1.1202	.0411	.7314	1.1544	.0379	.7748	1.1334	.0343	.8800	1.0724
.0214	.8889	1.0651	.0293	.7894	1.1201	.0385	.7333	1.1547	.0352	.7754	1.1335	.0321	.8806	1.0726
.0193	.8888	1.0650	.0269	.7874	1.1198	.0363	.7323	1.1546	.0322	.7745	1.1333	.0301	.8796	1.0723
.0171	.8874	1.0647	.0247	.7886	1.1199	.0344	.7330	1.1547	.0294	.7742	1.1333	.0280	.8787	1.0721
.0150	.8884	1.0649	.0224	.7877	1.1197	.0326	.7322	1.1545	.0274	.7734	1.1335	.0258	.8761	1.0715
.0132	.8874	1.0647	.0206	.7799	1.1181	.0309	.7290	1.1539	.0252	.7687	1.1321	.0237	.8714	1.0704
.0114	.8738	1.0615	.0191	.7644	1.1148	.0297	.7254	1.1529	.0234	.7658	1.1315	.0218	.8612	1.0680
.0102	.8523	1.0569	.0174	.7319	1.1083	.0287	.7177	1.1516	.0215	.7540	1.1290	.0199	.8506	1.0659
.0088	.8206	1.0497	.0159	.6922	1.1008	.0275	.7063	1.1494	.0198	.7402	1.1262	.0184	.8377	1.0627
.0080	.7924	1.0438	.0145	.6468	1.0929	.0266	.6987	1.1479	.0185	.7219	1.1225	.0170	.8213	1.0590
.0072	.7651	1.0378	.0134	.6099	1.0869	.0256	.6855	1.1454	.0172	.7006	1.1201	.0154	.8010	1.0547
.0062	.7272	1.0312	.0125	.5712	1.0811	.0240	.6586	1.1404	.0157	.6911	1.1166	.0138	.7793	1.0502
.0055	.6975	1.0246	.0115	.5319	1.0756	.0224	.6249	1.1346	.0144	.6844	1.1121	.0124	.7623	1.0468
.0046	.6543	1.0187	.0104	.4878	1.0700	.0213	.5976	1.1301	.0131	.6427	1.1080	.0107	.7355	1.0417
.0037	.6111	1.0121	.0092	.4447	1.0630	.0200	.5623	1.1242	.0120	.6239	1.1048	.0091	.7174	1.0383
.0033	.5794	1.0074	.0078	.3906	1.0545	.0188	.5383	1.1212	.0103	.6013	1.1012	.0073	.6973	1.0347
.0031	.5657	1.0057	.0066	.3457	1.0555	.0178	.5106	1.1174	.0092	.5748	1.0971	.0062	.6837	1.0323
.0027	.5340	1.0016	.0054	.3047	1.0523	.0163	.4767	1.1130	.0084	.5645	1.0956	.0047	.6684	1.0297
.0024	.5208	.9999	.0047	.2772	1.0504	.0151	.4441	1.1091	.0073	.5492	1.0934	.0036	.6501	1.0262
.0019	.4956	.9969	.0037	.2463	1.0484	.0135	.4035	1.1047	.0062	.5297	1.0906	.0029	.6362	1.0248
.0013	.4421	.9911	.0034	.2414	1.0481	.0123	.3723	1.1016	.0051	.5206	1.0894	.0021	.6422	1.0255
.0004	.3724	.9845	.0030	.2241	1.0472	.0112	.3416	1.0989	.0044	.5066	1.0876	.0014	.6370	1.0246
			.0025	.2061	1.0463	.0100	.3169	1.0966	.0034	.4937	1.0859	.0014	.6277	1.0232
			.0019	.1959	1.0458	.0089	.2900	1.0948	.0028	.4886	1.0853	.0010	.6123	1.0208
			.0013	.1812	1.0451	.0078	.2685	1.0933	.0020	.4829	1.0846	.0007	.5903	1.0176
			.0010	.1739	1.0448	.0066	.2472	1.0919	.0012	.4633	1.0822	.0004	.5506	1.0121
			.0006	.1644	1.0444	.0055	.2345	1.0911	.0006	.4544	1.0812	.0003	.5202	1.0082
						.0047	.2229	1.0905						
						.0038	.2010	1.0893						
						.0031	.1892	1.0887						
						.0023	.1840	1.0885						
						.0015	.1798	1.0883						
						.0006	.1766	1.0882						

GP11-0232-62

X/C = 1.050 RUN 142			X/C = 1.100 RUN 143			X/C = 1.200 RUN 144			X/C = .300U RUN 85			X/C = .450U RUN 87		
z/c	u/u_∞	ρ/ρ_∞	z/c	u/u_∞	ρ/ρ_∞	z/c	u/u_∞	ρ/ρ_∞	z/c	u/u_∞	ρ/ρ_∞	z/c	u/u_∞	ρ/ρ_∞
.0262	.9028	1.0512	.0216	.9041	1.0484	.0521	.9076	1.0429	.0057	1.3724	.7138	.0118	1.3525	.7256
.0235	.9050	1.0517	.0177	.9067	1.0490	.0414	.9070	1.0428	.0053	1.3739	.7143	.0080	1.3550	.7264
.0203	.9070	1.0522	.0135	.9101	1.0498	.0284	.9058	1.0425	.0050	1.3733	.7141	.0070	1.3525	.7266
.0178	.9093	1.0527	.0102	.9126	1.0504	.0165	.9078	1.0430	.0044	1.3728	.7139	.0059	1.3551	.7264
.0154	.9094	1.0527	.0069	.9135	1.0506	.0077	.9115	1.0438	.0081	1.3740	.7143	.0054	1.3538	.7260
.0132	.9091	1.0526	.0064	.9131	1.0505	.0043	.9133	1.0442	.0063	1.3728	.7139	.0047	1.3489	.7245
.0114	.9076	1.0523	.0035	.9069	1.0491	.0019	.9138	1.0444	.0043	1.3715	.7135	.0044	1.3480	.7243
.0097	.9025	1.0511	.0012	.8944	1.0461	.0003	.9120	1.0439	.0041	1.3717	.7136	.0037	1.3264	.7179
.0080	.8914	1.0485	-.0007	.8702	1.0406	-.0016	.9097	1.0434	.0038	1.3707	.7133	.0032	1.3020	.7109
.0063	.8741	1.0445	-.0025	.8455	1.0351	-.0041	.9015	1.0415	.0036	1.3710	.7136	.0027	1.2647	.7008
.0050	.8609	1.0415	-.0040	.8188	1.0295	-.0069	.8849	1.0377	.0035	1.3716	.7135	.0024	1.2367	.6936
.0033	.8305	1.0340	-.0056	.7884	1.0234	-.0088	.8707	1.0345	.0032	1.3719	.7137	.0021	1.1940	.6831
.0018	.7743	1.0182	-.0074	.7491	1.0139	-.0108	.8494	1.0298	.0028	1.3705	.7132	.0017	1.1411	.6711
.0007	.7625	1.0214	-.0093	.7000	1.0073	-.0129	.8252	1.0247	.0028	1.3641	.7113	.0016	1.1106	.6645
-.0015	.7244	1.0144	-.0111	.6627	1.0012	-.0153	.8017	1.0199	.0025	1.3563	.7089	.0013	.0616	.6547
-.0027	.6892	1.0084	-.0129	.6164	.9941	-.0183	.7562	1.0112	.0023	1.3343	.7026	.0011	1.0154	.6460
-.0044	.6420	1.0008	-.0151	.5733	.9881	-.0201	.7335	1.0071	.0021	1.3109	.6958	.0008	.9487	.6380
-.0069	.5848	.9923	-.0174	.5435	.9843	-.0220	.7100	1.0031	.0018	1.2499	.6798	.0007	.9482	.6346
-.0094	.5073	.9828	-.0189	.5262	.9822	-.0238	.6899	.9997	.0016	1.1763	.6623			
-.0114	.4907	.9766	-.0211	.5170	.9811	-.0250	.6799	.9981	.0014	1.0727	.6407			
-.0138	.3902	.9709	-.0234	.5247	.9830	-.0274	.6679	.9961	.0011	.9949	.6124			
-.0159	.3516	.9677	-.0260	.5503	.9851	-.0295	.6544	.9940	.0008	.7991	.5980			
-.0184	.3410	.9669	-.0283	.5868	.9900	-.0318	.6535	.9939	.0008	.7557	.5928			
-.0206	.3679	.9690	-.0307	.6364	.9971	-.0348	.6610	.9951	.0007	.7257	.5894			
-.0228	.4286	.9744	-.0328	.6746	1.0031	-.0366	.6713	.9967						
-.0248	.5143	.9832	-.0349	.7142	1.0097	-.0389	.6800	.9996						
-.0269	.5459	.9941	-.0372	.7529	1.0166	-.0417	.7159	1.0041						
-.0289	.6654	1.0048	-.0397	.7741	1.0210	-.0442	.7460	1.0094						
-.0313	.7342	1.0144	-.0415	.8118	1.0281	-.0461	.7641	1.0127						
-.0333	.7552	1.0200	-.0445	.8462	1.0353	-.0485	.7919	1.0180						
-.0354	.7774	1.0242	-.0489	.8813	1.0431	-.0506	.8161	1.0228						
-.0375	.8023	1.0291	-.0519	.8964	1.0466	-.0527	.8357	1.0269						
-.0394	.8253	1.0332	-.0547	.9032	1.0482	-.0552	.8599	1.0321						
-.0419	.8490	1.0389	-.0578	.9103	1.0499	-.0581	.8814	1.0369						
-.0440	.8745	1.0446	-.0612	.9128	1.0505	-.0608	.8957	1.0401						
-.0468	.8871	1.0475	-.0643	.9123	1.0504	-.0636	.9058	1.0425						
-.0496	.8977	1.0499				-.0660	.9122	1.0440						
-.0529	.9062	1.0519				-.0691	.9168	1.0451						
-.0549	.9076	1.0523				-.0729	.9180	1.0454						
-.0591	.9089	1.0526				-.0769	.9192	1.0457						
-.0612	.9105	1.0530				-.0803	.9200	1.0458						
						-.0836	.9199	1.0458						

GP11-0232-63

TABLE 5. — Continued.

X/C = .700U RUN 89			X/C = .850U RUN 91			X/C = .900U RUN 93			X/C = .950U RUN 95			X/C - 1.000U RUN 83		
z/c	u/u_∞	ρ/ρ_∞	z/c	u/u_∞	ρ/ρ_∞	z/c	u/u_∞	ρ/ρ_∞	z/c	u/u_∞	ρ/ρ_∞	z/c	u/u_∞	ρ/ρ_∞
.0307	1.2016	.8447	.0244	1.0974	.9244	.0274	1.0396	.9666	.0321	.9664	1.0173	.0429	.9244	1.0416
.0264	1.2021	.8448	.0219	1.0978	.9245	.0241	1.0399	.9665	.0286	.9673	1.0175	.0380	.9262	1.0421
.0219	1.2032	.8452	.0195	1.0975	.9244	.0225	1.0415	.9669	.0258	.9673	1.0176	.0364	.9263	1.0422
.0192	1.2034	.8452	.0177	1.0978	.9245	.0207	1.0412	.9668	.0235	.9672	1.0175	.0344	.9268	1.0422
.0163	1.2037	.8453	.0166	1.0979	.9245	.0196	1.0408	.9667	.0215	.9651	1.0169	.0336	.9267	1.0422
.0146	1.2042	.8454	.0154	1.0970	.9243	.0180	1.0405	.9666	.0192	.9535	1.0138	.0328	.9265	1.0421
.0129	1.2044	.8455	.0141	1.0927	.9230	.0165	1.0386	.9661	.0172	.9194	1.0091	.0314	.9259	1.0420
.0120	1.2026	.8450	.0131	1.0852	.9200	.0150	1.0271	.9629	.0160	.8830	.9963	.0303	.9248	1.0417
.0110	1.1992	.8440	.0122	1.0685	.9162	.0139	1.0043	.9568	.0141	.8290	.9843	.0288	.9200	.0407
.0101	1.1897	.8412	.0110	1.0402	.9086	.0122	.9758	.9494	.0126	.7786	.9737	.0283	.9184	.0401
.0096	1.1773	.8376	.0102	1.0089	.9005	.0113	.9455	.9419	.0115	.7345	.9653	.0256	.8853	.0318
.0093	1.1742	.8367	.0092	.9689	.8907	.0100	.9032	.9320	.0100	.6872	.9569	.0245	.8554	1.0247
.0089	1.1597	.8315	.0077	.9051	.8763	.0090	.8650	.9236	.0084	.6059	.9442	.0226	.8218	.0171
.0083	1.1407	.8274	.0068	.8601	.8671	.0080	.8230	.9130	.0070	.5513	.9367	.0220	.7886	1.0100
.0078	1.1143	.8204	.0058	.8131	.8580	.0069	.7648	.9039	.0058	.4935	.9297	.0203	.7483	1.0019
.0068	1.0673	.8086	.0052	.7856	.8530	.0061	.7298	.8978	.0046	.4408	.9239	.0194	.7190	.9964
.0062	1.0428	.8028	.0042	.7437	.8459	.0051	.7061	.8939	.0035	.3934	.9174	.0176	.6907	.9844
.0056	.9948	.7920	.0036	.7148	.8413	.0045	.6662	.8876	.0024	.3364	.9147	.0160	.6934	.9727
.0052	.9808	.7890	.0031	.6925	.8379	.0037	.6325	.8827	.0013	.2790	.9108	.0143	.5313	.9672
.0045	.9537	.7775	.0024	.6670	.8341	.0029	.6067	.8791	.0008	.2508	.9091	.0126	.4632	.9591
.0043	.8962	.7723	.0019	.6484	.8314	.0021	.5532	.8722				.0102	.3733	.9503
.0027	.7664	.7562	.0015	.6286	.8288	.0016	.5352	.8699				.0091	.3246	.9463
.0025	.7699	.7511	.0012	.5999	.8251	.0011	.4966	.8658				.0080	.2782	.9431
.0011	.6385	.7359	.0009	.5735	.8216	.0006	.4391	.8600				.0070	.2334	.9405
.0007	.6535	.7352	.0005	.5483	.8189							.0060	.1963	.9406
.0005	.6077	.7249										.0049	.2030	.9349
												.0041	.1853	.9382
												.0028	.1372	.9364
												.0017	.0936	.9353
												.0007	.0380	.9344

GP11-0232-64

X/C = .500L RUN 146			X/C = .750L RUN 148			X/C = .910L RUN 176			X/C = .985L RUN 174			X/C = 1.000L RUN 150		
z/c	u/u_∞	ρ/ρ_∞	z/c	u/u_∞	ρ/ρ_∞	z/c	u/u_∞	ρ/ρ_∞	z/c	u/u_∞	ρ/ρ_∞	z/c	u/u_∞	ρ/ρ_∞
.0168	1.0978	.9312	.0393	.8148	1.1159	.0498	.7612	1.1516	.0444	.7727	1.1432	.0436	.8870	1.0747
.0143	1.0978	.9312	.0364	.8151	1.1160	.0453	.7611	1.1516	.0419	.7733	1.1433	.0399	.8876	1.0749
.0131	1.0978	.9312	.0334	.8148	1.1159	.0420	.7611	1.1516	.0383	.7736	1.1434	.0368	.8876	1.0749
.0119	1.0978	.9312	.0306	.8152	1.1160	.0400	.7612	1.1516	.0346	.7730	1.1433	.0339	.8872	1.0748
.0105	1.0978	.9312	.0284	.8148	1.1159	.0380	.7590	1.1511	.0324	.7736	1.1434	.0310	.8869	1.0747
.0095	1.0975	.9311	.0257	.8136	1.1157	.0357	.7556	1.1503	.0298	.7713	1.1429	.0280	.8856	1.0743
.0086	1.0938	.9300	.0235	.8045	1.1135	.0336	.7510	1.1493	.0277	.7643	1.1413	.0253	.8809	1.0731
.0079	1.0867	.9280	.0219	.7862	1.1092	.0312	.7349	1.1451	.0252	.7532	1.1388	.0222	.8699	1.0704
.0072	1.0739	.9244	.0202	.7463	1.1004	.0310	.7385	1.1465	.0233	.7433	1.1366	.0190	.8525	.0661
.0066	1.0590	.9203	.0190	.7137	.0940	.0298	.7127	1.1410	.0208	.7191	1.1314	.0160	.8148	1.0575
.0058	1.0389	.9149	.0170	.6558	1.0825	.0281	.6943	1.1372	.0188	.6838	1.1243	.0136	.7847	1.0506
.0052	1.0216	.9104	.0151	.5829	1.0702	.0254	.6396	1.1266	.0168	.6544	1.1187	.0115	.7567	1.0447
.0042	.9811	.9004	.0133	.5140	1.0607	.0235	.5978	1.1192	.0148	.6169	1.1119	.0097	.7278	1.0389
.0038	.9595	.8952	.0110	.4414	1.0509	.0219	.5465	1.1109	.0136	.5938	1.1080	.0079	.7015	.0338
.0030	.9282	.8881	.0088	.3654	1.0439	.0202	.5179	1.1066	.0123	.5675	1.1038	.0056	.6735	1.0287
.0026	.9041	.8829	.0073	.3030	1.0376	.0186	.4715	1.1003	.0108	.5446	1.0992	.0039	.6560	.0257
.0021	.8852	.8789	.0062	.2742	1.0355	.0161	.3892	1.0907	.0093	.5228	1.0970	.0029	.6506	1.0247
.0018	.8767	.8771	.0046	.2202	1.0321	.0142	.3652	1.0882	.0078	.5005	1.0939	.0023	.6410	1.0231
.0017	.8595	.8737	.0036	.2019	1.0311	.0127	.3310	1.0851	.0061	.4693	1.0898	.0017	.6374	.0225
.0015	.8433	.8709	.0027	.1892	1.0303	.0112	.3013	.0826	.0047	.4333	1.0878	.0014	.6310	1.0214
.0013	.8366	.8642	.0019	.1692	1.0296	.0098	.2482	1.0787	.0037	.4412	1.0864	.0010	.6268	1.0208
.0012	.8193	.8659	.0014	.1567	1.0291	.0040	.1706	1.0744	.0027	.4327	1.0853	.0007	.6217	1.0199
.0010	.8045	.8632	.0005	.1281	1.0281	.0033	.1622	1.0741	.0018	.4245	1.0846	.0006	.6184	1.0195
.0008	.7794	.8588				.0023	.1529	1.0737	.0009	.3945	1.0817	.0004	.6092	1.0179
.0006	.7663	.8565				.0016	.1532	1.0737						
.0005	.7518	.8541				.0006	.1691	1.0744						

GP11-0232-65

TABLE 5. — Continued.

X/C = 1.000L RUN 97			X/C = 1.100 RUN 98			X/C = 1.200 RUN 100		
z/c	u/u_∞	ρ/ρ_∞	z/c	u/u_∞	ρ/ρ_∞	z/c	u/u_∞	ρ/ρ_∞
.0405	.8800	1.0727	.0347	.8908	1.0631	.0973	.8989	1.0543
.0337	.8801	1.0728	.0265	.8950	1.0642	.0635	.8966	1.0538
.0309	.8784	1.0723	.0217	.8960	1.0645	.0567	.8971	1.0539
.0291	.8777	1.0722	.0186	.8955	1.0643	.0498	.8962	1.0537
.0281	.8772	1.0720	.0152	.8859	1.0619	.0407	.8960	1.0536
.0268	.8748	1.0714	.0119	.8631	1.0563	.0341	.8979	1.0541
.0253	.8716	1.0706	.0087	.8018	1.0422	.0274	.8992	1.0544
.0237	.8661	1.0693	.0066	.7589	1.0331	.0217	.9020	1.0551
.0227	.8629	1.0685	.0025	.6528	1.0134	.0146	.9004	1.0547
.0212	.8526	1.0660	-.0001	.5983	1.0047	.0111	.8931	1.0529
.0205	.8498	1.0653	-.0026	.5222	.9940	.0091	.8822	1.0501
.0185	.8353	1.0619	-.0058	.4807	.9888	.0047	.8547	1.0434
.0169	.8149	1.0572	-.0096	.4619	.9866	.0019	.8250	1.0366
.0145	.7850	1.0506	-.0131	.4803	.9898	.0004	.8058	1.0323
.0127	.7614	1.0455	-.0165	.5427	.9967	-.0022	.7683	1.0243
.0111	.7370	1.0406	-.0192	.5978	1.0046	-.0044	.7471	1.0200
.0090	.7094	1.0352	-.0232	.6730	1.0169	-.0053	.7274	1.0161
.0076	.6919	1.0320	-.0264	.7296	1.0273	-.0101	.6730	1.0062
.0063	.6742	1.0288	-.0297	.7753	1.0365	-.0134	.6506	1.0023
.0053	.6668	1.0275	-.0317	.7975	1.0412	-.0169	.6382	1.0003
.0046	.6553	1.0255	-.0358	.8395	1.0507	-.0202	.6407	1.0007
.0040	.6521	1.0249	-.0392	.8609	1.0558	-.0216	.6447	1.0014
.0029	.6453	1.0238	-.0427	.8766	1.0596	-.0246	.6664	1.0050
.0027	.6408	1.0230	-.0476	.8873	1.0623	-.0300	.7030	1.0115
.0023	.6353	1.0221	-.0560	.8913	1.0633	-.0346	.7521	1.0210
.0017	.6326	1.0217				-.0395	.8016	1.0313
.0015	.6296	1.0212				-.0449	.8494	1.0422
.0012	.6229	1.0201				-.0504	.8807	1.0498
.0010	.6187	1.0189				-.0538	.8971	1.0539
.0007	.6046	1.0172				-.0608	.9041	1.0557
						-.0659	.9063	1.0563

GP11-0232-66

X/C = .300U RUN 102			X/C = .500U RUN 104			X/C = .700U RUN 106			X/C = .800U RUN 108			X/C = .900U RUN 110		
z/c	u/u_∞	ρ/ρ_∞	z/c	u/u_∞	ρ/ρ_∞	z/c	u/u_∞	ρ/ρ_∞	z/c	u/u_∞	ρ/ρ_∞	z/c	u/u_∞	ρ/ρ_∞
.0147	1.2278	.9111	.0177	1.1872	.9221	.0250	1.1691	.9311	.0274	1.1581	.9358	.0396	1.0793	.9674
.0129	1.2273	.9110	.0161	1.1868	.9220	.0233	1.1693	.9312	.0250	1.1575	.9357	.0371	1.0789	.9673
.0124	1.2276	.9111	.0153	1.1865	.9220	.0213	1.1686	.9310	.0233	1.1573	.9357	.0348	1.0793	.9674
.0105	1.2279	.9111	.0137	1.1868	.9220	.0198	1.1691	.9311	.0219	1.1570	.9357	.0328	1.0784	.9672
.0098	1.2274	.9110	.0123	1.1863	.9220	.0189	1.1690	.9311	.0206	1.1573	.9357	.0307	1.0791	.9674
.0091	1.2279	.9111	.0113	1.1827	.9214	.0179	1.1685	.9310	.0193	1.1561	.9355	.0289	1.0789	.9673
.0083	1.2270	.9109	.0101	1.1817	.9212	.0171	1.1683	.9310	.0180	1.1563	.9355	.0279	1.0791	.9674
.0077	1.2249	.9106	.0090	1.1765	.9204	.0161	1.1665	.9307	.0170	1.1549	.9353	.0266	1.0789	.9673
.0073	1.2211	.9100	.0090	1.1637	.9183	.0152	1.1650	.9305	.0159	1.1526	.9350	.0253	1.0793	.9674
.0068	1.2146	.9090	.0085	1.1560	.9171	.0144	1.1647	.9304	.0152	1.1483	.9343	.0250	1.0795	.9674
.0066	1.2143	.9088	.0079	1.1370	.9142	.0138	1.1583	.9294	.0140	1.1413	.9332	.0234	1.0791	.9674
.0064	1.2066	.9076	.0070	1.1084	.9099	.0128	1.1522	.9284	.0130	1.1283	.9312	.0221	1.0780	.9672
.0060	1.2010	.9067	.0063	1.0816	.9060	.0116	1.1362	.9259	.0120	1.1107	.9284	.0220	1.0745	.9667
.0058	1.1910	.9050	.0058	1.0623	.9033	.0107	1.1235	.9240	.0109	1.0938	.9259	.0206	1.0777	.9671
.0052	1.1746	.9025	.0051	1.0309	.8990	.0100	1.1072	.9215	.0100	1.0727	.9228	.0201	1.0766	.9670
.0050	1.1672	.9013	.0045	1.0088	.8961	.0090	1.0769	.9170	.0094	1.0555	.9204	.0200	1.0762	.9669
.0044	1.1473	.8982	.0040	.9721	.8914	.0082	1.0561	.9141	.0087	1.0270	.9164	.0197	1.0732	.9665
.0041	1.1312	.8958	.0032	.9411	.8876	.0078	1.0410	.9120	.0078	1.0027	.9131	.0185	1.0731	.9664
.0038	1.1060	.8922	.0028	.9136	.8844	.0065	1.0036	.9069	.0070	.9789	.9100	.0175	1.0670	.9655
.0035	1.0968	.8908	.0023	.8845	.8811	.0049	.9304	.8988	.0061	.9495	.9063	.0160	1.0530	.9635
.0034	1.0845	.8891	.0019	.8493	.8773	.0043	.9202	.8965	.0048	.9183	.9026	.0147	1.0402	.9616
.0030	1.0596	.8856	.0010	.7857	.8709	.0039	.8963	.8938	.0039	.8859	.8988	.0138	1.0204	.9587
.0029	1.0359	.8821	.0008	.7378	.8665	.0025	.8561	.8891	.0031	.8483	.8946	.0128	1.0035	.9564
.0026	1.0345	.8822	.0006	.6876	.8622	.0020	.8101	.8845	.0024	.8189	.8913	.0118	.9795	.9531
.0024	1.0175	.8794				.0015	.7796	.8815	.0018	.7830	.8880	.0104	.9469	.9488
.0020	.9972	.8774				.0012	.7509	.8788	.0012	.7524	.8850	.0094	.9169	.9451
.0018	.9636	.8733				.0004	.6551	.8705	.0004	.6575	.8768	.0080	.8853	.9413
.0015	.9238	.8686										.0071	.8565	.9379
.0013	.8861	.8644										.0063	.8331	.9353
.0009	.8485	.8604										.0054	.8014	.9319
.0006	.7813	.8538										.0046	.7780	.9286
												.0039	.7450	.9262
												.0033	.7210	.9240
												.0027	.7009	.9221
												.0022	.6766	.9200
												.0016	.6432	.9172
												.0013	.6233	.9156
												.0011	.5894	.9130
												.0008	.5558	.9106
												.0004	.5140	.9078

GP11-0232-67

TABLE 5. — Continued.

X/C = 0.950U RUN 112

z/c	u/u_∞	ρ/ρ_∞
.0413	1.0022	.9965
.0381	1.0012	.9964
.0350	1.0014	.9964
.0331	1.0006	.9963
.0308	1.0012	.9964
.0292	1.0004	.9963
.0279	.9986	.9960
.0266	.9984	.9960
.0250	.9988	.9960
.0228	.9962	.9954
.0209	.9849	.9941
.0196	.9717	.9922
.0181	.9439	.9884
.0174	.9232	.9857
.0153	.8958	.9822
.0138	.8557	.9773
.0122	.8237	.9736
.0111	.7738	.9684
.0096	.7411	.9648
.0083	.6986	.9607
.0071	.6539	.9567
.0062	.6232	.9541
.0056	.6038	.9525
.0046	.5744	.9502
.0041	.5346	.9475
.0034	.5147	.9460
.0028	.4855	.9441
.0021	.4519	.9421
.0013	.4115	.9398
.0010	.3774	.9381
.0006	.3560	.9371

X/C = 1.000U RUN 114

z/c	u/u_∞	ρ/ρ_∞
.0404	.9386	1.0189
.0379	.9380	1.0188
.0351	.9378	1.0188
.0332	.9376	1.0188
.0314	.9360	1.0186
.0295	.9330	1.0182
.0278	.9262	1.0173
.0262	.9177	1.0161
.0248	.8927	1.0129
.0238	.8780	1.0111
.0228	.8569	1.0084
.0219	.8359	1.0059
.0206	.8177	1.0038
.0196	.7919	1.0008
.0186	.7674	.9982
.0178	.7427	.9956
.0167	.7224	.9935
.0159	.6946	.9908
.0145	.6614	.9878
.0138	.6561	.9873
.0129	.6391	.9841
.0128	.5949	.9821
.0120	.5799	.9809
.0114	.5584	.9793
.0109	.5346	.9775
.0102	.5127	.9760
.0092	.4728	.9734
.0080	.4368	.9712
.0073	.4064	.9695
.0065	.3574	.9671
.0056	.3337	.9660
.0042	.2745	.9637
.0031	.2292	.9622
.0027	.2090	.9616
.0018	.1836	.9610
.0010	.1575	.9604
.0009	.1575	.9604

X/C = 0.300L RUN 100

z/c	u/u_∞	ρ/ρ_∞
.0143	1.0391	.9825
.0108	1.0389	.9855
.0090	1.0395	.9856
.0078	1.0395	.9856
.0068	1.0395	.9856
.0060	1.0387	.9854
.0053	1.0381	.9854
.0048	1.0358	.9850
.0045	1.0333	.9846
.0043	1.0309	.9843
.0038	1.0246	.9834
.0032	1.0085	.9810
.0031	.9944	.9781
.0026	.9893	.9783
.0023	.9659	.9751
.0018	.9414	.9719
.0016	.9297	.9704
.0014	.8995	.9666
.0010	.8563	.9614
.0007	.8180	.9571
.0004	.7698	.9519

X/C = 0.500L RUN 88

z/c	u/u_∞	ρ/ρ_∞
.0156	1.0757	.9719
.0135	1.0756	.9719
.0120	1.0756	.9719
.0105	1.0754	.9719
.0095	1.0757	.9719
.0090	1.0754	.9719
.0081	1.0754	.9719
.0076	1.0754	.9719
.0071	1.0728	.9715
.0062	1.0660	.9705
.0057	1.0550	.9688
.0054	1.0492	.9680
.0048	1.0456	.9674
.0044	1.0243	.9644
.0042	1.0089	.9622
.0038	.9993	.9608
.0033	.9846	.9590
.0029	.9660	.9563
.0027	.9578	.9553
.0025	.9375	.9526
.0022	.9180	.9502
.0019	.9060	.9487
.0017	.8835	.9460
.0012	.8539	.9426
.0010	.8139	.9381
.0006	.7657	.9331

X/C = 0.600L RUN 90

z/c	u/u_∞	ρ/ρ_∞
.0156	1.0321	.9836
.0136	1.0353	.9837
.0119	1.0353	.9837
.0113	1.0349	.9836
.0103	1.0347	.9837
.0094	1.0337	.9837
.0083	1.0336	.9834
.0077	1.0322	.9832
.0068	1.0253	.9822
.0062	1.0111	.9802
.0056	.9950	.9779
.0052	.9754	.9752
.0045	.9602	.9731
.0042	.9424	.9708
.0038	.9319	.9694
.0035	.9118	.9668
.0032	.8958	.9649
.0028	.8802	.9630
.0026	.8575	.9603
.0023	.8392	.9582
.0018	.8083	.9548
.0015	.7831	.9521
.0009	.7418	.9479
.0006	.6992	.9438
.0004	.6558	.9400

GP11-0232-68

X/C = 0.650L RUN 92

z/c	u/u_∞	ρ/ρ_∞
.0255	.9651	1.0099
.0224	.9645	1.0098
.0207	.9647	1.0099
.0190	.9634	1.0097
.0173	.9645	1.0098
.0160	.9634	1.0097
.0150	.9640	1.0098
.0139	.9647	1.0099
.0128	.9647	1.0099
.0120	.9651	1.0099
.0111	.9640	1.0098
.0102	.9626	1.0096
.0090	.9574	1.0088
.0081	.9424	1.0068
.0075	.9269	1.0047
.0071	.9189	1.0036
.0066	.8976	1.0009
.0061	.8796	.9986
.0053	.8565	.9958
.0048	.8280	.9924
.0043	.8003	.9892
.0040	.7805	.9877
.0036	.7729	.9862
.0032	.7512	.9839
.0030	.7240	.9812
.0026	.7046	.9793
.0024	.6834	.9773
.0023	.6977	.9777
.0019	.6913	.9744
.0014	.5959	.9697
.0008	.5084	.9633

X/C = 0.750L RUN 94

z/c	u/u_∞	ρ/ρ_∞
.0309	.8151	1.0586
.0276	.8161	1.0588
.0245	.8154	1.0587
.0228	.8164	1.0588
.0211	.8156	1.0587
.0196	.8150	1.0587
.0178	.8151	1.0586
.0160	.8139	1.0585
.0142	.8009	1.0569
.0131	.7794	1.0544
.0120	.7540	1.0516
.0111	.7218	1.0481
.0103	.6988	1.0457
.0098	.6761	1.0435
.0090	.6397	1.0400
.0081	.6053	1.0370
.0077	.5830	1.0351
.0065	.5357	1.0314
.0058	.4919	1.0282
.0052	.4559	1.0258
.0041	.4029	1.0227
.0033	.3745	1.0211
.0022	.3187	1.0185
.0013	.2873	1.0172
.0010	.2743	1.0167
.0009	.2408	1.0158
.0006	.2367	1.0154
.0004	.2398	1.0155

X/C = 0.910L RUN 96

z/c	u/u_∞	ρ/ρ_∞
.0384	.7463	1.0819
.0353	.7461	1.0819
.0331	.7463	1.0819
.0310	.7463	1.0819
.0286	.7463	1.0819
.0263	.7461	1.0819
.0248	.7463	1.0819
.0232	.7416	1.0814
.0215	.7302	1.0801
.0199	.7119	1.0781
.0188	.6893	1.0758
.0173	.6640	1.0732
.0162	.6446	1.0713
.0152	.6161	1.0687
.0140	.5887	1.0662
.0124	.5457	1.0627
.0108	.5061	1.0596
.0090	.4602	1.0564
.0074	.4247	1.0541
.0061	.3882	1.0520
.0050	.3665	1.0508
.0043	.3512	1.0501
.0031	.3286	1.0490
.0021	.3157	1.0484
.0011	.3024	1.0478
.0008	.2850	1.0471
.0009	.2875	1.0472
.0006	.2699	1.0465
.0005	.2690	1.0464

X/C = 1.000L RUN 98

z/c	u/u_∞	ρ/ρ_∞
.0340	.8984	1.0311
.0307	.9000	1.0314
.0282	.8993	1.0313
.0259	.8996	1.0313
.0237	.8984	1.0311
.0219	.8980	1.0311
.0203	.8948	1.0307
.0185	.8885	1.0298
.0168	.8784	1.0285
.0156	.8657	1.0269
.0139	.8496	1.0249
.0129	.8393	1.0226
.0113	.8177	1.0205
.0099	.7948	1.0184
.0089	.7793	1.0167
.0071	.7502	1.0135
.0060	.7400	1.0124
.0048	.7283	1.0112
.0040	.7127	1.0096
.0033	.7119	1.0095
.0025	.7027	1.0086
.0022	.6976	1.0081
.0018	.6947	1.0078
.0013	.6895	1.0073
.0011	.6827	1.0067
.0009	.6714	1.0056
.0004	.6147	1.0005

X/C = 1.000L RUN 120

z/c	u/u_∞	ρ/ρ_∞
.0366	.9020	1.0315
.0321	.9024	1.0316
.0287	.9009	1.0314
.0250	.9015	1.0315
.0227	.9004	1.0314
.0202	.8989	1.0311
.0181	.8957	1.0307
.0154	.8844	1.0292
.0137	.8682	1.0271
.0117	.8431	1.0240
.0100	.8152	1.0207
.0083	.7857	1.0173
.0069	.7674	1.0153
.0050	.7393	1.0123
.0037	.7243	1.0108
.0032	.7194	1.0103
.0022	.7063	1.0090
.0015	.6952	1.0079
.0005	.6828	1.0067

GP11-0232-69

TABLE 5. — Continued.

X/C = 1.050 RUN 115			X/C = 1.100 RUN 116			X/C = 1.200 RUN 118			X/C = .300U RUN 4			X/C = .400U RUN 24		
z/c	u/u_∞	ρ/ρ_∞	z/c	u/u_∞	ρ/ρ_∞	z/c	u/u_∞	ρ/ρ_∞	z/c	u/u_∞	ρ/ρ_∞	z/c	u/u_∞	ρ/ρ_∞
.0447	.9279	1.0224	.0306	.9319	1.0214	.0268	.9387	1.0188	.0090	1.4447	.6738	.0118	1.4291	.6826
.0363	.9285	1.0225	.0267	.9319	1.0214	.0196	.9392	1.0188	.0079	1.4457	.6741	.0101	1.4314	.6833
.0306	.9277	1.0223	.0229	.9316	1.0214	.0160	.9390	1.0188	.0064	1.4461	.6743	.0092	1.4319	.6834
.0259	.9277	1.0223	.0199	.9319	1.0214	.0129	.9383	1.0187	.0056	1.4466	.6744	.0081	1.4330	.6837
.0232	.9266	1.0222	.0170	.9301	1.0212	.0095	.9364	1.0184	.0050	1.4467	.6744	.0073	1.4331	.6838
.0201	.9222	1.0216	.0137	.9241	1.0203	.0058	.9284	1.0174	.0048	1.4467	.6744	.0060	1.4338	.6840
.0175	.9016	1.0189	.0115	.9174	1.0188	.0038	.9190	1.0161	.0045	1.4468	.6744	.0061	1.4313	.6832
.0147	.8686	1.0147	.0095	.8971	1.0168	.0017	.9001	1.0136	.0042	1.4461	.6742	.0058	1.4275	.6821
.0120	.8417	1.0113	.0080	.8674	1.0130	-.0010	.8702	1.0098	.0038	1.4445	.6738	.0054	1.4226	.6807
.0115	.8141	1.0082	.0065	.8458	1.0103	-.0031	.8386	1.0060	.0036	1.4437	.6735	.0052	1.4175	.6793
.0098	.7772	1.0041	.0046	.8075	1.0058	-.0045	.8193	1.0037	.0033	1.4430	.6733	.0047	1.4070	.6763
.0081	.7362	.9998	.0029	.7713	1.0018	-.0060	.7833	1.0008	.0031	1.4408	.6727	.0043	1.3919	.6724
.0068	.6998	.9962	.0019	.7538	.9999	-.0083	.7480	.9960	.0029	1.4378	.6719	.0040	1.3757	.6678
.0048	.6505	.9916	.0015	.7345	.9979	-.0108	.7108	.9921	.0026	1.4334	.6706	.0037	1.3543	.6622
.0032	.6081	.9880	.0003	.6969	.9942	-.0143	.6716	.9884	.0025	1.4294	.6695	.0033	1.3277	.6555
.0018	.5570	.9840	-.0015	.6593	.9906	-.0169	.6615	.9875	.0023	1.4245	.6681	.0031	1.3159	.6526
.0003	.5151	.9810	-.0041	.6088	.9863	-.0193	.6619	.9875	.0020	1.4145	.6653	.0030	1.2941	.6474
-.0014	.4739	.9783	-.0050	.5847	.9843	-.0219	.6760	.9888	.0019	1.3936	.6597	.0026	1.2620	.6400
-.0022	.4525	.9770	-.0070	.5674	.9830	-.0234	.6904	.9902	.0016	1.3871	.6580	.0023	1.2143	.6296
-.0036	.4414	.9763	-.0090	.5577	.9822	-.0237	.6966	.9908	.0015	1.3424	.6466	.0021	1.1868	.6240
-.0050	.4346	.9759	-.0108	.5662	.9826	-.0253	.7130	.9923	.0013	1.2845	.6329	.0018	1.1471	.6143
-.0056	.4380	.9761	-.0129	.5916	.9849	-.0261	.7209	.9931	.0011	1.2458	.6244	.0014	1.0853	.6031
-.0064	.4458	.9772	-.0149	.6299	.9880	-.0278	.7447	.9955	.0010	1.1762	.6103	.0012	1.0390	.5974
-.0075	.4837	.9789	-.0170	.6828	.9928	-.0296	.7670	.9979	.0009	1.1255	.6010	.0011	1.0135	.5934
-.0086	.5272	.9818	-.0188	.7284	.9973	-.0315	.7922	1.0006	.0007	1.0497	.5882	.0007	.9541	.5846
-.0097	.5723	.9852	-.0204	.7648	1.0011	-.0332	.8204	1.0038	.0005	.9558	.5742			
-.0103	.6030	.9876	-.0218	.7968	1.0046	-.0336	.8479	1.0071						
-.0114	.6429	.9910	-.0246	.8286	1.0083	-.0380	.8726	1.0101						
-.0125	.6910	.9953	-.0264	.8576	1.0118	-.0401	.8935	1.0126						
-.0134	.7208	.9982	-.0290	.8833	1.0150	-.0431	.9121	1.0152						
-.0147	.7606	1.0023	-.0316	.9048	1.0178	-.0457	.9247	1.0169						
-.0161	.7864	1.0051	-.0331	.9210	1.0199	-.0490	.9334	1.0180						
-.0176	.8104	1.0078	-.0387	.9286	1.0209	-.0521	.9368	1.0185						
-.0195	.8338	1.0105	-.0415	.9306	1.0212	-.0552	.9379	1.0186						
-.0215	.8579	1.0134	-.0445	.9306	1.0212	-.0588	.9387	1.0188						
-.0236	.8826	1.0165	-.0481	.9308	1.0212	-.0620	.9381	1.0187						
-.0264	.9052	1.0194	-.0517	.9310	1.0213	-.0664	.9383	1.0187						
-.0291	.9184	1.0211												
-.0310	.9248	1.0220												
-.0350	.9261	1.0221												
-.0381	.9268	1.0222												
-.0416	.9270	1.0223												
-.0453	.9277	1.0223												

GP11-0232-70

X/C - .450U RUN 6			X/C =.600U RUN 8			X/C = .750U RUN 10			X/C = .850U RUN 12			X/C = .900U RUN 14		
z/c	u/u_∞	ρ/ρ_∞	z/c	u/u_∞	ρ/ρ_∞	z/c	u/u_∞	ρ/ρ_∞	z/c	u/u_∞	ρ/ρ_∞	z/c	u/u_∞	ρ/ρ_∞
.0144	1.4272	.6870	.0210	1.1191	.9219	.0252	1.1463	.9018	.0289	1.0888	.9350	.0314	1.0348	.9709
.0118	1.4277	.6871	.0195	1.1180	.9216	.0225	1.1467	.9020	.0261	1.0905	.9354	.0293	1.0354	.9711
.0109	1.4287	.6874	.0174	1.1181	.9216	.0216	1.1470	.9020	.0245	1.0908	.9355	.0274	1.0364	.9714
.0101	1.4263	.6867	.0158	1.1193	.9219	.0201	1.1470	.9020	.0233	1.0908	.9355	.0261	1.0368	.9715
.0093	1.4296	.6877	.0150	1.1194	.9220	.0188	1.1468	.9020	.0223	1.0916	.9357	.0247	1.0375	.9716
.0083	1.4281	.6872	.0143	1.1185	.9217	.0179	1.1468	.9020	.0211	1.0916	.9357	.0234	1.0390	.9720
.0074	1.4285	.6873	.0134	1.1194	.9220	.0169	1.1456	.9017	.0201	1.0904	.9354	.0219	1.0368	.9715
.0070	1.4263	.6867	.0125	1.1185	.9217	.0157	1.1437	.9011	.0196	1.0901	.9353	.0202	1.0347	.9709
.0062	1.4194	.6847	.0116	1.1165	.9210	.0145	1.1362	.8991	.0185	1.0894	.9353	.0192	1.0311	.9700
.0059	1.4195	.6848	.0109	1.1125	.9196	.0133	1.1272	.8967	.0177	1.0863	.9343	.0180	1.0238	.9681
.0055	1.4014	.6808	.0098	.0908	.9144	.0125	1.1156	.8937	.0167	1.0839	.9337	.0168	1.0114	.9650
.0051	1.3911	.6748	.0093	1.0742	.9102	.0119	1.1007	.8897	.0156	1.0751	.9314	.0156	.9967	.9614
.0048	1.3754	.6726	.0089	1.0606	.9068	.0112	1.0880	.8865	.0147	1.0642	.9286	.0144	.9772	.9567
.0045	1.3641	.6696	.0085	1.0439	.9027	.0102	1.0671	.8812	.0134	1.0459	.9239	.0135	.9600	.9527
.0043	1.3502	.6660	.0079	1.0221	.8976	.0096	1.0534	.8779	.0129	1.0200	.9176	.0127	.9408	.9484
.0039	1.3296	.6608	.0075	.9924	.8907	.0085	1.0370	.8734	.0113	1.0058	.9142	.0116	.9202	.9438
.0036	1.3090	.6558	.0067	.9474	.8811	.0075	.9881	.8630	.0104	.9909	.9107	.0107	.8988	.9393
.0034	1.2877	.6507	.0062	.9169	.8749	.0067	.9646	.8580	.0096	.9724	.9066	.0099	.8767	.9347
.0029	1.2606	.6445	.0057	.9016	.8719	.0057	.9357	.8520	.0087	.9494	.9015	.0090	.8532	.9301
.0026	1.2278	.6373	.0053	.8717	.8662	.0052	.9189	.8487	.0081	.9335	.8981	.0079	.8294	.9255
.0024	1.2055	.6326	.0044	.8004	.8537	.0045	.9008	.8452	.0074	.9139	.8940	.0068	.7919	.9186
.0022	1.1878	.6290	.0037	.7754	.8497	.0039	.8865	.8425	.0069	.8970	.8906	.0057	.7694	.9148
.0018	1.1315	.6181	.0036	.7432	.8447	.0031	.8717	.8362	.0063	.8834	.8880	.0051	.7479	.9112
.0014	1.0806	.6106	.0029	.7287	.8425	.0022	.8180	.8304	.0051	.8553	.8826	.0042	.7146	.9059
.0012	1.0558	.6049	.0026	.7137	.8404	.0021	.8058	.8284	.0046	.8363	.8791	.0037	.7018	.9039
.0006	.9707	.5917	.0022	.6759	.8352	.0018	.7895	.8258	.0042	.8234	.8768	.0034	.6940	.9026
			.0020	.6617	.8333	.0013	.7780	.8240	.0037	.8078	.8741	.0028	.6693	.8991
			.0015	.6136	.8273	.0012	.7582	.8209	.0033	.7966	.8722	.0026	.6522	.8967
			.0007	.5618	.8214	.0009	.7197	.8153	.0031	.7813	.8696	.0024	.6420	.8953
			.0004	.6044	.8262				.0027	.7704	.8678	.0020	.6208	.8925
									.0022	.7447	.8637	.0018	.6085	.8909
									.0017	.7310	.8616	.0014	.5814	.8876
									.0011	.6751	.8536	.0011	.5637	.8857
									.0009	.6568	.8511	.0009	.5268	.8813

GP11-0232-71

TABLE 5. — Continued.

X/C = .950U RUN 16			X/C = 1.000U RUN 18			X/C = .300L RUN 26			X/C = .500L RUN 28			X/C = .600L RUN 30		
z/c	u/u_∞	ρ/ρ_∞	z/c	u/u_∞	ρ/ρ_∞	z/c	u/u_∞	ρ/ρ_∞	z/c	u/u_∞	ρ/ρ_∞	z/c	u/u_∞	ρ/ρ_∞
.0361	.9304	1.0239	.0465	.8922	1.0568	.0101	1.0011	.9405	.0156	1.1149	.9235	.0197	1.0350	.9769
.0339	.9318	1.0243	.0444	.8956	1.0574	.0088	1.0012	.9402	.0136	1.1130	.9235	.0172	1.0335	.9770
.0318	.9327	1.0245	.0418	.8967	1.0576	.0079	1.0011	.9405	.0121	1.1153	.9236	.0150	1.0337	.9771
.0303	.9333	1.0247	.0400	.8967	1.0578	.0074	1.0011	.9405	.0106	1.1152	.9235	.0137	1.0341	.9771
.0289	.9344	1.0249	.0382	.8975	1.0580	.0069	1.0005	.9403	.0103	1.1152	.9235	.0126	1.0353	.9770
.0275	.9344	1.0249	.0361	.8980	1.0582	.0066	1.0012	.9405	.0094	1.1155	.9236	.0117	1.0355	.9770
.0260	.9332	1.0246	.0345	.8974	1.0580	.0062	1.0002	.9403	.0085	1.1142	.9233	.0108	1.0355	.9770
.0244	.9500	1.0238	.0328	.8970	1.0579	.0057	1.0074	.9395	.0073	1.1066	.9212	.0099	1.0327	.9763
.0229	.9437	1.0223	.0310	.8937	1.0571	.0051	1.0013	.9370	.0068	1.0987	.9181	.0091	1.0301	.9751
.0214	.9334	1.0203	.0295	.8874	1.0557	.0046	1.0691	.9347	.0064	1.0880	.9163	.0084	1.0208	.9722
.0202	.9210	1.0189	.0278	.8739	1.0525	.0042	1.0587	.9321	.0058	1.0747	.9128	.0074	1.0016	.9685
.0185	.8986	1.0117	.0266	.8607	1.0495	.0039	1.0395	.9272	.0053	1.0580	.9086	.0069	.9885	.9653
.0174	.8808	1.0078	.0253	.8425	1.0455	.0034	1.0190	.9222	.0050	1.0460	.9056	.0063	.9661	.9599
.0161	.8556	1.0024	.0235	.8153	1.0397	.0032	1.0023	.9183	.0048	1.0351	.9030	.0054	.9452	.9552
.0150	.8349	.9980	.0224	.7906	1.0347	.0027	.9757	.9122	.0044	1.0222	.8999	.0048	.9120	.9479
.0138	.8070	.9925	.0200	.7452	1.0259	.0024	.9590	.9083	.0041	1.0046	.8958	.0039	.8791	.9410
.0126	.7751	.9864	.0187	.7205	1.0214	.0022	.9418	.9048	.0036	.9882	.8920	.0035	.8595	.9371
.0114	.7452	.9810	.0175	.6812	1.0146	.0020	.9323	.9027	.0033	.9709	.8882	.0033	.8408	.9334
.0103	.7212	.9768	.0162	.6305	1.0097	.0017	.9118	.8985	.0032	.9600	.8858	.0028	.8124	.9281
.0096	.6960	.9727	.0146	.6066	1.0031	.0016	.8912	.8944	.0028	.9386	.8813	.0024	.7888	.9238
.0088	.6729	.9690	.0130	.5337	.9958	.0013	.8568	.8877	.0023	.9106	.8756	.0020	.7627	.9193
.0080	.6464	.9650	.0116	.5128	.9907	.0011	.8443	.8854	.0020	.8985	.8732	.0017	.7327	.9144
.0069	.6073	.9594	.0106	.4796	.9869	.0008	.8175	.8806	.0018	.8809	.8698	.0013	.7083	.9106
.0061	.5794	.9557	.0094	.4479	.9835	.0007	.7914	.8762	.0015	.8589	.8657	.0012	.6867	.9071
.0052	.5488	.9518	.0081	.4057	.9794	.0005	.7758	.8736	.0012	.8432	.8620	.0008	.6696	.9048
.0043	.5109	.9474	.0070	.3765	.9769				.0011	.8132	.8575	.0002	.6217	.8982
.0036	.4960	.9457	.0056	.3285	.9730				.0007	.7651	.8496			
.0033	.4726	.9432	.0045	.2939	.9706									
.0028	.4480	.9408	.0039	.2743	.9694									
.0023	.4249	.9386	.0028	.2446	.9677									
.0020	.4115	.9374	.0021	.2279	.9668									
.0016	.3921	.9359	.0015	.2195	.9664									
.0013	.3781	.9345	.0013	.2123	.9661									
.0010	.3559	.9328	.0010	.2014	.9656									
.0007	.3393	.9316												

GP11-0232-72

X/C = .650L RUN 32			X/C .750L RUN 34			X/C = .910L RUN 36			X/C = 1.000L RUN 20			X/C = 1.050 RUN 21		
z/c	u/u_∞	ρ/ρ_∞	z/c	u/u_∞	ρ/ρ_∞	z/c	u/u_∞	ρ/ρ_∞	z/c	u/u_∞	ρ/ρ_∞	z/c	u/u_∞	ρ/ρ_∞
.0228	.9250	1.0405	.0377	.8291	1.0968	.0501	.7679	1.1365	.0434	.8677	1.0808	.0418	.8667	1.0694
.0207	.9250	1.0405	.0351	.8281	1.0967	.0466	.7679	1.1365	.0408	.8677	1.0808	.0373	.8694	1.0700
.0189	.9247	1.0404	.0328	.8283	1.0966	.0449	.7674	1.1364	.0382	.8677	1.0808	.0342	.8711	1.0704
.0175	.9254	1.0406	.0310	.8290	1.0970	.0430	.7669	1.1355	.0363	.8673	1.0807	.0322	.8736	1.0710
.0164	.9264	1.0408	.0295	.8298	1.0970	.0412	.7679	1.1365	.0340	.8673	1.0807	.0300	.8748	1.0713
.0149	.9259	1.0407	.0273	.8291	1.0968	.0391	.7662	1.1362	.0320	.8665	1.0805	.0273	.8754	1.0714
.0136	.9248	1.0404	.0254	.8280	1.0966	.0374	.7646	1.1358	.0302	.8631	1.0797	.0244	.8723	1.0707
.0123	.9238	1.0402	.0240	.8232	1.0955	.0355	.7576	1.1344	.0282	.8595	1.0788	.0219	.8631	1.0686
.0115	.9189	1.0390	.0226	.8103	1.0926	.0336	.7488	1.1325	.0260	.8537	1.0775	.0195	.8423	1.0639
.0104	.9026	1.0352	.0214	.7878	1.0878	.0320	.7333	1.1294	.0248	.8470	1.0760	.0176	.8198	1.0590
.0095	.8839	1.0309	.0204	.7654	1.0832	.0304	.7141	1.1256	.0231	.8407	1.0746	.0152	.7833	1.0515
.0087	.8603	1.0257	.0194	.7373	1.0777	.0288	.6900	1.1210	.0211	.8245	1.0711	.0138	.7563	1.0462
.0076	.8236	1.0180	.0185	.7099	1.0725	.0273	.6610	1.1158	.0197	.8065	1.0672	.0117	.7175	1.0390
.0068	.7937	1.0120	.0174	.6768	1.0666	.0258	.6238	1.1093	.0176	.7826	1.0623	.0100	.6808	1.0326
.0061	.7594	1.0055	.0167	.6487	1.0618	.0240	.5809	1.1027	.0154	.7469	1.0553	.0077	.6257	1.0237
.0054	.7317	1.0005	.0157	.6160	1.0566	.0220	.5387	1.0966	.0140	.7301	1.0521	.0063	.5910	1.0186
.0047	.6940	.9941	.0147	.5797	1.0501	.0207	.4981	1.0912	.0130	.7109	1.0486	.0044	.5392	1.0116
.0041	.6632	.9892	.0141	.5580	1.0481	.0192	.4563	1.0862	.0115	.6909	1.0450	.0031	.5063	1.0076
.0035	.6321	.9845	.0132	.5198	1.0430	.0172	.4122	1.0813	.0101	.6722	1.0419	.0013	.4627	1.0026
.0032	.6063	.9808	.0119	.4661	1.0366	.0154	.3585	1.0762	.0089	.6597	1.0389	-.0009	.4297	.9982
.0029	.5766	.9767	.0110	.4232	1.0319	.0135	.3239	1.0733	.0081	.6445	1.0374	-.0023	.4208	.9983
.0025	.5568	.9742	.0098	.3765	1.0275	.0118	.2791	1.0699	.0075	.6357	1.0360	-.0043	.4341	.9996
.0022	.5312	.9710	.0084	.3194	1.0228	.0105	.2457	1.0678	.0066	.6289	1.0350	-.0062	.4711	1.0035
.0018	.4954	.9669	.0067	.2734	1.0176	.0092	.2239	1.0666	.0056	.6155	1.0329	-.0083	.5277	1.0102
.0009	.4374	.9590	.0050	.2433	1.0170	.0075	.1821	1.0645	.0050	.6127	1.0324	-.0103	.5884	1.0183
.0005	.3589	.9540	.0041	.2148	1.0162	.0067	.1600	1.0636	.0044	.6054	1.0314	-.0125	.6295	1.0243
			.0033	.1896	1.0150	.0056	.1352	1.0627	.0040	.6019	1.0309	-.0143	.6550	1.0283
			.0022	.1807	1.0147	.0046	.1110	1.0620	.0034	.5971	1.0302	-.0162	.6776	1.0320
			.0000	.1572	1.0137	.0034	.1020	1.0617	.0028	.5914	1.0294	-.0181	.7017	1.0362
			.0005	.1482	1.0133	.0028	.1004	1.0617	.0025	.5891	1.0291	-.0204	.7278	1.0408
				.1405	1.0132	.0023	.0921	1.0615	.0021	.5858	1.0286	-.0223	.7502	1.0450
						.0015	.0849	1.0614	.0020	.5845	1.0284	-.0243	.7742	1.0497
						.0007	.0682	1.0610	.0018	.5838	1.0283	-.0265	.7964	1.0541
									.0015	.5815	1.0280	-.0288	.8177	1.0586
									.0011	.5774	1.0274	-.0314	.8346	1.0622
									.0007	.5661	1.0258	-.0339	.8503	1.0657
									.0005	.5638	1.0255	-.0360	.8572	1.0673
									.0004	.5611	1.0252	-.0381	.8635	1.0687
												-.0406	.8683	1.0698
												-.0430	.8704	1.0703
												-.0456	.8706	1.0703
												-.0483	.8714	1.0705
												-.0504	.8726	1.0708
												-.0528	.8728	1.0708

GP11-0232-73

TABLE 5. — Continued.

X/C = 1.100 RUN 22			X/C = 1.200 RUN 37		
z/c	u/u_∞	ρ/ρ_∞	z/c	u/u_∞	ρ/ρ_∞
.0356	.8696	1.0672	.0310	.8786	1.0522
.0307	.8739	1.0681	.0273	.8811	1.0527
.0277	.8741	1.0682	.0239	.8834	1.0534
.0253	.8755	1.0682	.0220	.8840	1.0534
.0231	.8755	1.0689	.0201	.8840	1.0534
.0205	.8761	1.0687	.0180	.8844	1.0535
.0179	.8690	1.0670	.0156	.8843	1.0535
.0153	.8547	1.0638	.0135	.8799	1.0525
.0131	.8316	1.0587	.0114	.8711	1.0505
.0106	.7993	1.0519	.0096	.8625	1.0485
.0091	.7724	1.0465	.0076	.8459	1.0448
.0072	.7389	1.0402	.0056	.8247	1.0403
.0049	.6922	1.0310	.0037	.8006	1.0353
.0031	.6592	1.0264	.0017	.7727	1.0268
.0012	.6215	1.0205	-.0004	.7446	1.0245
-.0007	.5848	1.0152	-.0025	.7137	1.0189
-.0024	.5539	1.0110	-.0041	.6896	1.0148
-.0047	.5304	1.0080	-.0061	.6705	1.0116
-.0062	.5264	1.0072	-.0076	.6520	1.0087
-.0067	.5261	1.0072	-.0089	.6410	1.0069
-.0083	.5284	1.0070	-.0107	.6283	1.0050
-.0099	.5427	1.0096	-.0122	.6281	1.0050
-.0118	.5643	1.0124	-.0139	.6239	1.0044
-.0140	.5940	1.0165	-.0154	.6242	1.0044
-.0160	.6266	1.0213	-.0168	.6302	1.0053
-.0181	.6588	1.0263	-.0189	.6443	1.0075
-.0199	.6832	1.0304	-.0209	.6608	1.0101
-.0221	.7109	1.0351	-.0229	.6784	1.0129
-.0243	.7364	1.0391	-.0249	.6989	1.0163
-.0268	.7620	1.0445	-.0269	.7160	1.0193
-.0287	.7836	1.0487	-.0291	.7371	1.0231
-.0310	.8020	1.0525	-.0308	.7532	1.0261
-.0333	.8201	1.0563	-.0326	.7695	1.0291
-.0358	.8390	1.0603	-.0345	.7877	1.0327
-.0380	.8503	1.0628	-.0364	.8003	1.0352
-.0411	.8591	1.0648	-.0385	.8178	1.0388
-.0435	.8642	1.0662	-.0408	.8345	1.0424
-.0461	.8693	1.0671	-.0427	.8469	1.0451
-.0485	.8714	1.0676	-.0449	.8549	1.0468
-.0514	.8737	1.0681	-.0467	.8634	1.0487
-.0539	.8745	1.0683	-.0491	.8707	1.0504
			-.0518	.8764	1.0517
			-.0541	.8799	1.0525
			-.0574	.8837	1.0533
			-.0605	.8864	1.0540
			-.0633	.8869	1.0541
			-.0666	.8882	1.0544
			-.0703	.8882	1.0544

GP11-0232-74

X/C = .300U RUN 125			X/C = .450U RUN 123			X/C = .650U RUN 127			X/C = .800U RUN 129			X/C = .900U RUN 131		
z/c	u/u_∞	ρ/ρ_∞	z/c	u/u_∞	ρ/ρ_∞	z/c	u/u_∞	ρ/ρ_∞	z/c	u/u_∞	ρ/ρ_∞	z/c	u/u_∞	ρ/ρ_∞
.0074	1.4746	.6528	.0104	1.4608	.6601	.0215	1.1122	.9195	.0248	1.1153	.9173	.0361	1.0316	.9716
.0058	1.4761	.6532	.0091	1.4626	.6606	.0191	1.1123	.9195	.0217	1.1159	.9175	.0324	1.0361	.9727
.0045	1.4761	.6535	.0082	1.4636	.6609	.0170	1.1122	.9195	.0199	1.1158	.9175	.0300	1.0391	.9733
.0038	1.4741	.6528	.0071	1.4646	.6612	.0153	1.1125	.9195	.0185	1.1152	.9173	.0273	1.0396	.9736
.0036	1.4740	.6526	.0065	1.4649	.6613	.0144	1.1126	.9196	.0176	1.1145	.9171	.0251	1.0402	.9738
.0033	1.4756	.6531	.0057	1.4626	.6606	.0135	1.1118	.9194	.0163	1.1132	.9168	.0226	1.0400	.9738
.0032	1.4753	.6530	.0052	1.4576	.6592	.0123	1.1091	.9186	.0150	1.1089	.9156	.0206	1.0376	.9731
.0030	1.4745	.6527	.0048	1.4558	.6587	.0112	1.0994	.9161	.0138	1.0977	.9126	.0189	1.0332	.9720
.0028	1.4727	.6522	.0045	1.4496	.6569	.0104	1.0850	.9123	.0129	1.0892	.9104	.0176	1.0265	.9702
.0026	1.4698	.6514	.0043	1.4413	.6549	.0096	1.0546	.9046	.0121	1.0763	.9070	.0158	1.0085	.9657
.0026	1.4663	.6504	.0040	1.4321	.6519	.0091	1.0220	.8967	.0113	1.0595	.9028	.0145	.9896	.9610
.0025	1.4654	.6501	.0037	1.4250	.6499	.0084	1.0190	.8960	.0106	1.0392	.8978	.0132	.9656	.9542
.0024	1.4585	.6482	.0034	1.4077	.6452	.0087	.9816	.8875	.0097	1.0182	.8928	.0121	.9403	.9464
.0023	1.4384	.6426	.0033	1.3849	.6392	.0084	.9786	.8868	.0084	.9818	.8845	.0108	.9074	.9421
.0023	1.4497	.6457	.0029	1.3656	.6343	.0078	.9269	.8758	.0077	.9570	.8791	.0097	.8816	.9367
.0021	1.4357	.6419	.0028	1.3411	.6282	.0075	.9544	.8815	.0067	.9253	.8723	.0085	.8463	.9296
.0018	1.4033	.6333	.0026	1.3079	.6203	.0066	.8958	.8696	.0061	.9041	.8683	.0074	.8134	.9233
.0016	1.3618	.6230	.0024	1.2842	.6137	.0060	.8563	.8621	.0052	.8732	.8623	.0062	.7837	.9180
.0014	1.2970	.6080	.0021	1.2642	.6080	.0056	.8435	.8598	.0042	.8362	.8556	.0048	.7470	.9117
.0013	1.2631	.6007	.0021	1.2638	.6104	.0053	.8311	.8542	.0037	.8142	.8518	.0034	.7061	.9051
.0011	1.1366	.5766	.0020	1.2473	.6070	.0048	.7855	.8499	.0030	.7856	.8470	.0031	.7009	.9043
.0009	1.0930	.5692	.0017	1.2050	.5983	.0042	.7264	.8408	.0020	.7511	.8415	.0024	.6735	.9006
.0008	.9021	.5423	.0013	1.1682	.5912	.0037	.7260	.8407	.0014	.7333	.8389	.0022	.6721	.9001
			.0011	1.0878	.5770	.0034	.6734	.8333	.0011	.7148	.8361	.0016	.6544	.8975
			.0009	1.0075	.5644	.0027	.6266	.8273	.0008	.6733	.8252	.0015	.6232	.8935
						.0026	.6183	.8262	.0005	.6534		.0013	.6085	.8913
						.0021	.5854	.8224				.0011	.6020	.8905
						.0019	.5798	.8218				.0007	.5516	.8844
						.0015	.5495	.8165				.0006	.5416	.8832
						.0013	.5083	.8143				.0005	.5224	.8811
						.0010	.5196	.8134						
						.0007	.4678	.8105						
						.0004	.4595	.8098						

GP11-0232-75

TABLE 5. — Continued.

X/C = .950U RUN 133			X/C = 1.000U RUN 135			X/C =.300L RUN 150			X/C = .500L RUN 144			X/C = .600L RUN 146		
z/c	u/u_∞	ρ/ρ_∞	z/c	u/u_∞	ρ/ρ_∞	z/c	u/u_∞	ρ/ρ_∞	z/c	u/u_∞	ρ/ρ_∞	z/c	u/u_∞	ρ/ρ_∞
.0381	.9954	.9966	.0453	.8888	1.0595	.0115	1.0568	.9557	.0150	1.0911	.9397	.0151	1.0262	.9820
.0341	1.0000	.9978	.0411	.8951	1.0610	.0083	1.0575	.9549	.0117	1.0912	.9398	.0137	1.0263	.9821
.0316	1.0025	.9984	.0388	.8965	1.0613	.0075	1.0569	.9558	.0101	1.0911	.9397	.0119	1.0273	.9823
.0293	1.0021	.9983	.0366	.8990	1.0619	.0066	1.0567	.9557	.0088	1.0906	.9396	.0107	1.0269	.9822
.0277	1.0025	.9984	.0342	.8994	1.0620	.0058	1.0551	.9553	.0076	1.0891	.9392	.0102	1.0274	.9823
.0260	1.0015	.9981	.0324	.8989	1.0618	.0050	1.0485	.9535	.0068	1.0828	.9375	.0096	1.0266	.9821
.0244	.9981	.9975	.0311	.8969	1.0614	.0047	1.0391	.9511	.0067	1.0810	.9370	.0090	1.0254	.9818
.0226	.9923	.9958	.0292	.8884	1.0594	.0041	1.0226	.9468	.0062	1.0738	.9351	.0082	1.0218	.9809
.0203	.9829	.9935	.0274	.8764	1.0566	.0036	1.0056	.9426	.0039	1.0774	.9347	.0078	1.0180	.9799
.0190	.9652	.9891	.0256	.8582	1.0525	.0034	.9794	.9362	.0035	1.0519	.9320	.0074	1.0173	.9777
.0171	.9436	.9840	.0239	.8367	1.0478	.0029	.9335	.9302	.0052	1.0564	.9306	.0070	.9995	.9752
.0158	.9152	.9774	.0222	.8201	1.0443	.0026	.8964	.9224	.0043	1.0324	.9245	.0065	.9841	.9714
.0144	.8901	.9719	.0204	.7855	1.0372	.0021	.8586	.9177	.0040	1.0136	.9200	.0056	.9538	.9652
.0129	.8569	.9649	.0184	.7387	1.0283	.0017	.8134	.9100	.0035	.9970	.9160	.0052	.9293	.9586
.0112	.8188	.9574	.0168	.7006	1.0216	.0015	.7902	.9015	.0030	.9807	.9122	.0046	.9114	.9547
.0096	.7801	.9518	.0146	.6485	1.0130	.0014	.7461	.8938	.0027	.9601	.9076	.0044	.8907	.9521
.0084	.7597	.9448	.0126	.6006	1.0059	.0013	.7902	.8973	.0024	.9405	.9033	.0038	.8733	.9466
.0068	.7151	.9390	.0108	.5413	.9980	.0011	.7778	.8951	.0023	.9162	.8982	.0033	.8418	.9403
.0054	.6770	.9331	.0085	.4882	.9916	.0010	.7598	.8921	.0016	.8869	.8922	.0028	.8022	.9328
.0041	.6340	.9268	.0067	.4342	.9859	.0009	.7487	.8902	.0012	.8443	.8841	.0025	.7795	.9287
.0033	.5978	.9219	.0057	.3975	.9825	.0006	.7525	.8909	.0009	.7849	.8736	.0019	.7374	.9249
.0029	.5980	.9220	.0050	.3756	.9806				.0007	.7691	.8709	.0016	.7329	.9208
.0027	.5819	.9199	.0041	.3407	.9777				.0006	.7512	.8681	.0013	.7058	.9165
.0022	.5681	.9182	.0036	.3047	.9753				.0004	.7235	.8637	.0010	.6668	.9106
.0020	.5563	.9167	.0023	.2812	.9736							.0008	.6192	.9040
.0016	.5366	.9144	.0016	.2546	.9720							.0006	.5497	.9015
.0011	.5220	.9128	.0011	.2307	.9708							.0006	.5899	.9002
.0009	.5003	.9104	.0005	.2156	.9700									
.0005	.4868	.9090												

GP11-0232-76

X/C = .750L RUN 148			X/C = .910L RUN 142			X/C = 1.000L RUN 137			X/C = 1.100 RUN 140			X/C = 1.200 RUN 138		
z/c	u/u_∞	ρ/ρ_∞	z/c	u/u_∞	ρ/ρ_∞	z/c	u/u_∞	ρ/ρ_∞	z/c	u/u_∞	ρ/ρ_∞	z/c	u/u_∞	ρ/ρ_∞
.0296	.8160	1.1101	.0471	.7420	1.1513	.0426	.8633	1.0762	.0338	.8590	1.0697	.0260	.8761	1.0554
.0266	.8168	1.1103	.0435	.7418	1.1512	.0396	.8639	1.0763	.0292	.8712	1.0725	.0238	.8766	1.0555
.0248	.8172	1.1104	.0400	.7420	1.1513	.0365	.8607	1.0756	.0265	.8730	1.0730	.0197	.8805	1.0564
.0228	.8174	1.1105	.0371	.7410	1.1511	.0338	.8629	1.0761	.0240	.8703	1.0724	.0231	.8752	1.0553
.0215	.8166	1.1102	.0343	.7394	1.1507	.0311	.8637	1.0762	.0220	.8682	1.0719	.0204	.8777	1.0558
.0189	.8079	1.1083	.0317	.7323	1.1493	.0288	.8629	1.0761	.0203	.8636	1.0708	.0173	.8817	1.0567
.0191	.8016	1.1069	.0294	.7204	1.1469	.0266	.8569	1.0747	.0177	.8490	1.0675	.0147	.8817	1.0567
.0184	.7862	1.1036	.0272	.7000	1.1428	.0243	.8519	1.0736	.0157	.8340	1.0641	.0119	.8724	1.0557
.0175	.7681	1.0998	.0251	.6647	1.1362	.0224	.8439	1.0718	.0135	.8068	1.0583	.0093	.8696	1.0539
.0165	.7290	1.0920	.0226	.6164	1.1278	.0205	.8324	1.0693	.0115	.7715	1.0511	.0071	.8568	1.0511
.0155	.7001	1.0862	.0204	.5601	1.1190	.0189	.8171	1.0660	.0092	.7370	1.0444	.0050	.8453	1.0486
.0143	.6513	1.0770	.0183	.5074	1.1116	.0172	.7973	1.0619	.0077	.7034	1.0383	.0029	.8194	1.0430
.0134	.6165	1.0723	.0159	.4493	1.1043	.0154	.7807	1.0585	.0053	.6561	1.0303	.0006	.7890	1.0349
.0124	.5735	1.0657	.0134	.3866	1.0976	.0133	.7472	1.0520	.0032	.6091	1.0230	-.0018	.7575	1.0308
.0118	.5359	1.0632	.0116	.3456	1.0938	.0113	.7232	1.0479	.0012	.5806	1.0189	-.0045	.7165	1.0234
.0112	.5272	1.0543	.0097	.3044	1.0908	.0102	.7017	1.0437	-.0009	.5449	1.0141	-.0068	.6966	1.0200
.0104	.4982	1.0256	.0076	.2668	1.0877	.0086	.6895	1.0416	-.0015	.5438	1.0139	-.0092	.6718	1.0159
.0094	.4586	1.0490	.0060	.2412	1.0859	.0070	.6777	1.0396	-.0031	.5231	1.0113	-.0116	.6484	1.0121
.0087	.4148	1.0463	.0043	.2088	1.0843	.0067	.6652	1.0376	-.0056	.5248	1.0115	-.0135	.6406	1.0110
.0071	.3419	1.0396	.0030	.1928	1.0838	.0059	.6524	1.0355	-.0081	.5457	1.0142	-.0138	.6426	1.0113
.0056	.2852	1.0353	.0021	.1811	1.0829	.0053	.6485	1.0349	-.0104	.5798	1.0188	-.0164	.6379	1.0105
.0046	.2373	1.0323	.0014	.1703	1.0825	.0047	.6396	1.0335	-.0133	.6252	1.0255	-.0185	.6446	1.0116
.0036	.2141	1.0311	.0005	.1478	1.0816	.0044	.6414	1.0338	-.0160	.6733	1.0331	-.0211	.6991	1.0188
.0028	.1803	1.0295	.0003	.1431	1.0814	.0037	.6310	1.0322	-.0185	.7096	1.0394	-.0244	.6863	1.0192
.0019	.1728	1.0292				.0028	.6245	1.0311	-.0211	.7475	1.0448	-.0276	.7292	1.0242
.0014	.1443	1.0281				.0025	.6283	1.0317	-.0234	.7678	1.0502	-.0306	.7476	1.0290
.0005	.1283	1.0276				.0023	.6242	1.0311	-.0261	.7923	1.0553	-.0332	.7745	1.0341
						.0022	.6217	1.0307	-.0295	.8171	1.0605	-.0362	.8019	1.0395
						.0017	.6189	1.0303	-.0321	.8557	1.0645	-.0392	.8257	1.0444
						.0013	.6153	1.0298	-.0358	.8494	1.0676	-.0422	.8446	1.0484
						.0010	.6148	1.0297	-.0388	.8573	1.0694	-.0458	.8624	1.0523
						.0008	.6035	1.0281	-.0425	.8630	1.0707	-.0488	.8734	1.0548
						.0007	.5909	1.0262	-.0455	.8670	1.0710	-.0520	.8800	1.0563
									-.0486	.8677	1.0717	-.0546	.8841	1.0572
									-.0515	.8678	1.0718	-.0580	.8870	1.0579
									-.0546	.8690	1.0721	-.0625	.8891	1.0584
												-.0668	.8894	1.0585

GP11-0232-77

TABLE 5. — Continued.

X/C = .500L RUN 40			X/C = .600L RUN 43			X/C = .750L RUN 45			X/C = .910L RUN 47			X/C = 1.000L RUN 49		
z/c	u/u_∞	ρ/ρ_∞	z/c	u/u_∞	ρ/ρ_∞	z/c	u/u_∞	ρ/ρ_∞	z/c	u/u_∞	ρ/ρ_∞	z/c	u/u_∞	ρ/ρ_∞
.0175	1.1440	.9038	.0200	1.0444	.9704	.0374	.8678	1.0803	.0573	.7967	1.1201	.0512	.8607	1.0856
.0152	1.1431	.9036	.0181	1.0449	.9706	.0339	.8678	1.0803	.0539	.7967	1.1201	.0480	.8608	1.0856
.0141	1.1446	.9040	.0164	1.0449	.9706	.0320	.8676	1.0803	.0507	.7964	1.1200	.0451	.8608	1.0856
.0130	1.1434	.9036	.0155	1.0449	.9706	.0302	.8662	1.0804	.0479	.7967	1.1201	.0420	.8608	1.0856
.0123	1.1441	.9038	.0142	1.0449	.9705	.0272	.8657	1.0788	.0457	.7896	1.1186	.0400	.8597	1.0854
.0114	1.1435	.9037	.0130	1.0452	.9706	.0278	.8664	1.0796	.0435	.7876	1.1181	.0376	.8604	1.0855
.0107	1.1431	.9036	.0121	1.0449	.9706	.0259	.8538	1.0771	.0409	.7834	1.1173	.0354	.8565	1.0846
.0092	1.1386	.9023	.0106	1.0415	.9697	.0242	.8283	1.0715	.0382	.7679	1.1140	.0331	.8557	1.0844
.0086	1.1334	.9009	.0095	1.0304	.9668	.0236	.8014	1.0671	.0361	.7579	1.1120	.0304	.8518	1.0835
.0078	1.1212	.8976	.0084	1.0082	.9612	.0224	.7796	1.0612	.0339	.7231	1.1055	.0283	.8425	1.0814
.0070	1.1020	.8926	.0078	.9869	.9549	.0213	.7453	1.0546	.0320	.6990	1.1006	.0258	.8329	1.0782
.0066	1.0851	.8883	.0067	.9522	.9478	.0202	.7047	1.0471	.0299	.6661	1.0947	.0236	.8207	1.0766
.0062	1.0758	.8860	.0059	.9187	.9405	.0194	.6797	1.0428	.0278	.6149	1.0863	.0219	.8093	1.0717
.0055	1.0521	.8802	.0051	.8883	.9338	.0182	.6425	1.0340	.0261	.5827	1.0813	.0204	.7897	1.0649
.0051	1.0388	.8770	.0043	.8460	.9234	.0175	.5963	1.0294	.0241	.5178	1.0724	.0188	.7738	1.0667
.0046	1.0256	.8740	.0036	.8098	.9180	.0163	.5232	1.0237	.0215	.4381	1.0652	.0173	.7547	1.0429
.0046	1.0133	.8717	.0030	.7776	.9128	.0151	.4403	1.0169	.0192	.3882	1.0579	.0150	.7264	1.0384
.0042	1.0016	.8685	.0025	.7508	.9083	.0136	.4552	1.0120	.0175	.3512	1.0546	.0148	.7161	1.0296
.0038	.9836	.8646	.0024	.7247	.9040	.0122	.3892	1.0064	.0161	.3234	1.0524	.0133	.6971	1.0271
.0035	.9650	.8608	.0017	.7047	.9008	.0115	.3536	1.0024	.0144	.2764	1.0483	.0116	.6708	1.0476
.0033	.9551	.8585	.0014	.6766	.8967	.0095	.2490	.9983	.0126	.2221	1.0458	.0104	.6430	1.0430
.0031	.9437	.8562	.0009	.6278	.8899	.0085	.2728	.9966	.0110	.1826	1.0439	.0091	.6300	1.0409
.0026	.9209	.8516	.0005	.5741	.8832	.0074	.2284	.9941	.0089	.1294	1.0418	.0078	.6110	1.0380
.0022	.8993	.8475				.0057	.1838	.9920	.0074	.0747	1.0406	.0066	.5878	1.0345
.0018	.8740	.8428				.0044	.1499	.9907	.0057	0.0000	1.0400	.0051	.5608	1.0307
.0017	.8590	.8401				.0035	.1146	.9897	.0043	0.0000	1.0400	.0036	.5484	1.0291
.0015	.8419	.8370				.0027	.1066	.9895	.0027	0.0000	1.0400	.0028	.5430	1.0284
.0012	.8046	.8308				.0018	.1036	.9894	.0015	0.0000	1.0400	.0023	.5434	1.0284
.0009	.7822	.8288				.0014	.0928	.9892	.0005	0.0000	1.0400	.0018	.5417	1.0282
.0005	.7448	.8222				.0012	.1049	.9895				.0015	.5345	1.0272
						.0008	.0890	.9891				.0010	.5351	1.0273
												.0006	.5208	1.0255
												.0005	.5127	1.0245
												.0004	.5020	1.0232

GP11-0232-78

X/C = .500L RUN 52			X/C = .600L RUN 54			X/C = .750L RUN 56			X/C = .910L RUN 58			X/C = 1.000L RUN 60		
z/c	u/u_∞	ρ/ρ_∞	z/c	u/u_∞	ρ/ρ_∞	z/c	u/u_∞	ρ/ρ_∞	z/c	u/u_∞	ρ/ρ_∞	z/c	u/u_∞	ρ/ρ_∞
.0150	1.1460	.9035	.0178	1.0491	.9684	.0343	.8550	1.0886	.0661	.7854	1.1268	.0581	.8688	1.0801
.0126	1.1460	.9035	.0151	1.0491	.9684	.0318	.8554	1.0837	.0603	.7858	1.1270	.0544	.8684	1.0800
.0114	1.1460	.9035	.0130	1.0484	.9683	.0303	.8555	1.0807	.0588	.7860	1.1271	.0515	.8677	1.0799
.0102	1.1459	.9034	.0126	1.0486	.9684	.0291	.8542	1.0884	.0559	.7861	1.1271	.0486	.8667	1.0801
.0085	1.1432	.9032	.0118	1.0478	.9681	.0278	.8496	1.0874	.0538	.7853	1.1268	.0455	.8652	1.0800
.0081	1.1406	.9021	.0109	1.0449	.9673	.0267	.8448	1.0863	.0511	.7835	1.1265	.0428	.8662	1.0795
.0071	1.1284	.8987	.0101	1.0350	.9648	.0257	.8354	1.0842	.0486	.7779	1.1248	.0399	.8621	1.0786
.0064	1.1131	.8947	.0092	1.0241	.9620	.0241	.8067	1.0778	.0463	.7742	1.1248	.0377	.8519	1.0779
.0059	.0962	.8898	.0087	1.0147	.9587	.0228	.7791	1.0715	.0438	.7614	1.1219	.0348	.8515	1.0762
.0053	.0781	.8854	.0080	.9949	.9548	.0218	.7418	1.0645	.0416	.7544	1.1205	.0324	.8386	1.0733
.0048	.0650	.8825	.0074	.9773	.9507	.0202	.6810	1.0535	.0392	.7352	1.1165	.0300	.8274	1.0708
.0042	.0364	.8758	.0066	.9494	.9443	.0188	.6337	1.0457	.0372	.7036	1.1104	.0274	.8170	1.0665
.0034	1.0068	.8690	.0062	.9353	.9412	.0172	.5716	1.0364	.0356	.6758	1.1053	.0251	.7876	1.0624
.0030	.9955	.8665	.0057	.9213	.9381	.0160	.5116	1.0285	.0336	.6374	1.0986	.0230	.7673	1.0584
.0027	.9772	.8625	.0050	.8967	.9329	.0152	.4704	1.0246	.0304	.5780	1.0893	.0220	.7428	1.0536
.0022	.9587	.8587	.0047	.8751	.9285	.0134	.4206	1.0183	.0270	.5187	1.0791	.0198	.7092	1.0471
.0021	.9361	.8541	.0042	.8448	.9226	.0122	.3745	1.0140	.0247	.4719	1.0685	.0162	.6759	1.0417
.0019	.9318	.8532	.0036	.8151	.9171	.0111	.3158	1.0092	.0220	.3644	1.0640	.0132	.6414	1.0361
.0016	.9248	.8485	.0029	.7884	.9124	.0094	.2620	1.0056	.0200	.3086	1.0596	.0112	.6152	1.0324
.0013	.8827	.8438	.0022	.7396	.9042	.0079	.2109	1.0028	.0174	.2503	1.0554	.0087	.5843	1.0275
.0011	.8584	.8396	.0018	.6985	.8978	.0070	.1627	1.0007	.0153	.1780	1.0517	.0068	.5652	1.0248
.0006	.8309	.8347	.0012	.6608	.8924	.0058	.1386	.9999	.0139	.1597	1.0509	.0046	.5478	1.0226
.0003	.7830	.8269	.0008	.6176	.8866	.0047	.0796	.9984	.0127	.0970	1.0491	.0036	.5342	1.0211
			.0004	.5860	.8827	.0037	.0857	.9986	.0111	.0722	1.0480	.0031	.5342	1.0208
						.0028	.0399	.9979	.0093	0.0000	1.0479	.0022	.5395	1.0215
						.0022	0.0000	.9977	.0075	0.0000	1.0479	.0017	.5333	1.0207
						.0012	0.0000	.9977	.0057	0.0000	1.0479	.0014	.5268	1.0199
						.0004	0.0000	.9977	.0043	0.0000	1.0479	.0009	.5291	1.0202
									.0029	0.0000	1.0479	.0006	.5144	1.0185
									.0018	0.0000	1.0479	.0004	.4884	1.0152
									.0011	0.0000	1.0479			

GP11-0232-79

TABLE 5. — Concluded.

X/C = .500L RUN 63			X/C = .600L RUN 65			X/C = .750L RUN 67			X/C = .910L RUN 69			X/C = 1.000L RUN 71		
z/c	u/u_∞	ρ/ρ_∞	z/c	u/u_∞	ρ/ρ_∞	z/c	u/u_∞	ρ/ρ_∞	z/c	u/u_∞	ρ/ρ_∞	z/c	u/u_∞	ρ/ρ_∞
.0134	1.1446	.9032	.0179	1.0591	.9614	.0460	.8325	1.1017	.0903	.7598	1.1383	.0765	.8741	1.0772
.0134	1.1444	.9032	.0133	1.0494	.9615	.0429	.8327	1.1018	.0850	.7595	1.1382	.0726	.8741	1.0772
.0115	1.1451	.9034	.0130	1.0594	.9615	.0387	.8327	1.1016	.0804	.7607	1.1385	.0688	.8741	1.0772
.0103	1.1447	.9033	.0115	1.0577	.9610	.0357	.8316	1.1015	.0763	.7592	1.1379	.0649	.8724	1.0769
.0094	1.1441	.9031	.0105	1.0548	.9603	.0337	.8306	1.1015	.0729	.7586	1.1379	.0618	.8717	1.0767
.0092	1.1443	.9032	.0099	1.0513	.9594	.0322	.8272	1.1005	.0688	.7556	1.1374	.0583	.8682	1.0758
.0091	1.1444	.9032	.0092	1.0401	.9565	.0317	.8243	1.0999	.0650	.7523	1.1367	.0552	.8625	1.0745
.0081	1.1373	.9016	.0089	1.0343	.9550	.0306	.8184	1.0986	.0612	.7482	1.1359	.0524	.8588	1.0739
.0078	1.1352	.9007	.0079	1.0095	.9488	.0293	.8079	1.0958	.0574	.7378	1.1337	.0484	.8549	1.0705
.0069	1.1216	.8970	.0074	.9987	.9464	.0287	.8010	1.0948	.0535	.7140	1.1303	.0447	.8371	1.0689
.0061	1.1016	.8918	.0065	.9655	.9384	.0277	.7788	1.0900	.0504	.7031	1.1270	.0444	.8291	1.0671
.0054	1.0820	.8869	.0054	.9258	.9296	.0269	.7655	1.0873	.0479	.6741	1.1217	.0419	.8134	1.0637
.0047	1.0539	.8798	.0047	.8955	.9232	.0254	.7201	1.0784	.0450	.6396	1.1148	.0389	.7841	1.0607
.0042	1.0346	.8753	.0043	.8747	.9190	.0241	.6883	1.0691	.0421	.5983	1.1091	.0363	.7733	1.0544
.0036	1.0043	.8684	.0036	.8430	.9129	.0230	.6368	1.0638	.0395	.5721	1.1051	.0335	.7489	1.0507
.0030	.9839	.8639	.0028	.7936	.9042	.0223	.6004	1.0581	.0372	.5144	.0971	.0310	.7284	1.0469
.0029	.9527	.8570	.0021	.7507	.8967	.0209	.5404	1.0448	.0345	.4649	.0910	.0269	.7062	1.0428
.0022	.9310	.8528	.0016	.7137	.8908	.0193	.4727	1.0411	.0323	.4126	.0893	.0250	.6743	1.0374
.0016	.9158	.8499	.0012	.6820	.8861	.0161	.4260	1.0360	.0303	.3748	.0817	.0223	.6545	1.0341
.0015	.8887	.8447	.0007	.6168	.8773	.0165	.3458	1.0286	.0281	.3203	.0769	.0188	.6290	1.0301
.0014	.8724	.8416				.0146	.2936	1.0220	.0267	.2764	.0737	.0178	.6019	1.0269
.0012	.8567	.8388				.0126	.1565	.0174	.0247	.2327	.0710	.0148	.5889	1.0241
.0007	.8060	.8302				.0107	0.0000	1.0145	.0228	.2114	.0699	.0123	.5707	1.0227
.0005	.7156	.8253				.0089	0.0000	1.0145	.0211	.1846	.0670	.0101	.5521	1.0218
						.0072	0.0000	1.0145	.0204	.1526	.0649	.0084	.5339	1.0217
						.0059	0.0000	1.0145	.0183	0.0000	.0645	.0064	.5279	1.0199
						.0048	0.0000	1.0145	.0163	0.0000	.0645	.0050	.5573	1.0198
						.0040	0.0000	1.0145	.0149	0.0000	.0645	.0040	.5572	1.0198
						.0030	0.0000	1.0145	.0138	0.0000	.0645	.0032	.5546	1.0194
						.0019	0.0000	1.0145	.0127	0.0000	.0645	.0025	.5564	1.0196
						.0010	0.0000	1.0145	.0117	0.0000	.0645	.0021	.5496	1.0201
									.0107	0.0000	.0645	.0017	.5360	1.0196
									.0098	0.0000	.0645	.0010	.5257	1.0180
									.0084	0.0000	.0645	.0008	.5368	1.0171
									.0069	0.0000	.0645	.0006	.5224	1.0153
									.0058	0.0000	.0645	.0005	.5100	1.0138
									.0049	0.0000	.0645			
									.0040	0.0000	.0645			
									.0030	0.0000	.0645			
									.0023	0.0000	.0645			
									.0016	0.0000	.0645			
									.0009	0.0000	.0645			

GP11-0232-80

X/C = .500L RUN 74			X/C = .600L RUN 76			X/C = .750L RUN 78			X/C = .910L RUN 80			X/C = 1.000L RUN 82		
z/c	u/u_∞	ρ/ρ_∞	z/c	u/u_∞	ρ/ρ_∞	z/c	u/u_∞	ρ/ρ_∞	z/c	u/u_∞	ρ/ρ_∞	z/c	u/u_∞	ρ/ρ_∞
.0136	1.1460	.9016	.0132	1.0400	.9675	.0345	.8529	1.0830	.0515	.7753	1.1326	.0486	.8677	1.0811
.0124	1.1469	.9018	.0125	1.0400	.9675	.0314	.8526	1.0830	.0471	.7753	1.1326	.0437	.8677	1.0811
.0110	1.1472	.9020	.0116	1.0396	.9674	.0295	.8529	1.0830	.0445	.7753	1.1326	.0405	.8677	1.0811
.0101	1.1469	.9018	.0110	1.0397	.9674	.0274	.8524	1.0829	.0422	.7742	1.1323	.0382	.8677	1.0811
.0096	1.1471	.9019	.0103	1.0400	.9675	.0260	.8521	1.0828	.0395	.7716	1.1316	.0367	.8666	1.0809
.0086	1.1468	.9018	.0099	1.0391	.9672	.0247	.8508	1.0826	.0373	.7663	1.1307	.0342	.8673	1.0810
.0077	1.1430	.9007	.0093	1.0380	.9669	.0234	.8449	1.0812	.0353	.7586	1.1291	.0316	.8633	1.0801
.0070	1.1366	.8990	.0085	1.0339	.9659	.0223	.8328	1.0786	.0335	.7469	1.1266	.0292	.8598	1.0793
.0064	1.1269	.8964	.0082	1.0283	.9644	.0213	.8186	1.0755	.0310	.7225	1.1218	.0267	.8489	1.0768
.0058	1.1137	.8927	.0075	1.0174	.9617	.0202	.7900	1.0695	.0291	.6957	1.1166	.0242	.8431	1.0755
.0055	1.1006	.8896	.0071	1.0042	.9584	.0188	.7684	1.0652	.0276	.6691	1.1118	.0222	.8292	1.0724
.0052	1.0930	.8876	.0066	.9921	.9554	.0189	.7362	1.0590	.0257	.6219	1.1028	.0204	.8162	1.0697
.0049	1.0788	.8840	.0063	.9758	.9510	.0181	.7134	1.0549	.0241	.5789	1.0970	.0181	.7892	1.0627
.0044	1.0644	.8804	.0057	.9618	.9482	.0169	.6781	1.0487	.0223	.5380	.0912	.0165	.7727	1.0606
.0042	1.0494	.8768	.0050	.9338	.9419	.0162	.6475	1.0437	.0202	.4923	.0852	.0147	.7561	1.0573
.0037	1.0370	.8739	.0046	.9139	.9375	.0155	.6019	1.0368	.0190	.4561	.0812	.0134	.7386	1.0540
.0035	1.0189	.8697	.0042	.8971	.9339	.0146	.5737	1.0326	.0175	.4180	.0767	.0118	.7076	1.0483
.0032	1.0025	.8661	.0038	.8741	.9282	.0128	.5396	1.0282	.0164	.3875	.0736	.0100	.6840	1.0441
.0028	.9845	.8621	.0036	.8623	.9268	.0127	.4928	1.0225	.0148	.3483	.0701	.0084	.6597	1.0399
.0026	.9716	.8594	.0028	.8208	.9189	.0115	.4468	1.0174	.0138	.3140	.0673	.0069	.6422	1.0373
.0022	.9606	.8570	.0025	.8090	.9167	.0105	.3949	1.0123	.0125	.2719	.0643	.0054	.6240	1.0344
.0019	.9308	.8510	.0020	.7712	.9100	.0091	.3369	1.0074	.0113	.2550	.0632	.0038	.6048	1.0315
.0017	.9037	.8457	.0016	.7248	.9024	.0076	.2805	1.0035	.0102	.2023	.0602	.0025	.5928	1.0297
.0015	.8873	.8426	.0011	.6941	.8976	.0066	.2491	1.0016	.0086	.1693	.0588	.0014	.5810	1.0280
.0011	.8763	.8409	.0006	.6532	.8917	.0051	.2374	1.0007	.0070	.1422	.0577	.0007	.5701	1.0265
.0009	.8569	.8371	.0006	.6234	.8843	.0041	.1867	.9991	.0059	.1210	.0565	.0004	.5462	1.0233
.0008	.8537	.8331	.0005	.6053	.8854	.0032	.1910	.9987	.0038	.0614	.0558	.0005	.5266	1.0210
.0006	.8057	.8284				.0024	.1590	.9974	.0016	0.0000	.0553			
.0004	.7946	.8266				.0019	.1359	.9967	.0005	0.0000	.0553			
						.0014	.1491	.9971						
						.0008	.1334	.9966						
						.0004	.1046	.9958						
							.1213	.9963						

GP11-0232-81

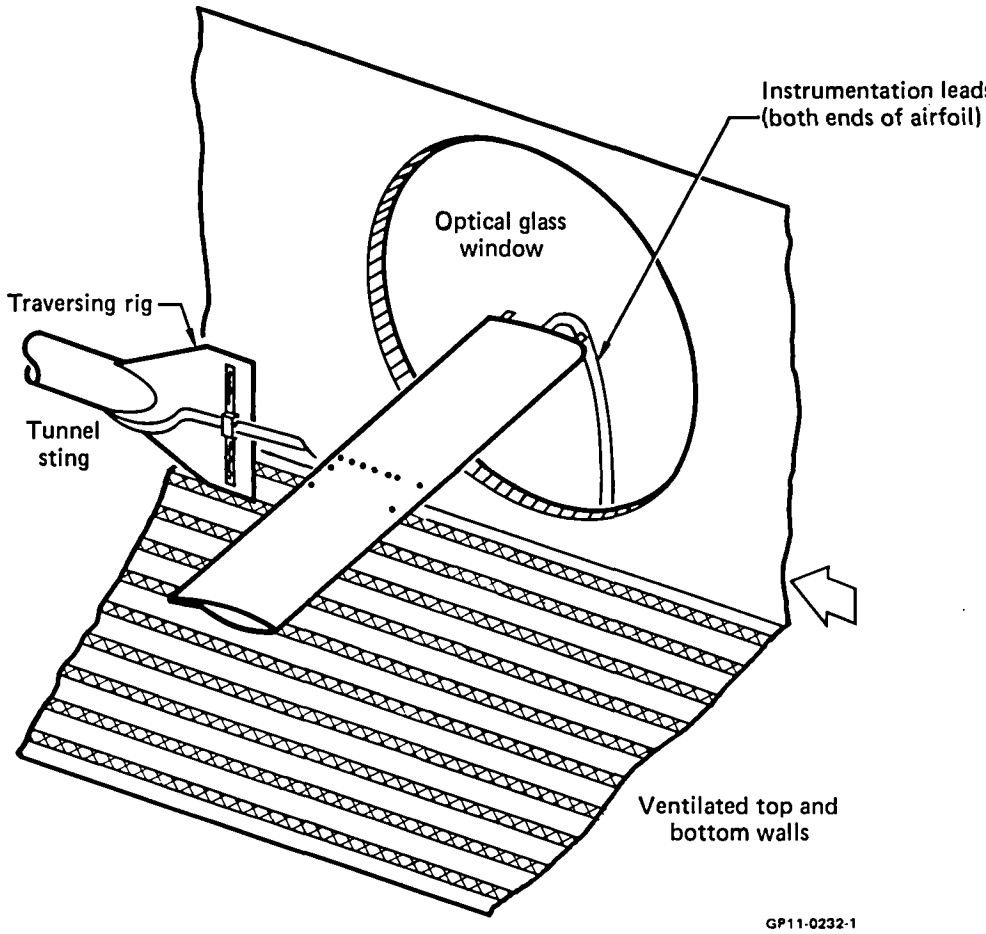

Figure 1. — Test section setup.

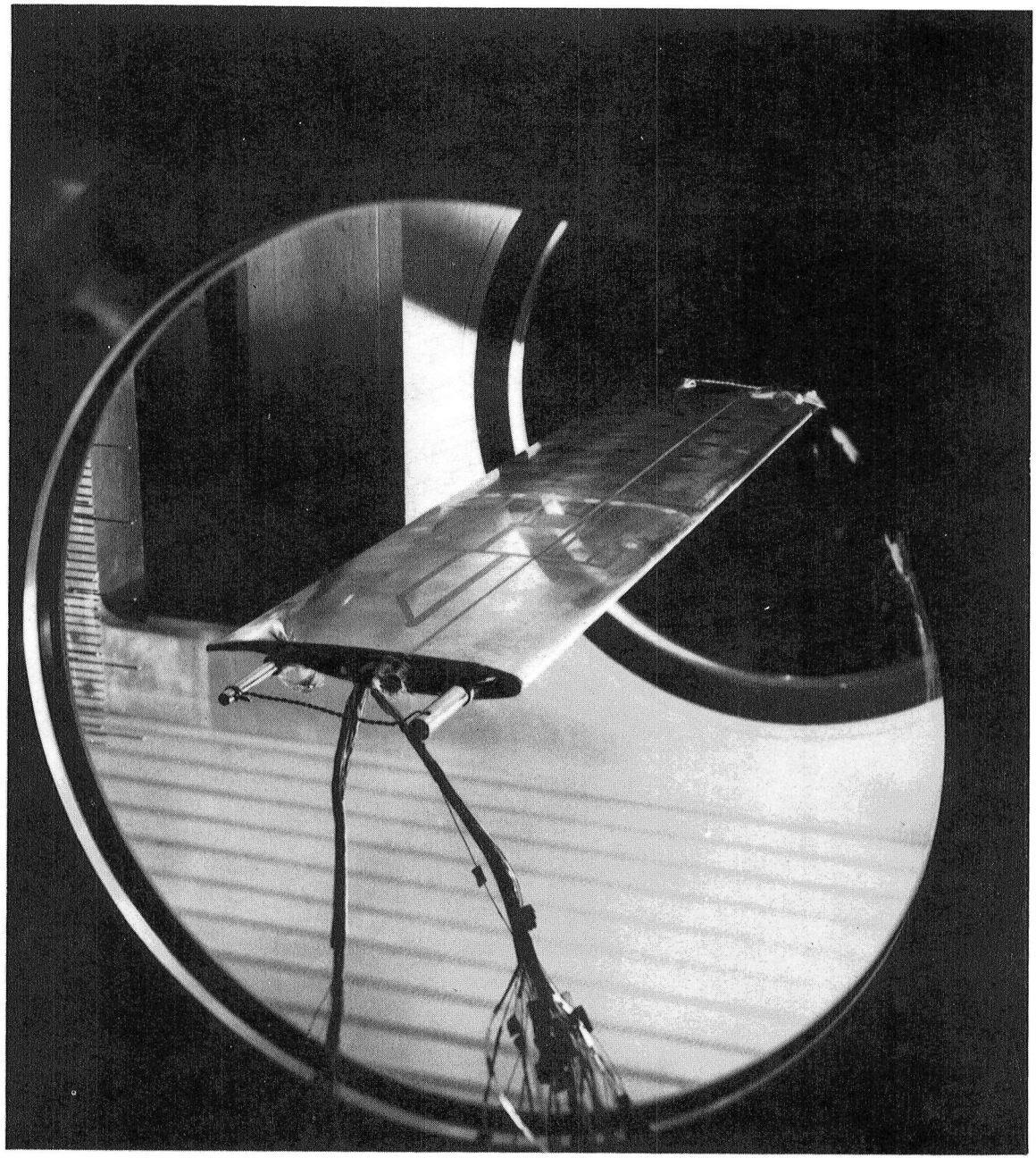

GP11-0232-2

Figure 2. — Two- by Two-Foot Transonic Wind Tunnel test section with blunt-trailing-edge model installed.

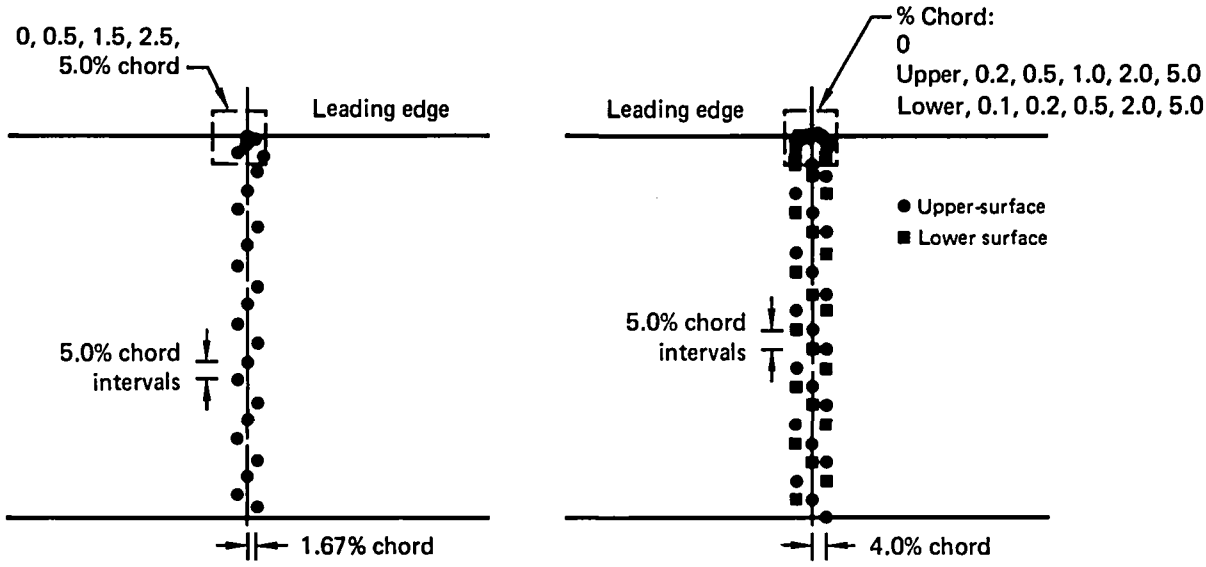

(a) Blunt-trailing-edge model, upper and lower surfaces.

(b) Sharp-trailing-edge model.

GP11-0232-3

Figure 3. — Distribution of static-pressure orifices at centerspan.

	Re_c	Boundary-layer trip			
		Upper		Lower	
		x/c	k (mm)	x/c	k (mm)
○	3×10^6, 4×10^6	0.35	0.05	0.188	0.05
Q	3×10^6, 4×10^6	0.35	0.05	0.06	0.08
□	14.6×10^6	Natural transition			

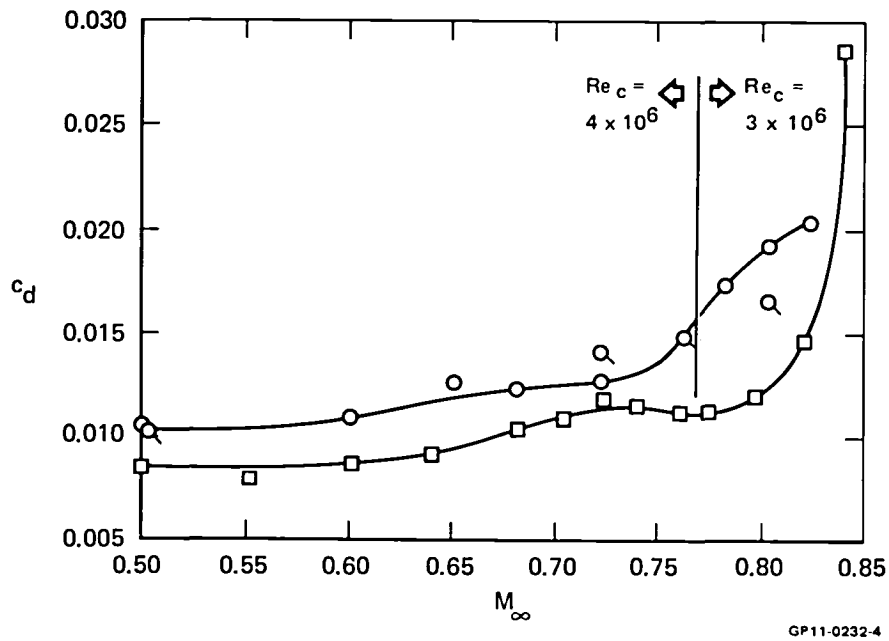

Figure 4. — Effect of boundary-layer trip configuration and Reynolds number on drag rise characteristics at $c_l \approx 0.6$.

Trip configurations				
x/c	k (mm)	k/k_{cr}		
		$Re_c = 3 \times 10^6$	$Re_c = 4 \times 10^6$	
0.35	0.08	0.9	1.2	Upper surface
○ 0.06	0.05	1.0	1.3	Lower surface
□ 0.18	0.08	1.2	1.4	Lower surface
△ 0.35	0.09	1.1	1.4	Lower surface
——— Data at $Re_c = 14.5 \times 10^6$				

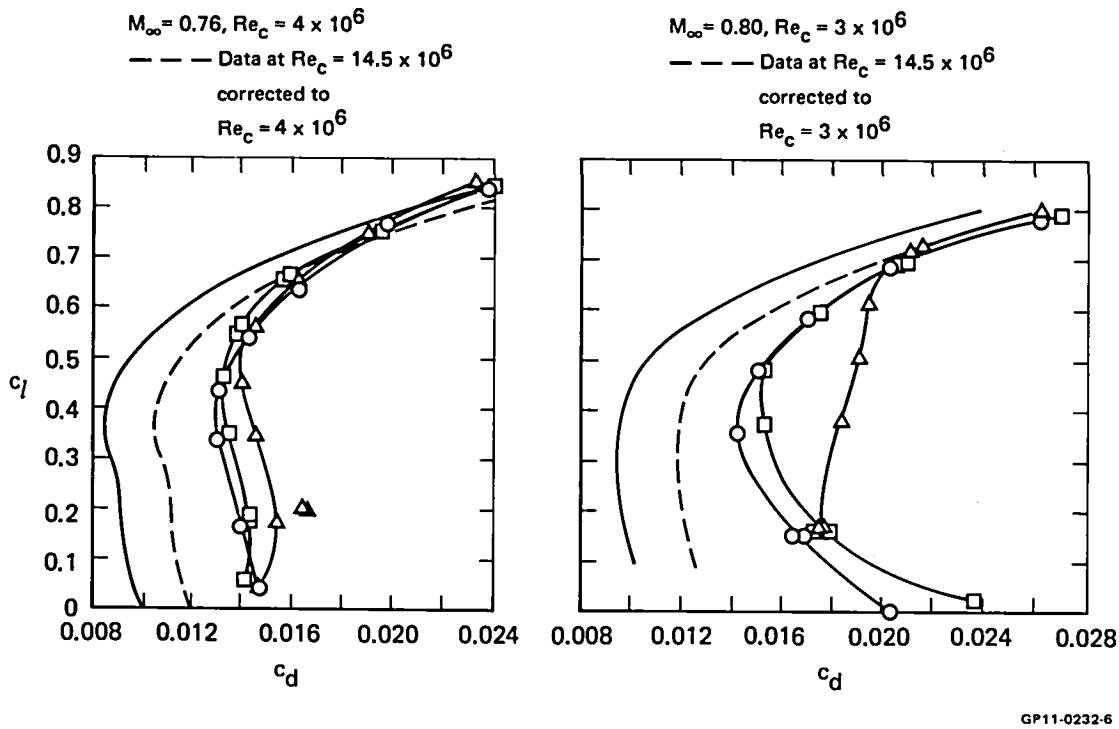

Figure 5. — Effect of lower-surface boundary-layer trip location on drag characteristics.

Trip configurations				
x/c	k (mm)	k/k_{cr}		
		$Re_c = 3 \times 10^6$	$Re_c = 4 \times 10^6$	
0.35	0.08	0.9	1.2	Upper surface
□ 0.18	0.08	1.2	1.4	Lower surface
◇ 0.18	0.10	1.5	1.8	Lower surface
△ 0.18	0.12	1.9	2.3	Lower surface
○ 0.18	0.16	2.4	3.0	Lower surface
——— Data at $Re_c = 14.5 \times 10^6$				

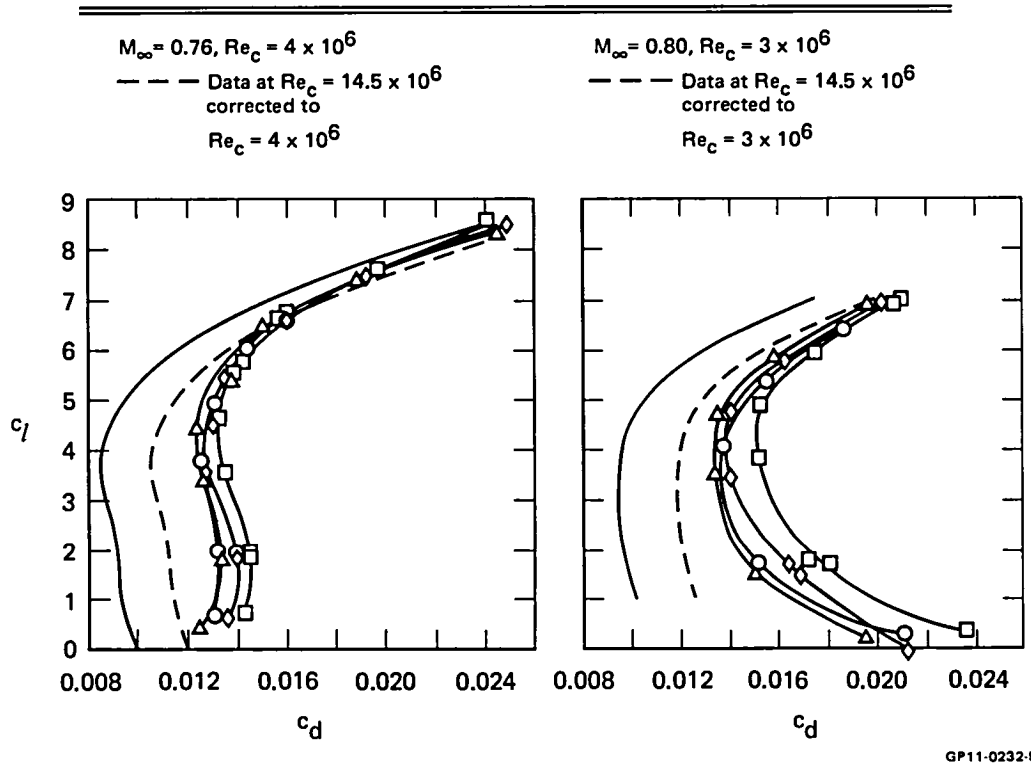

Figure 6. — Effect of lower-surface boundary-layer trip bead size on drag characteristics.

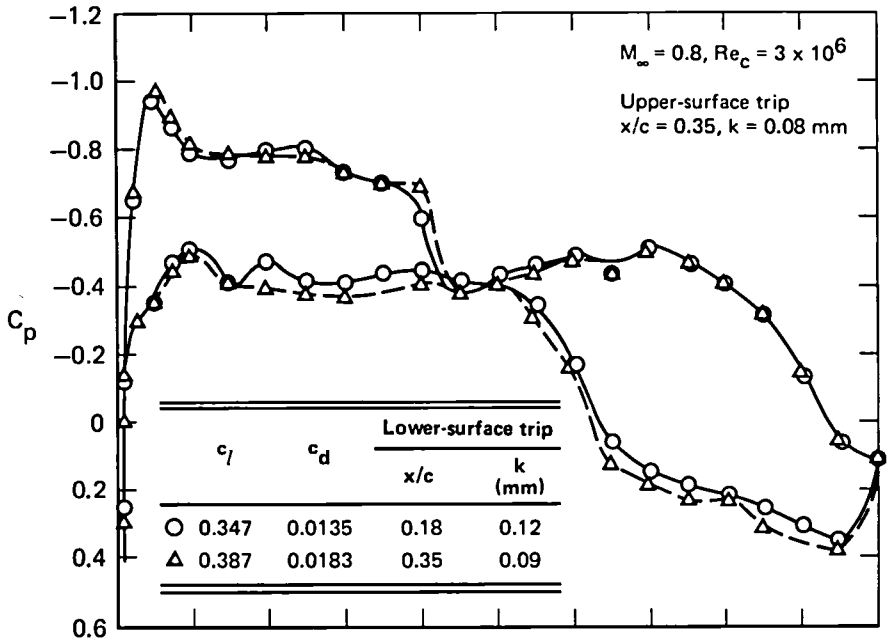

(a) $\alpha_{geom} = 1.0^o$.

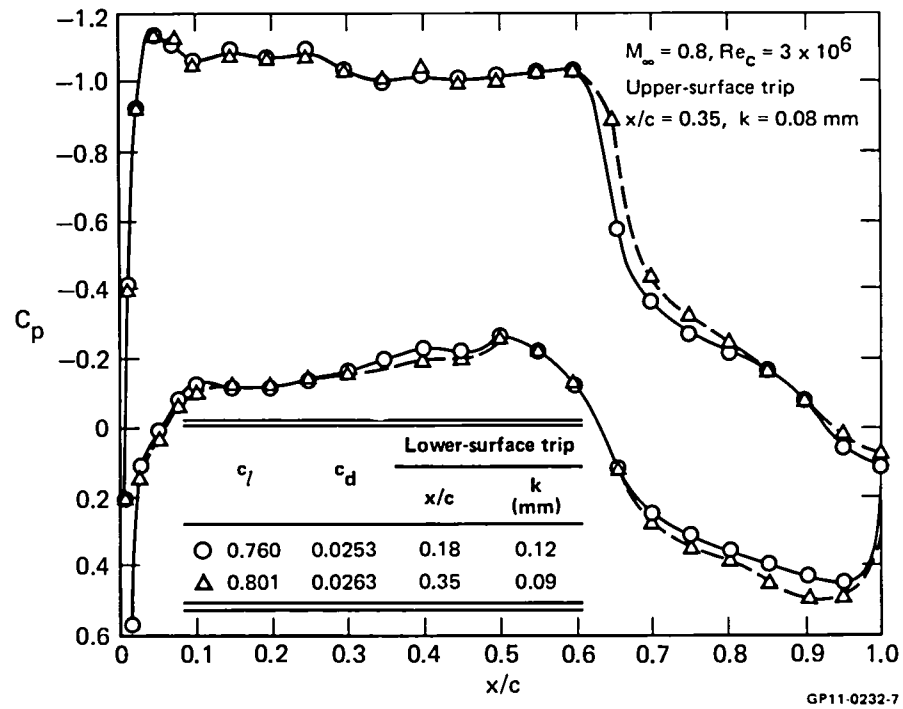

(b) $\alpha_{geom} = 3.0^o$.

Figure 7. — Static-pressure distributions corresponding to high- and low-drag conditions.

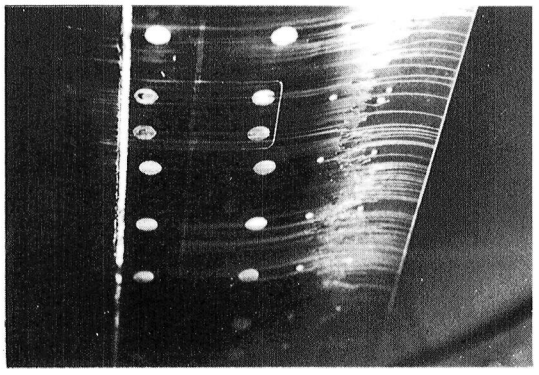

(a) $M_\infty = 0.6$, $Re_c = 4 \times 10^6$, $\alpha_{geom} = 2.0^o$, lower-surface trip, x/c = 0.18, k = 0.12 mm.

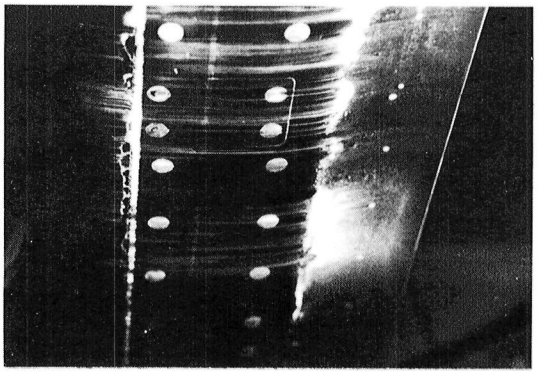

(b) $M_\infty = 0.8$, $\alpha_{geom} = 1.0^o$, $Re_c = 3 \times 10^6$, lower-surface trip, x/c = 0.18, k = 0.12 mm.

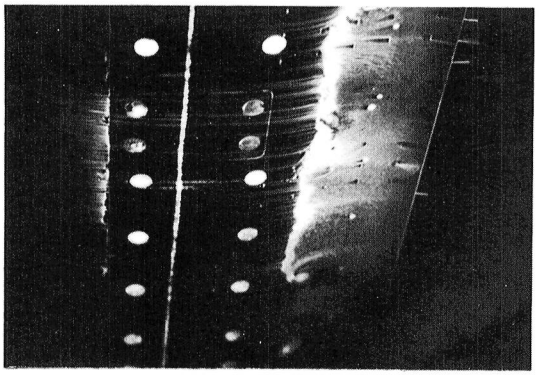

(c) $M_\infty = 0.8$ $\alpha_{geom} = 1.0^o$, $Re_c = 3 \times 10^6$, lower-surface trip, x/c = 0.35, k = 0.09 mm.

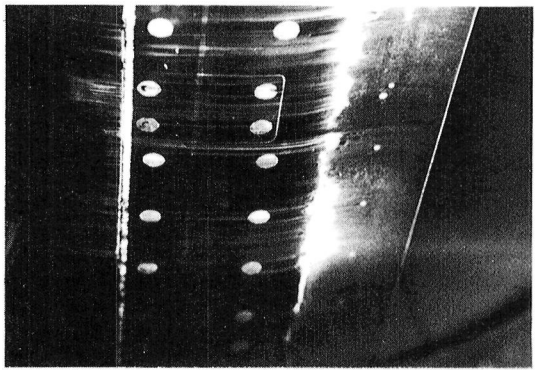

(d) $M_\infty = 0.8$, $\alpha_{geom} = 3.0^o$, $Re_c = 3 \times 10^6$, lower-surface trip, x/c = 0.18, k = 0.12 mm.

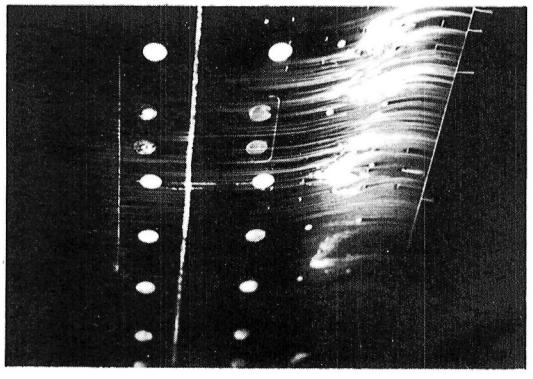

(e) $M_\infty = 0.8$ $\alpha_{geom} = 3.0^o$, $Re_c = 3 \times 10^6$, lower-surface trip, x/c = 0.35, k = 0.09 mm.

GP11-0232-8

Figure 8. — Lower-surface fluorescent oil-flow photographs.

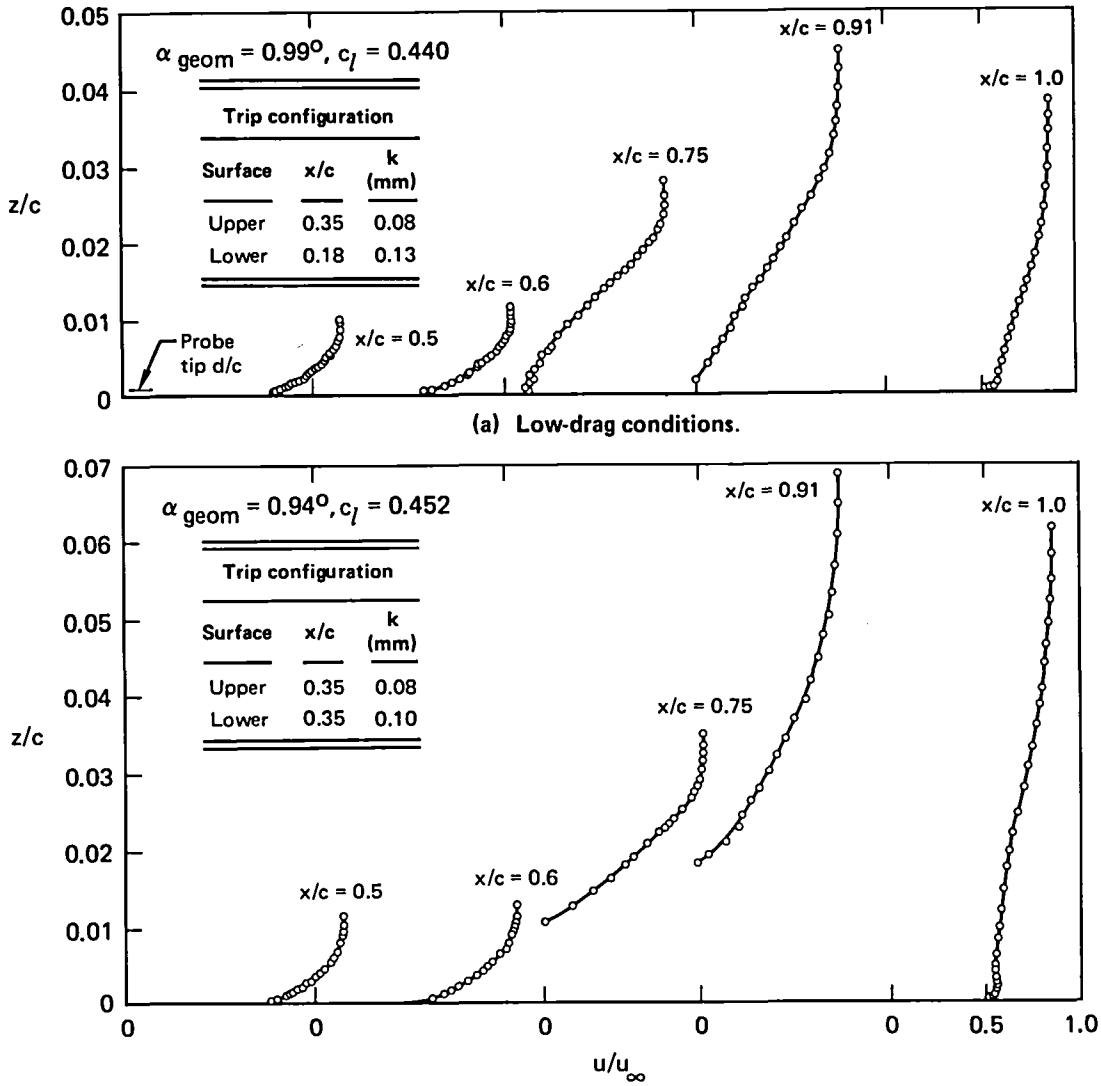

Figure 9. — Lower-surface boundary-layer profiles, $M_\infty = 0.8$, $Re_c = 3 \times 10^6$.

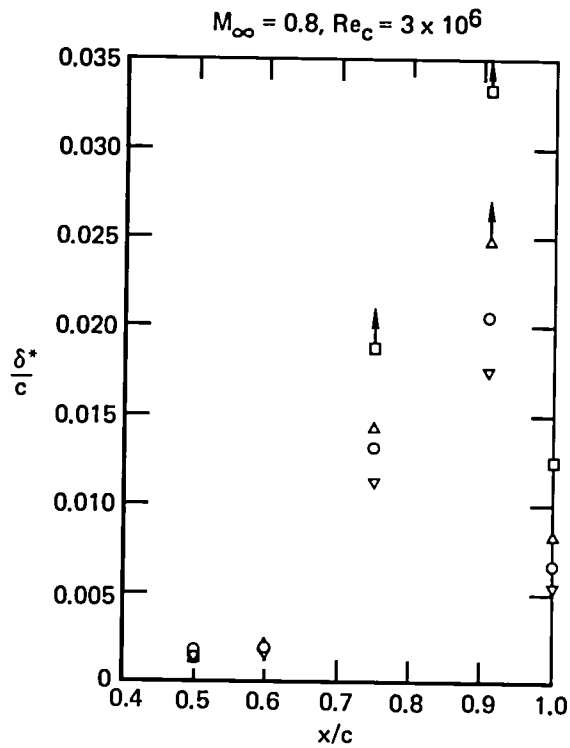

Trip configurations					
	α_{geom}	c_l	x/c	k (mm)	
○	1.05	0.435	0.06	0.05	Lower surface
△	0.98	0.432	0.18	0.08	Lower surface
▽	0.99	0.440	0.18	0.13	Lower surface
□	0.94	0.452	0.35	0.10	Lower surface
			0.35	0.08	Upper surface

GP11-0232-10

Figure 10. — Influence of lower-surface trip configuration on displacement thickness distribution.

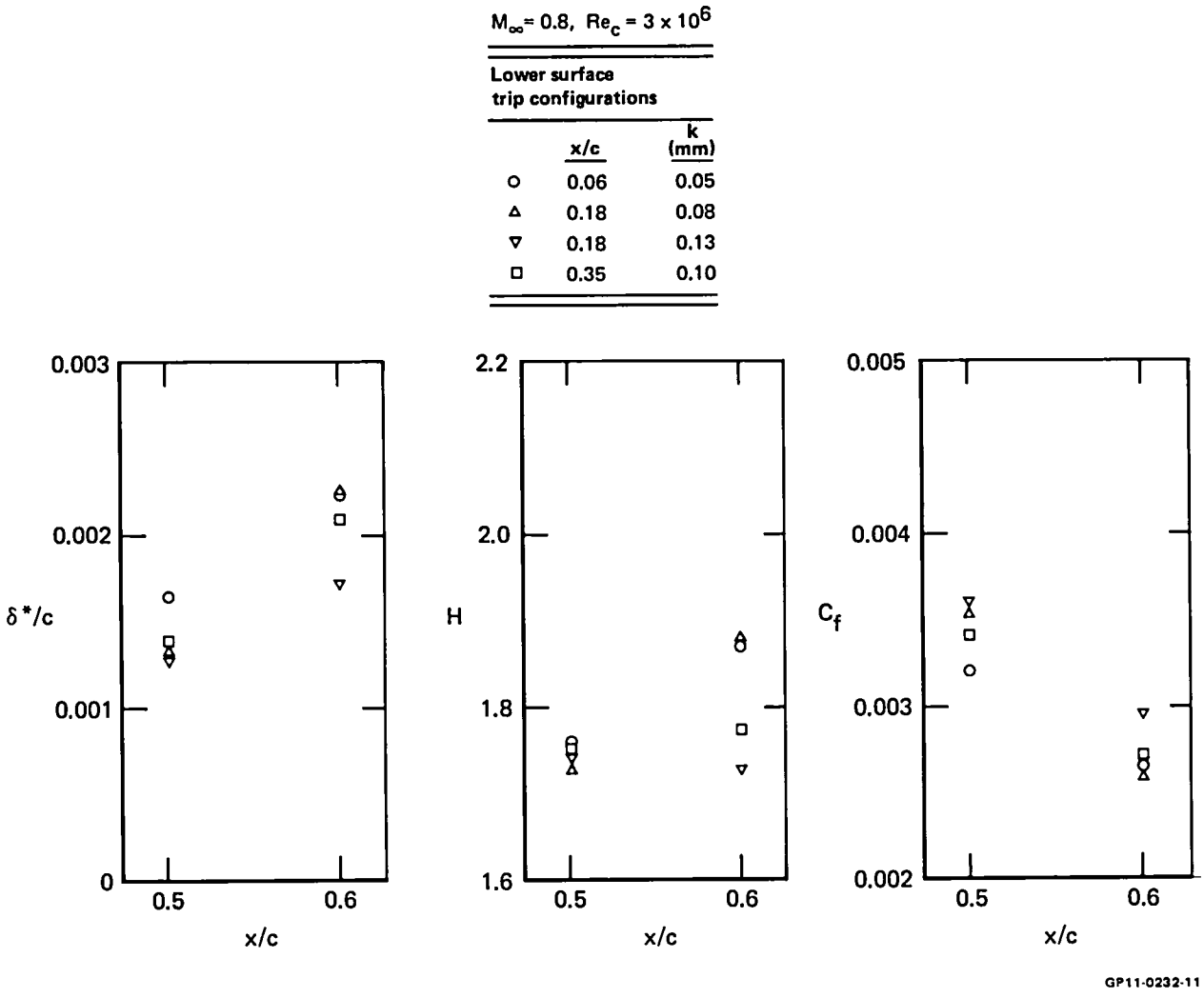

Figure 11. — Boundary-layer properties upstream of the lower-surface concavity.

Re_c	Trip configuration: Upper x/c	Upper k (mm)	Lower x/c	Lower k (mm)	Δc_d correction	
○ • 4×10^6	0.35	0.08	0.18	0.12		
⌕ 3×10^6	0.35	0.08	0.18	0.12	−0.0006	Sharp trailing edge
□ 4×10^6	0.35	0.06	0.18	0.06		
⌕ 3×10^6	0.35	0.06	0.18	0.06	−0.0006	
△ 2×10^6	0.05	0.09	0.18	0.12	−0.0015	Blunt trailing edge
▽ 2×10^6	0.35	0.12	0.18	0.13	−0.0015	
▼ 4×10^6	0.35	0.08	0.18	0.12		
— — — 14.5×10^6 Natural transition					+0.0020	Sharp trailing edge

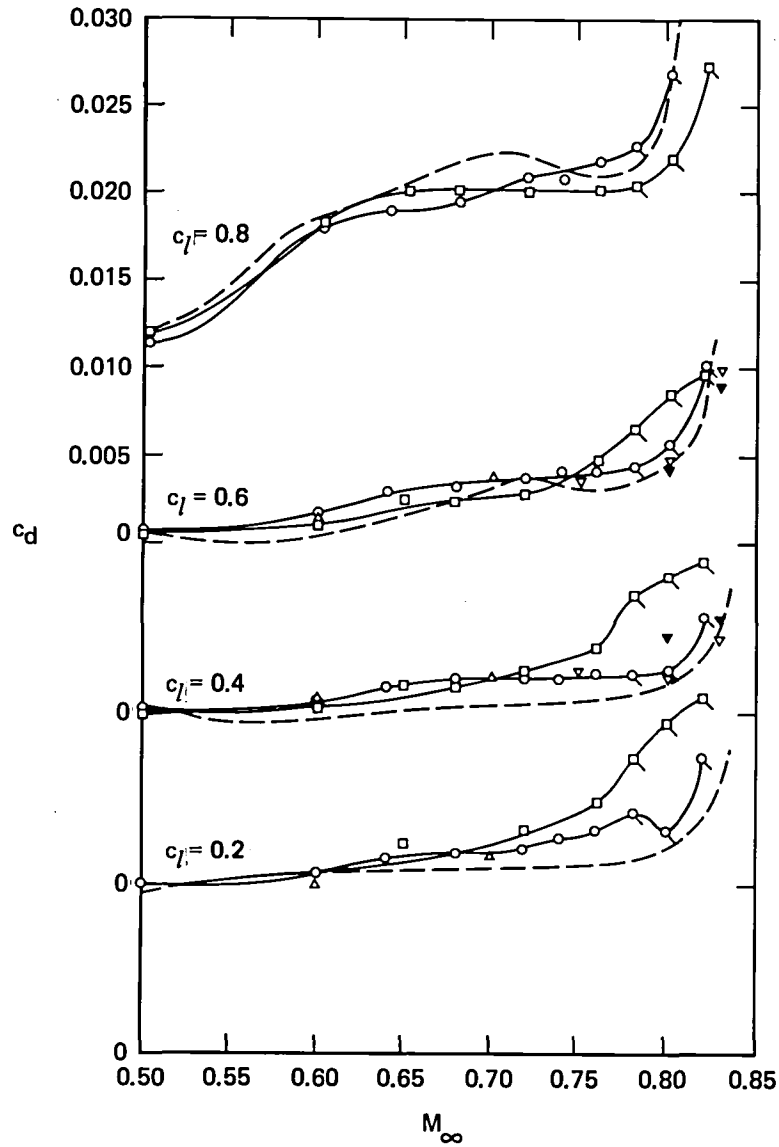

GP11-0232-12

Figure 12. — Drag data summary; various trip configurations at moderate Reynolds numbers and natural transition at higher Reynolds number.

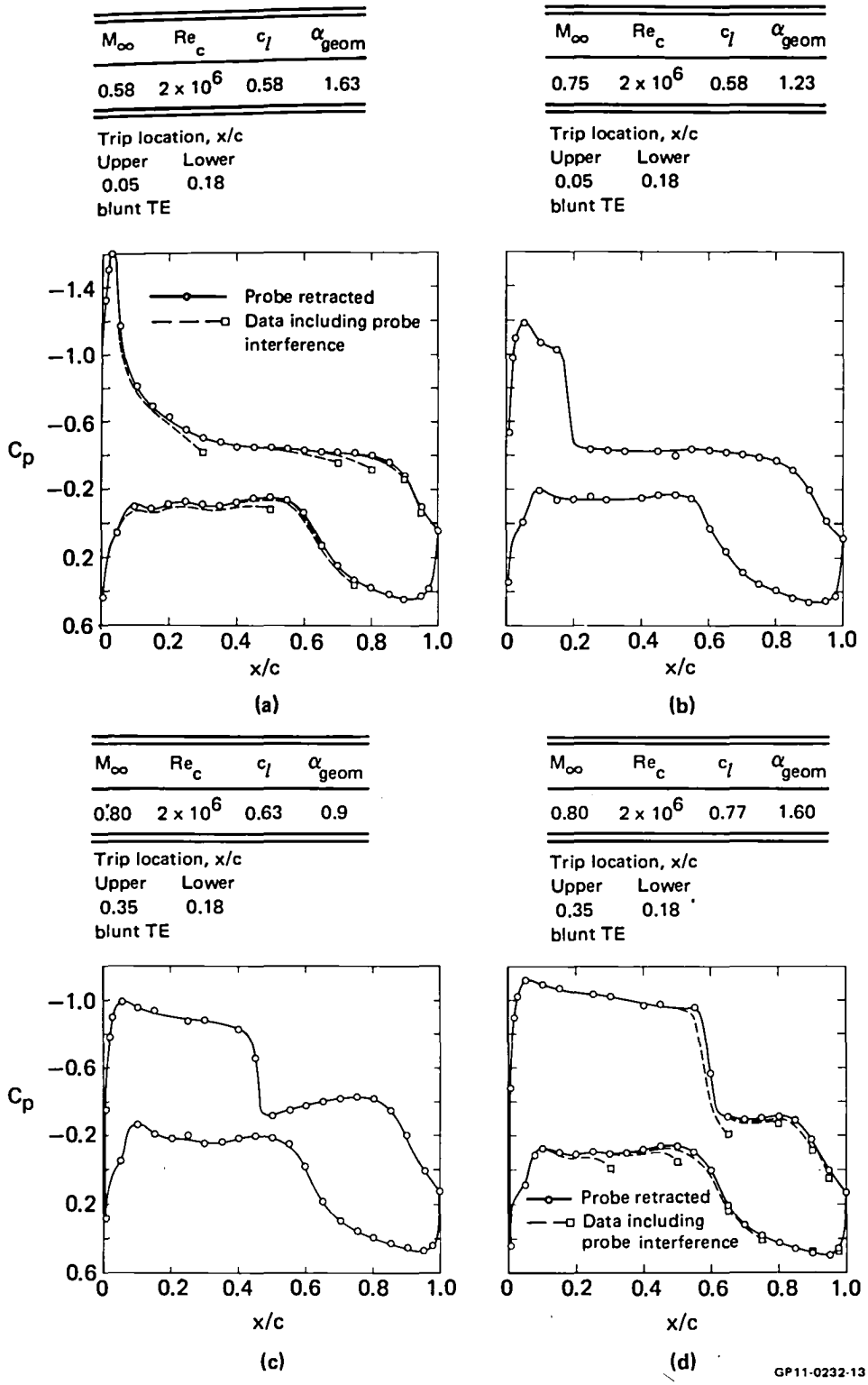

Figure 13. — Static pressure distributions, including examples of probe interference.

M_∞	Re_c	c_l	α_{geom}	Trailing edge
○ 0.6	2×10^6	0.58	1.63	Blunt
□ 0.6	4×10^6	0.58	2.60	Sharp

Trip location, x/c

Upper	Lower
0.35	0.18

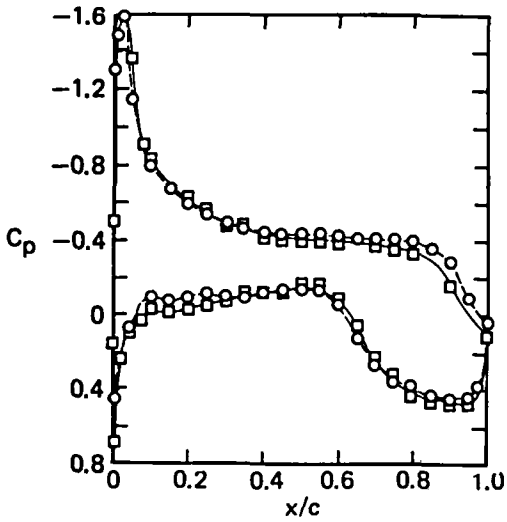

(e)

M_∞	Re_c	c_l	α_{geom}
○ 0.8	2×10^6	0.61	1.8
□ 0.8	3×10^6	0.71	2.4

Trip location, x/c

Upper	Lower
0.35	0.18
sharp TE	

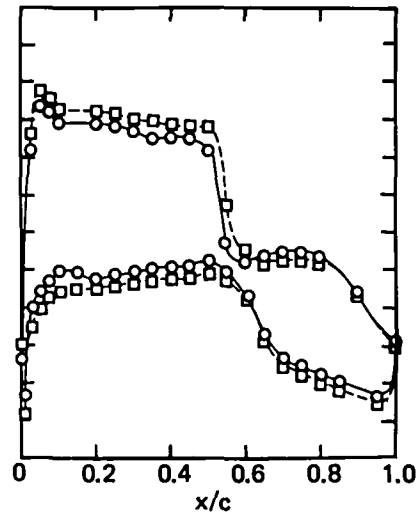

(f)

M_∞	Re_c	c_l	α_{geom}
○ 0.83	2×10^6	0.61	0.78
□ 0.83	3×10^6	0.54	1.03

Trip location, x/c

Upper	Lower
0.35	0.18
LE	LE
blunt TE	

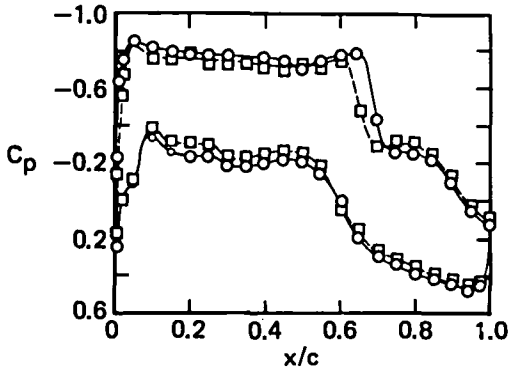

(g)

GP11-0232-46

Figure 13. — Concluded.

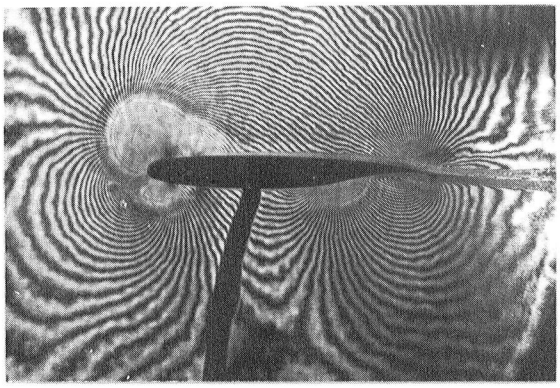

(a) Supercritical airfoil, $M_\infty = 0.6$, $Re_c = 4 \times 10^6$, $c_l = 0.58$.

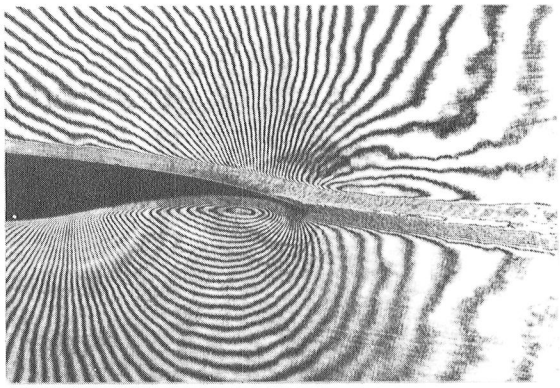

(b) Supercritical airfoil, $M_\infty = 0.6$, $Re_c = 4 \times 10^6$, $c_l = 0.58$, close-up of trailing-edge region.

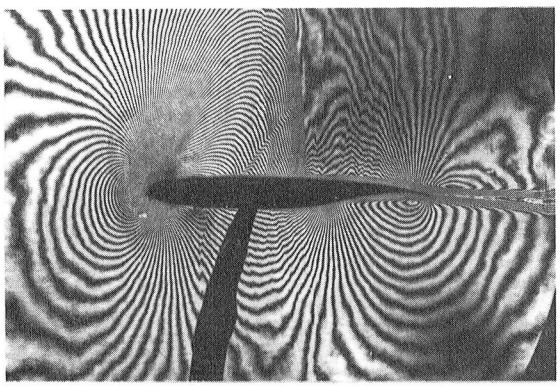

(c) Supercritical airfoil, $M_\infty = 0.8$, $Re_c = 2 \times 10^6$, $c_l = 0.61$.

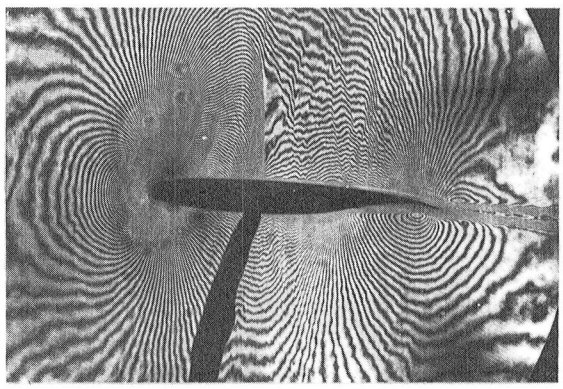

(d) Supercritical airfoil, $M_\infty = 0.8$, $Re_c = 3 \times 10^6$, $c_l = 0.44$.

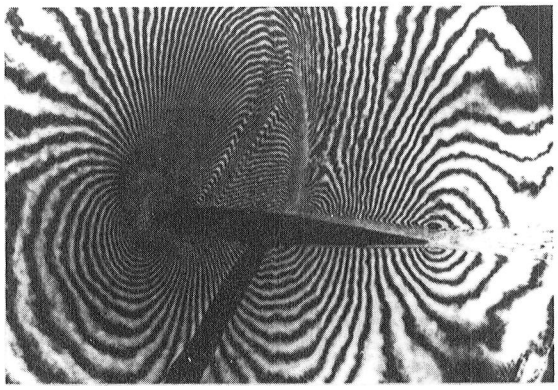

(e) NACA 64A010 airfoil, $M_\infty = 0.8$, $Re_c = 2 \times 10^6$, $c_l = 0.50$.

GP11-0232-40

Figure 14. — Interferograms of transonic airfoil flowfields.

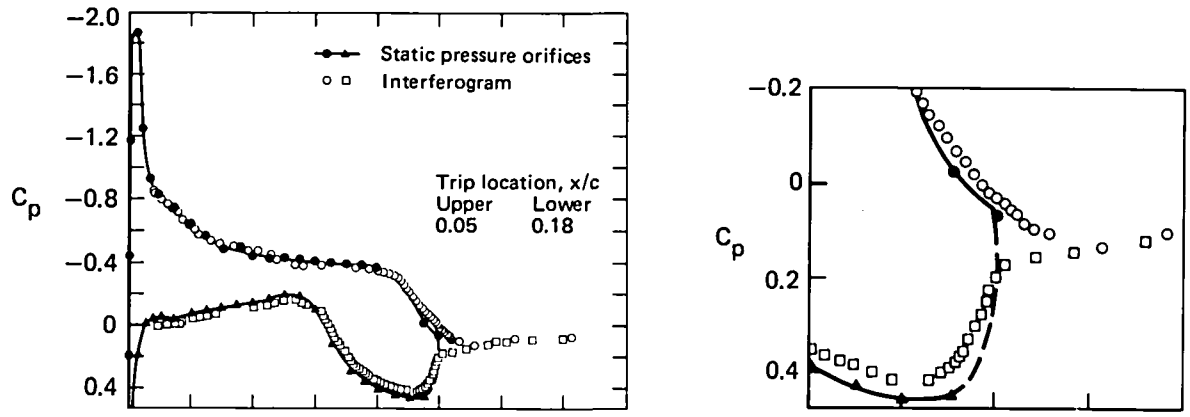

(a) Supercritical airfoil, $M_\infty = 0.6$, $Re_c = 4 \times 10^6$, $\alpha_{geom} = 2.6$ $c_l = 0.58$.

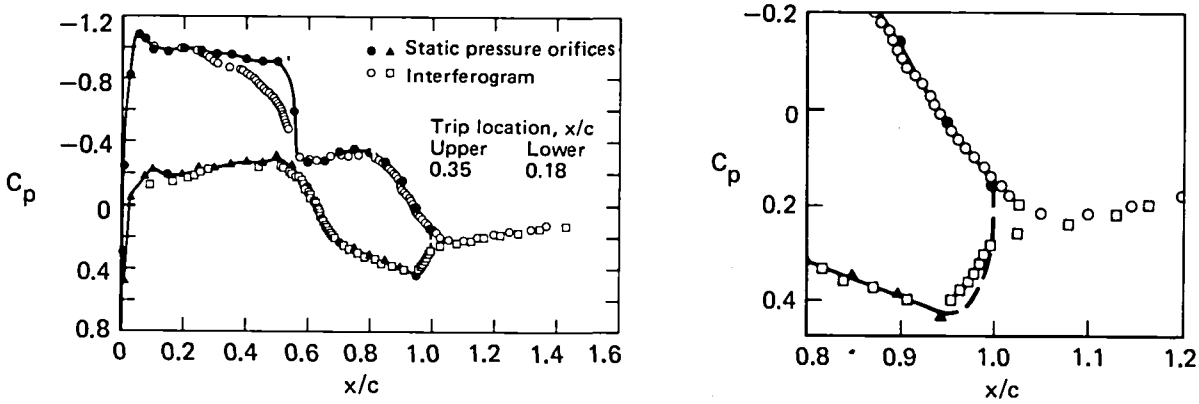

(b) Supercritical airfoil, $M_\infty = 0.8$, $Re_c = 2 \times 10^6$, $\alpha_{geom} = 1.8$, $c_l = 0.61$.

GP11-0232-14

Figure 15. — Comparison of data from static-pressure orifices and pressures determined from interferograms.

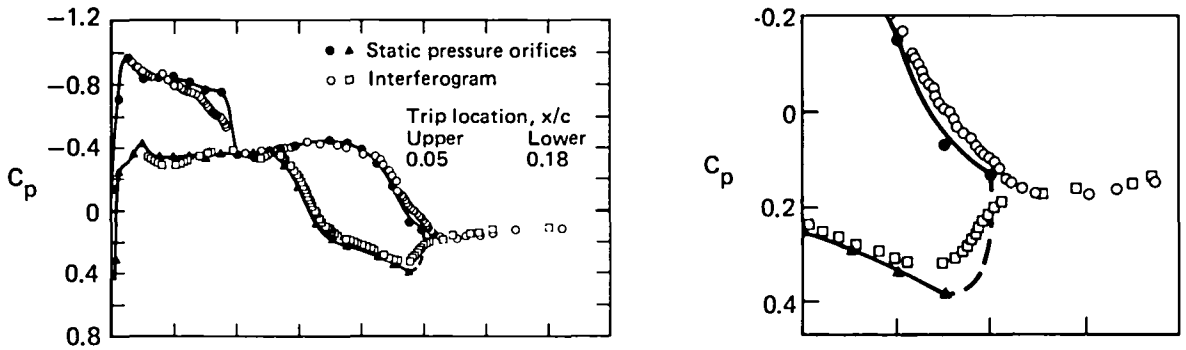

(c) Supercritical airfoil, $M_\infty = 0.8$, $Re_c = 3 \times 10^6$, $\alpha_{geom} = 1.0$, $c_l = 0.44$.

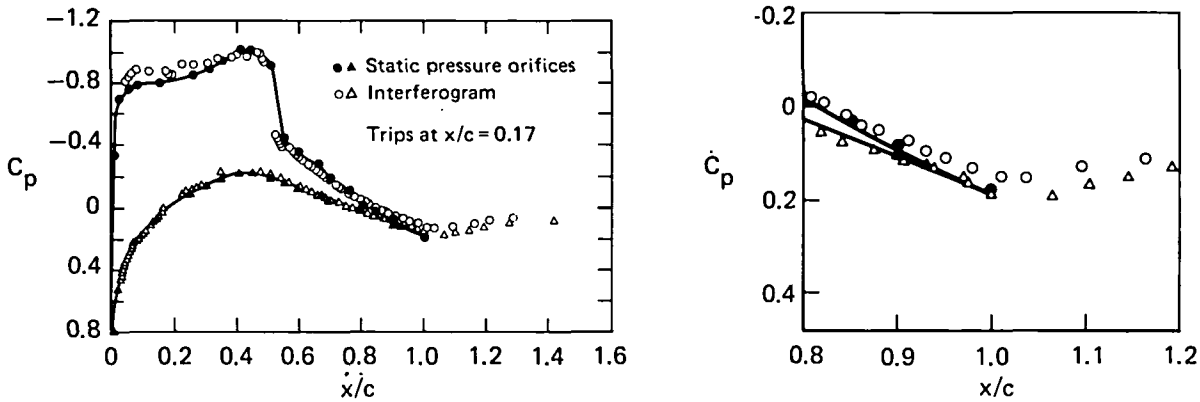

(d) NACA 64A010 airfoil, $M_\infty = 0.8$, $Re_c = 2 \times 10^6$, $\alpha_{geom} = 3.5$, $c_l = 0.50$.

GP11-0232-95

Figure 15. — Concluded.

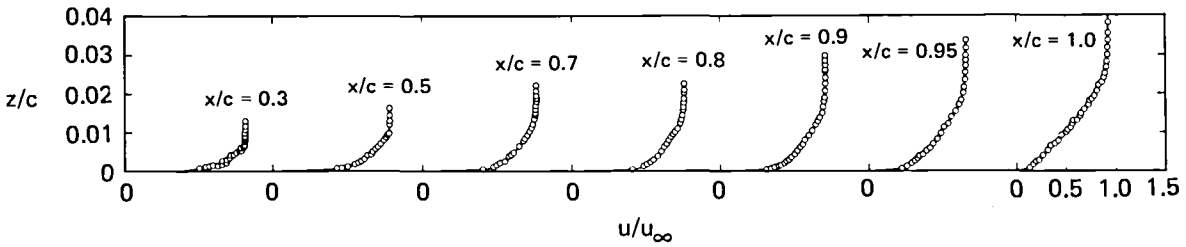

(a) Upper surface, trip at x/c = 0.05.

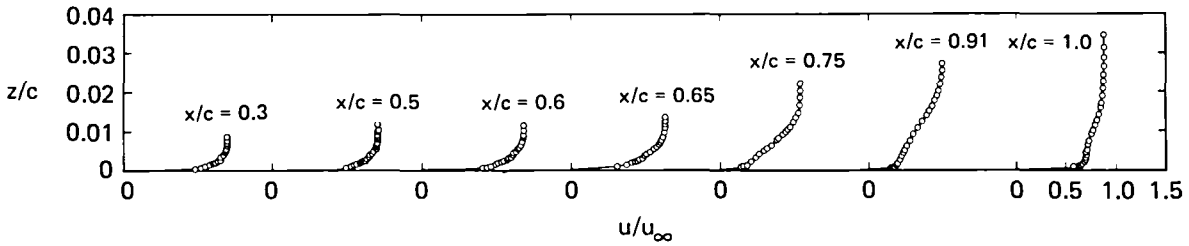

(b) Lower surface, trip at x/c = 0.18.

GP11-0232-15

Figure 16. — Boundary-layer profiles at $M_\infty = 0.6$; sharp trailing edge, $Re_c = 4 \times 10^6$, $\alpha_{geom} = 2.6$ (see fig. 13(e)).

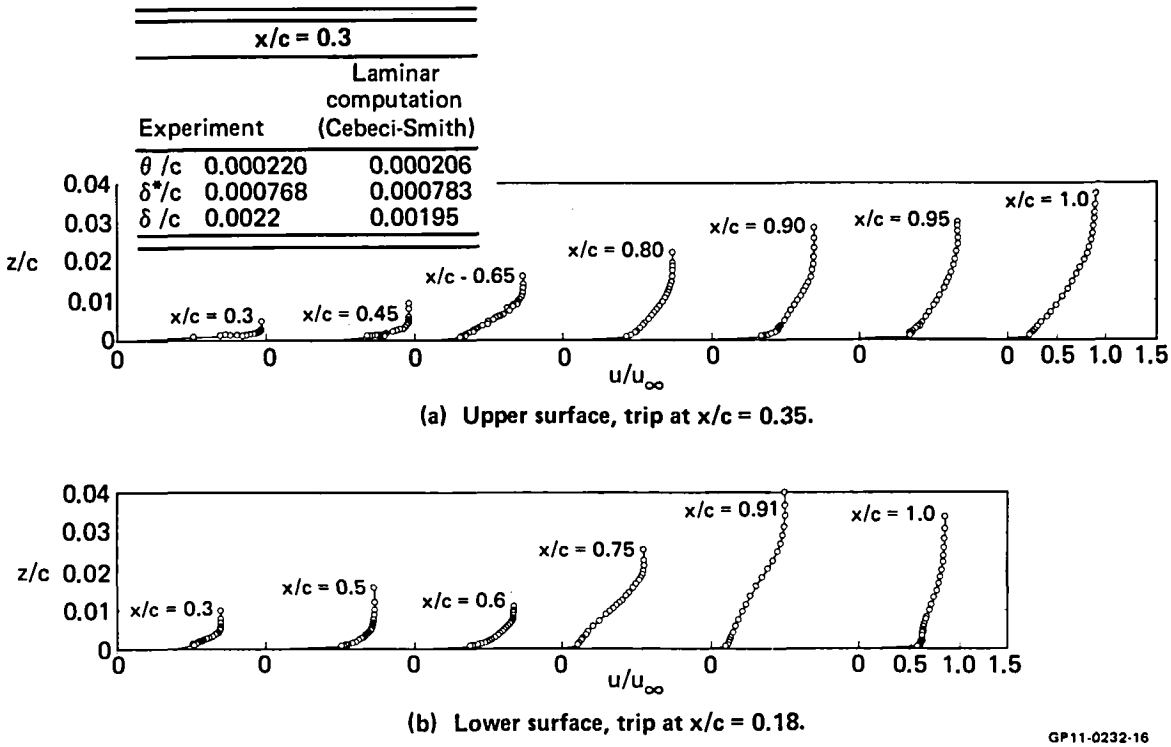

(a) Upper surface, trip at x/c = 0.35.

(b) Lower surface, trip at x/c = 0.18.

GP11-0232-16

Figure 17. — Boundary-layer profiles at $M_\infty = 0.8$; sharp trailing edge, $Re_c = 3 \times 10^6$, $\alpha_{geom} = 2.4$ (see fig. 13(f)).

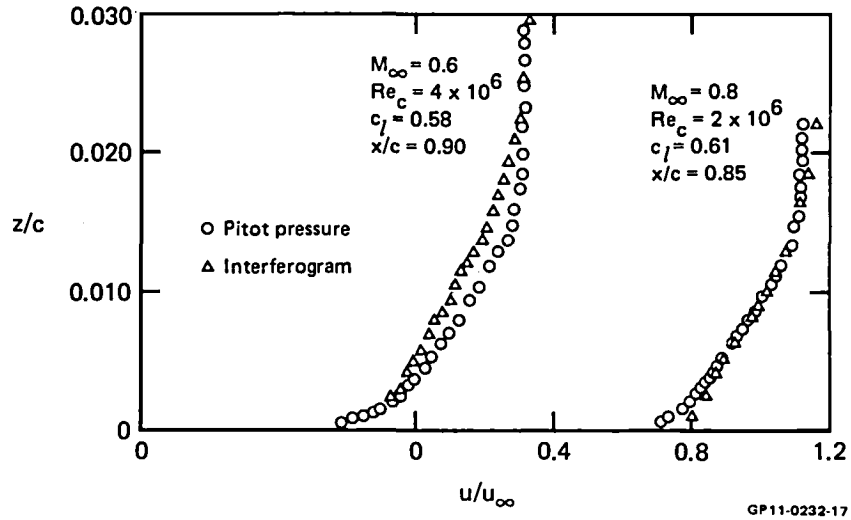

Figure 18. — Comparison of upper-surface boundary-layer profiles derived from pitot pressure measurements and from interferograms.

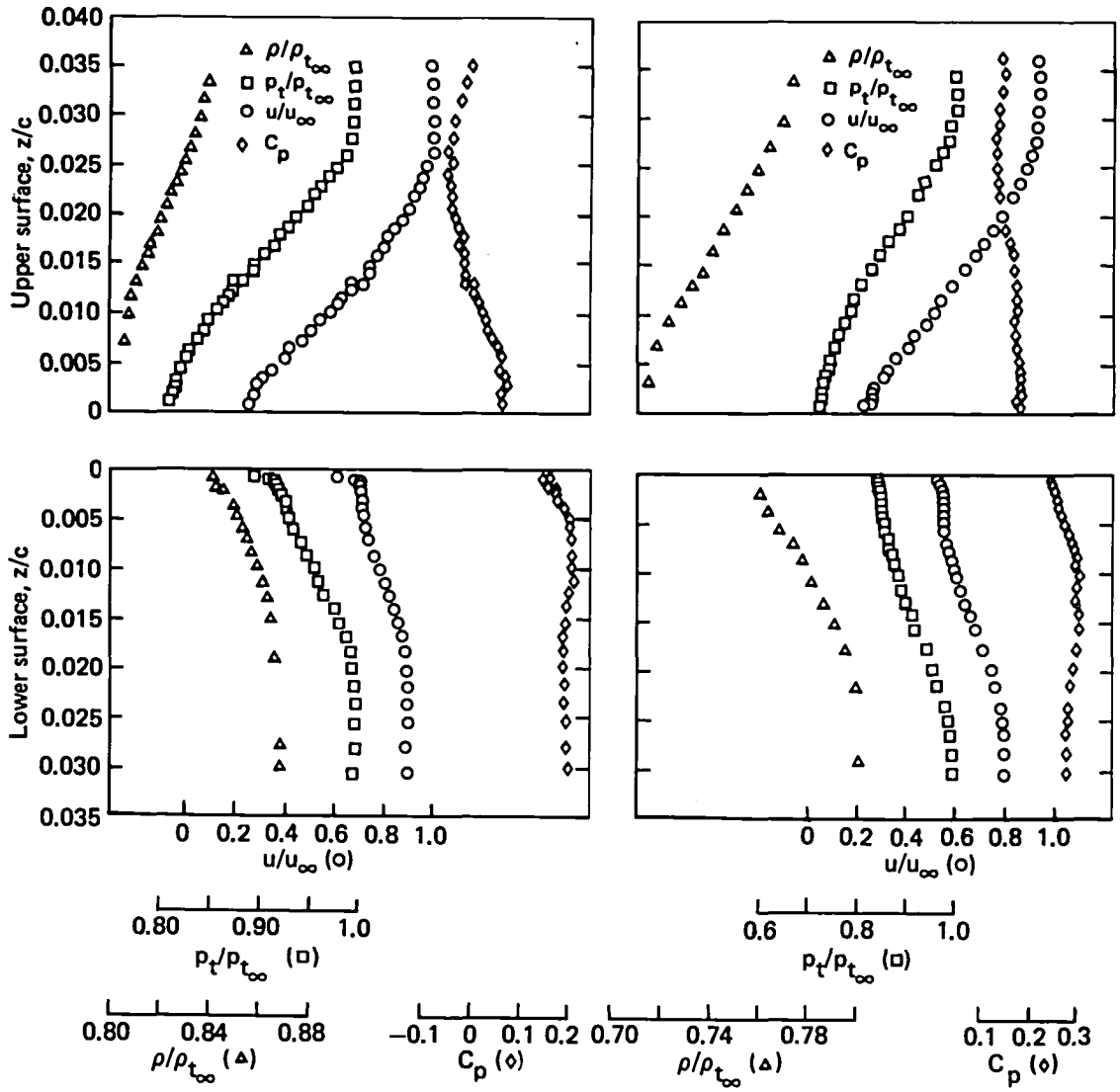

(a) $M_\infty = 0.6$, $Re_c = 4 \times 10^6$, $\alpha_{geom} = 2.6^o$ (see fig. 15(a)).

(b) $M_\infty = 0.8$, $Re_c = 2 \times 10^6$, $\alpha_{geom} = 1.8^o$ (see fig. 15(b)).

GP11-0232-18

Figure 19. — Trailing-edge boundary-layer profiles derived from pitot-pressure and interferogram data.

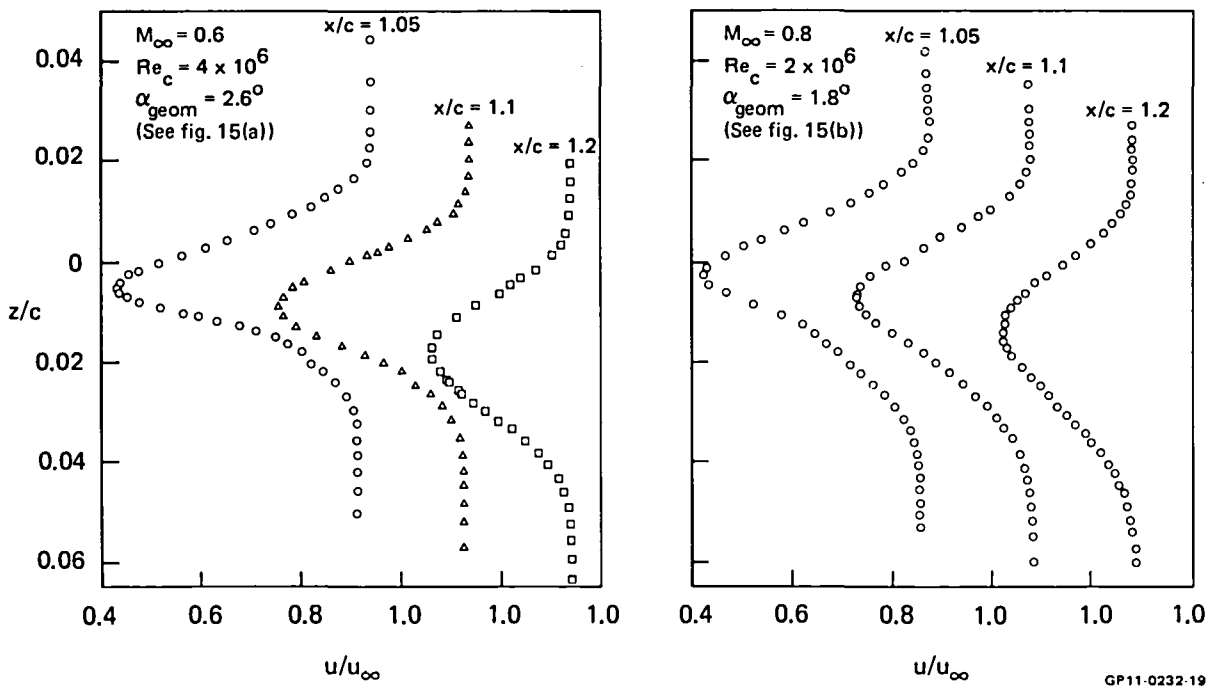

Figure 20. — Examples of near-wake profiles.

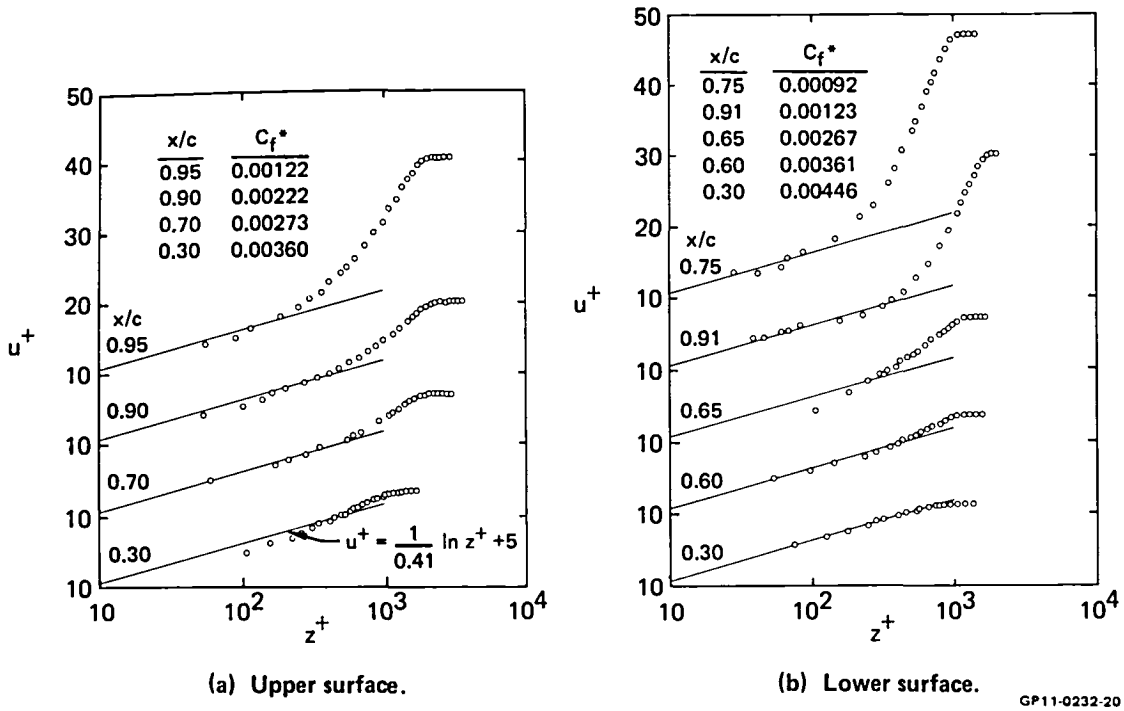

(a) Upper surface.

(b) Lower surface.

GP11-0232-20

Figure 21. — Transformed boundary-layer profiles in law-of-the-wall coordinates; sharp trailing edge, $M_\infty = 0.6$, $Re_c = 4 \times 10^6$, $\alpha_{geom} = 2.6$ (see fig. 16).

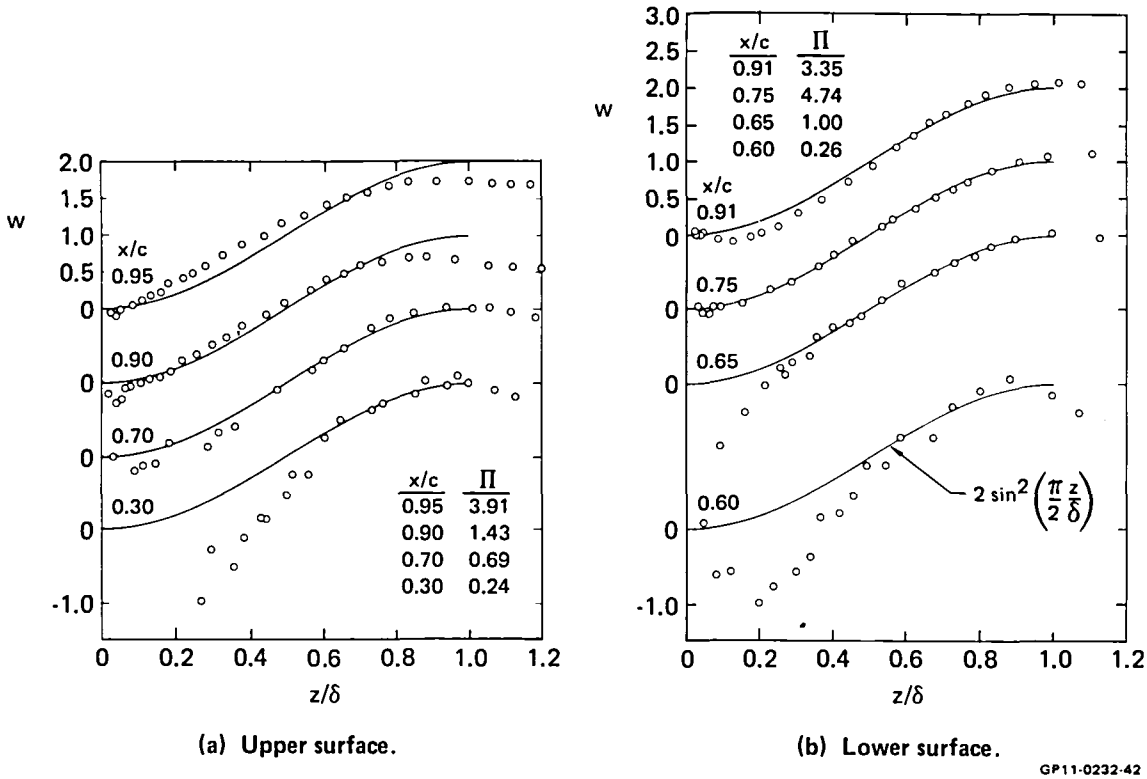

Figure 22. — Wake components of transformed boundary-layer profiles, sharp trailing edge, $M_\infty = 0.6$, $Re_c = 4 \times 10^6$, $\alpha_{geom} = 2.6$ (see fig. 16).

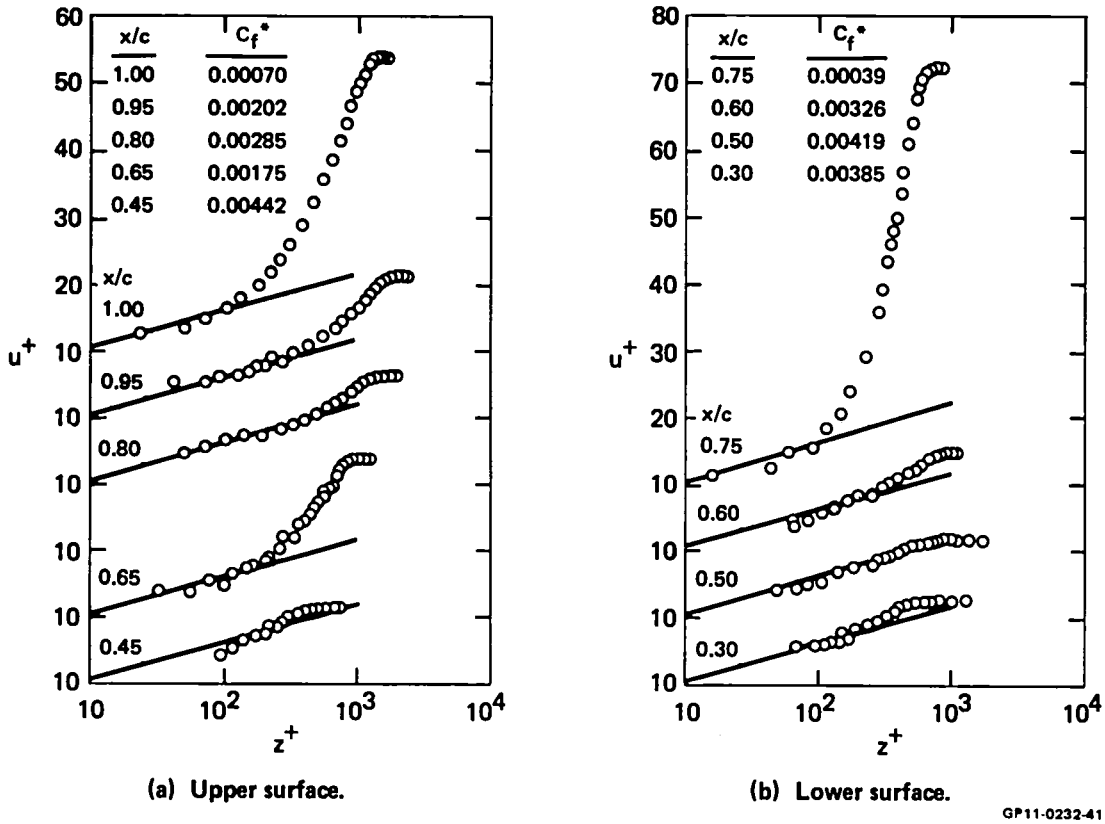

Figure 23. — Transformed boundary-layer profiles in law-of-the-wall coordinates; sharp trailing edge, $M_\infty = 0.8$, $Re_c = 3 \times 10^6$, $\alpha_{geom} = 2.4$ (see fig. 17).

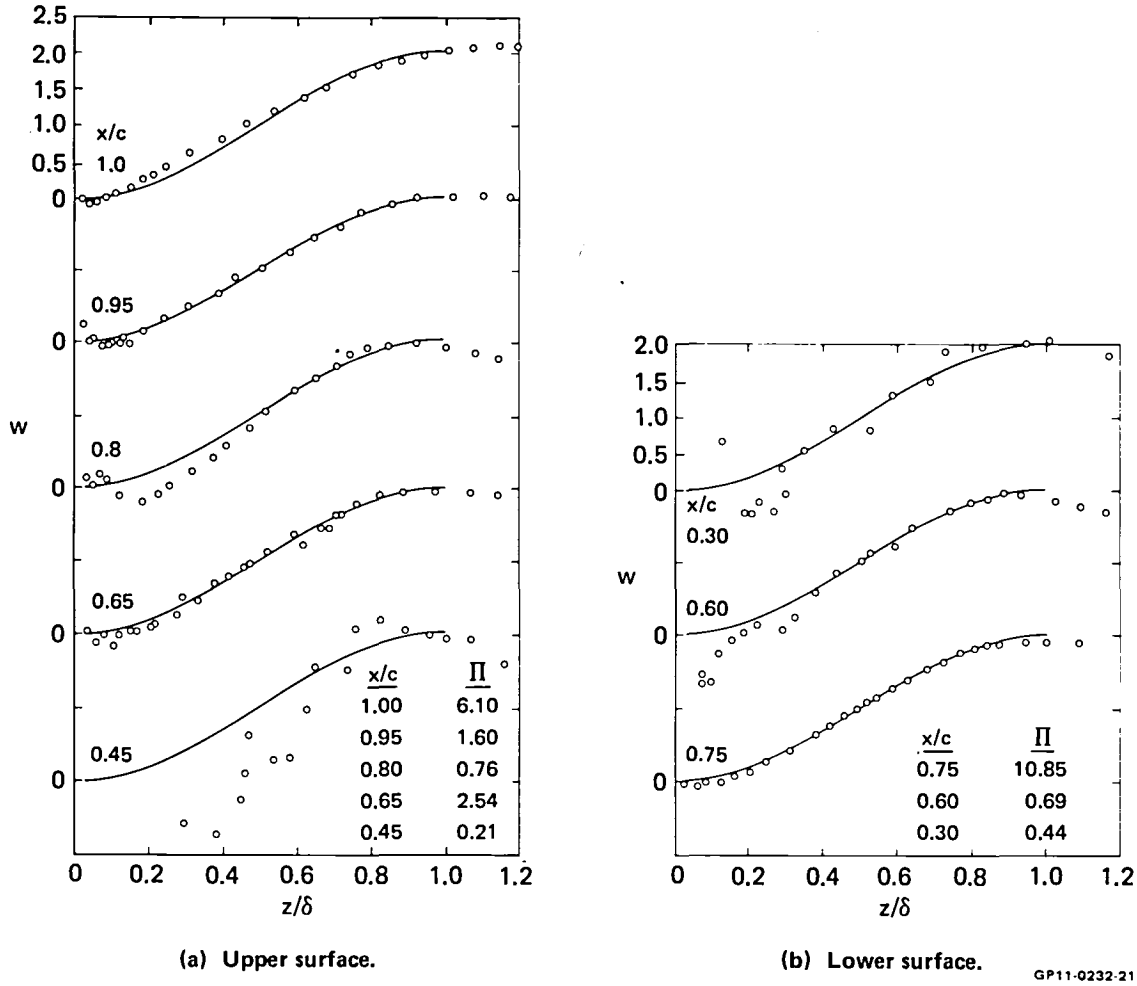

(a) Upper surface.

(b) Lower surface.

Figure 24. — Wake components of transformed boundary-layer profiles; sharp trailing edge, $M_\infty = 0.8$, $Re_c = 3 \times 10^6$, $\alpha_{geom} = 2.4$ (see fig. 17).

Case	Trailing edge	M_∞	Re_c	α_{geom}
(a)	blunt	0.75	2×10^6	1.0
(b)	blunt	0.83	2×10^6	0.8
(c)	sharp	0.60	4×10^6	2.6
(d)	sharp	0.80	2×10^6	1.8
(e)	sharp	0.80	3×10^6	2.4

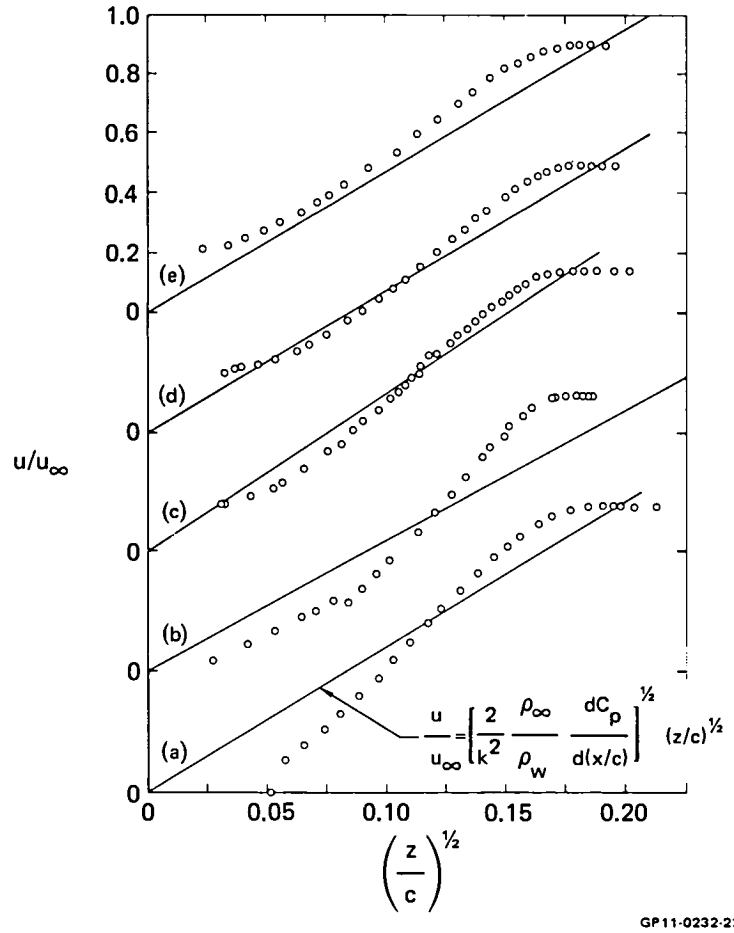

Figure 25. — Comparison of upper-surface trailing-edge profiles with Stratford's separation profile.

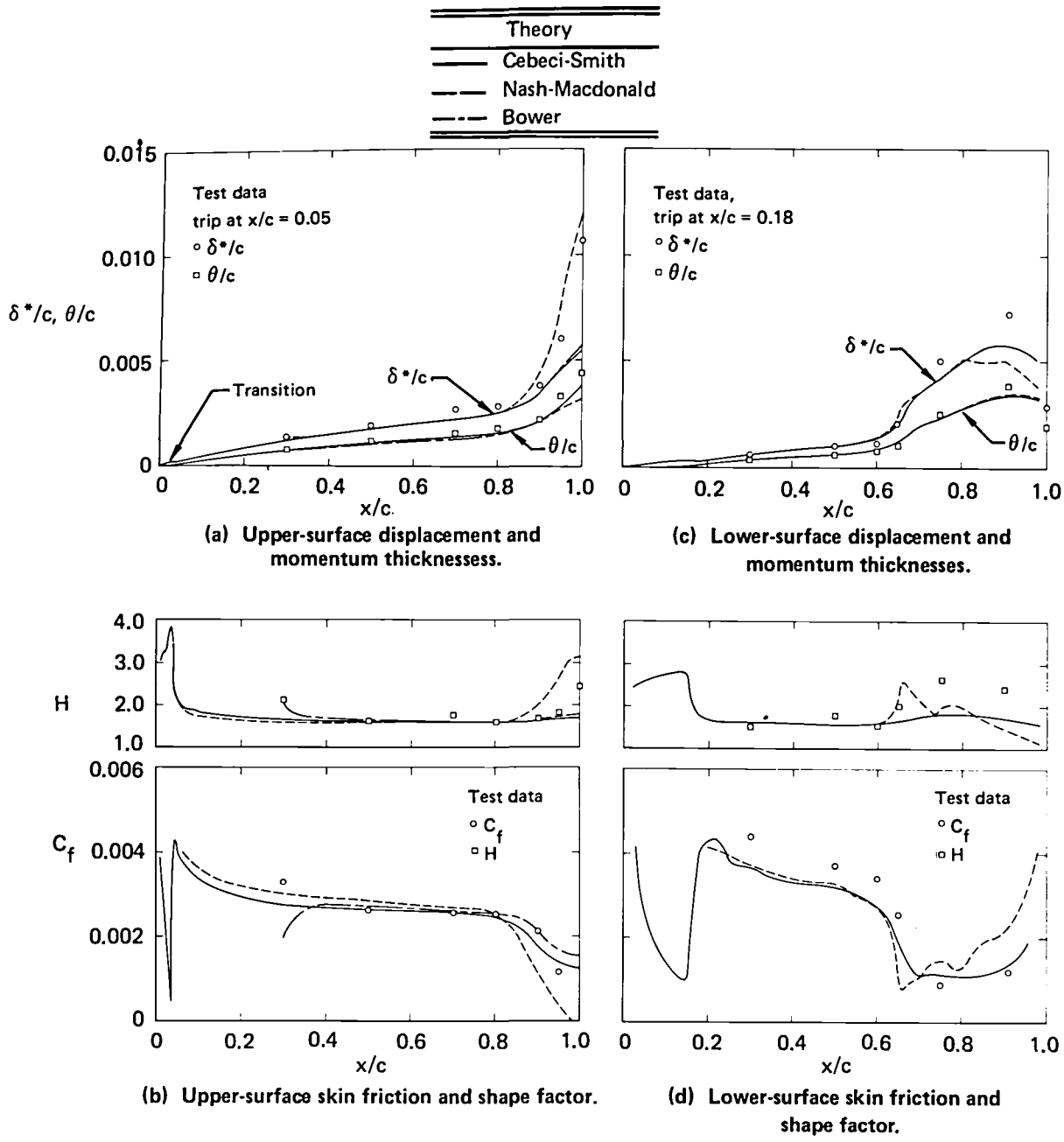

Figure 26. — Comparison of measured and calculated boundary-layer properties; sharp trailing edge, $M_\infty = 0.6$, $Re_c = 4 \times 10^6$, $\alpha_{geom} = 2.6$ (see fig. 13(e)).

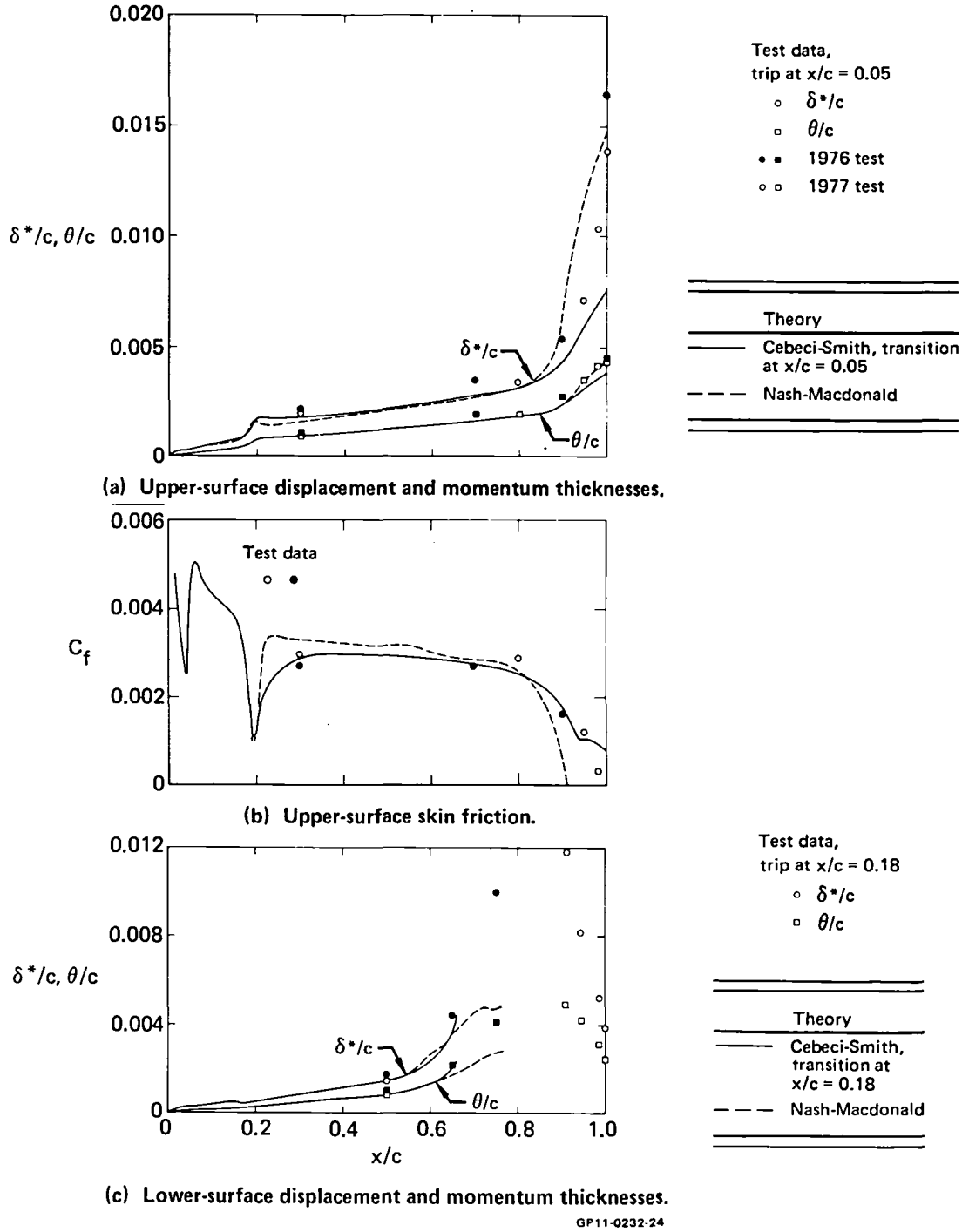

Figure 27. — Comparison of measured and calculated boundary-layer properties; blunt trailing edge, $M_\infty = 0.75$, $Re_c = 2 \times 10^6$, $\alpha_{geom} = 1.23$ (see fig. 13(b)).

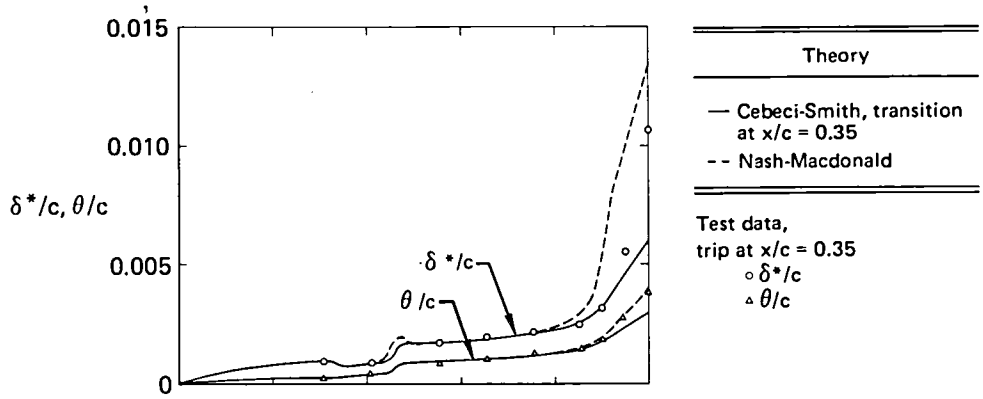

(a) Upper-surface displacement and momentum thicknesses.

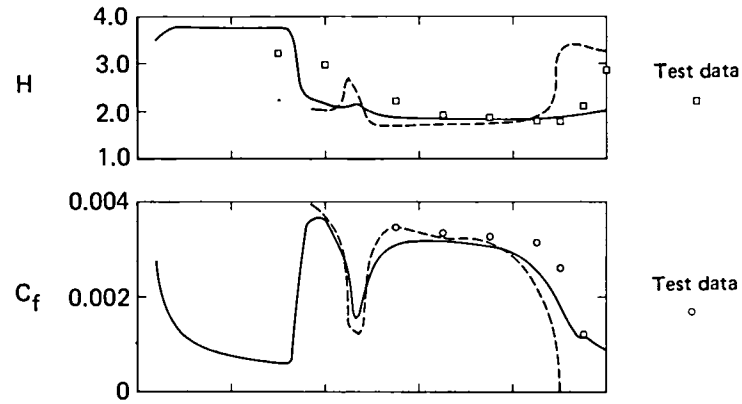

(b) Upper-surface skin friction and shape factor.

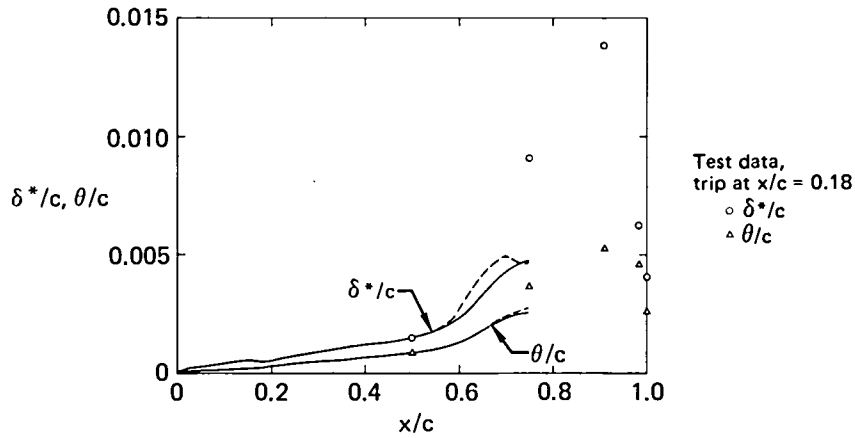

(c) Lower-surface displacement and momentum thicknesses.

GP11-0232-25

Figure 28. — Comparisons of measured and calculated boundary layer properties; blunt trailing edge, $M_\infty = 0.8$, $Re_c = 2 \times 10^6$, $\alpha_{geom} = 0.9$ (see fig. 13(c)).

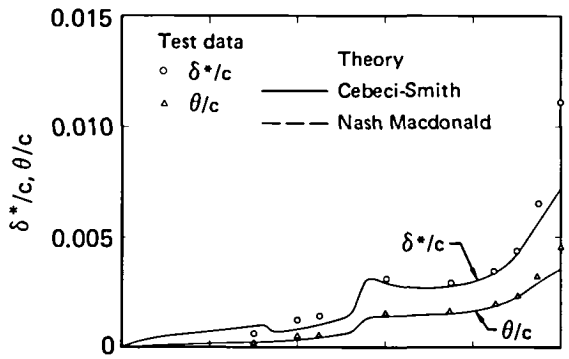

(a) Sharp trailing edge, $M_\infty = 0.8$, $Re_c = 2 \times 10^6$. $\alpha_{geom} = 1.8$ (see fig. 13(f)).

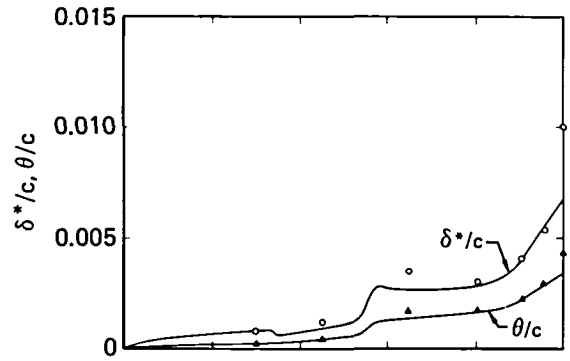

(b) Sharp trailing edge, $M_\infty = 0.8$, $Re_c = 3 \times 10^6$, $\alpha_{geom} = 2.4$ (see fig. 13(f)).

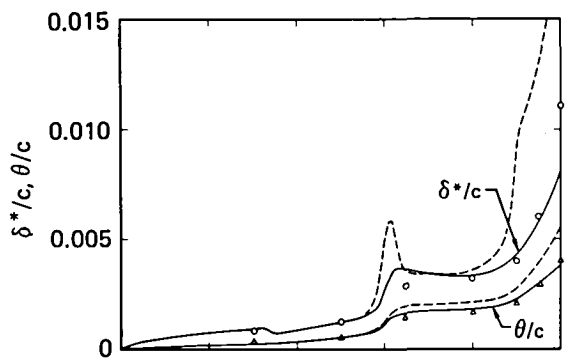

(c) Blunt trailing edge, $M_\infty = 0.8$, $Re_c = 2 \times 10^6$, $\alpha_{geom} = 1.6$ (see fig. 13(d)).

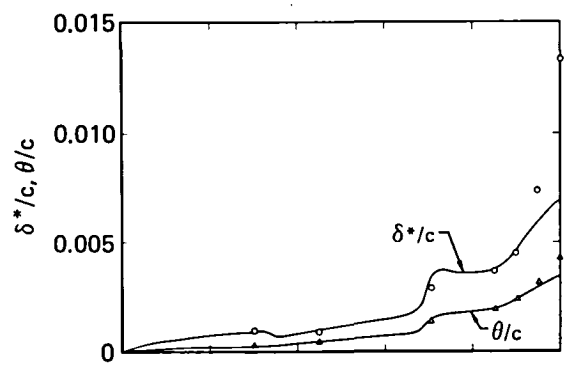

(d) Blunt trailing edge, $M_\infty = 0.83$, $Re_c = 2 \times 10^6$, $\alpha_{geom} = 0.78$ (see fig. 13(g)).

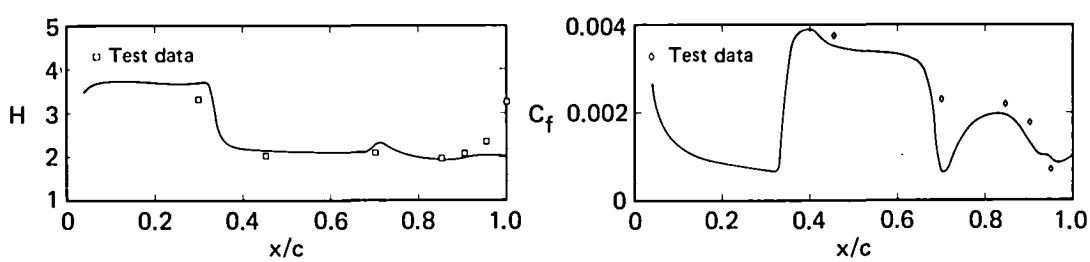

(e) Upper-surface skin friction and shape factor, blunt trailing edge, $M_\infty = 0.83$, $Re_c = 2 \times 10^6$, $\alpha_{geom} = 0.78$.

GP11-0232-26

Figure 29. — Comparisons of measured and calculated upper-surface boundary-layer properties; boundary-layer trip at x/c = 0.35, shocks aft of x/c = 0.5.

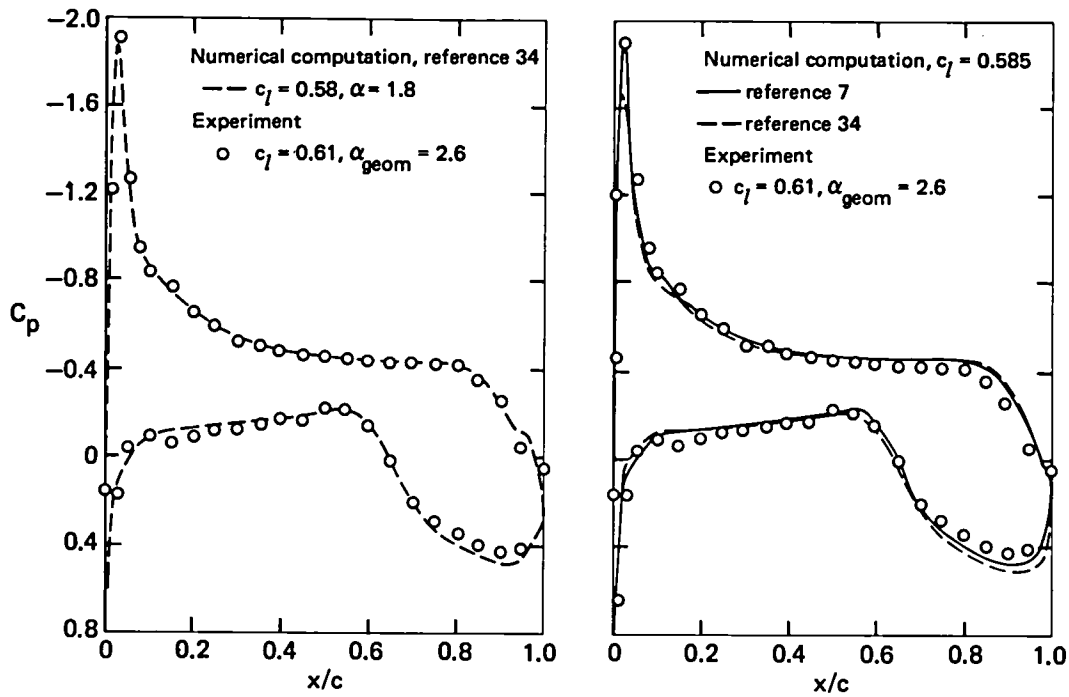

(a) Computation for airfoil coordinates plus experimental δ^*.

(b) Viscous-inviscid computations.

GP11-0232-27

Figure 30. — Calculated static-pressure distribution compared with experiment; $M_\infty = 0.6$, $Re_c = 4 \times 10^6$ (see fig. 15(a)).

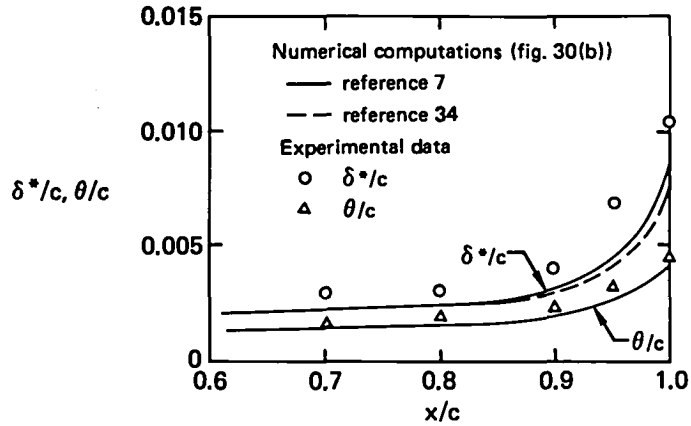

(a) Upper-surface displacement and momentum thicknesses.

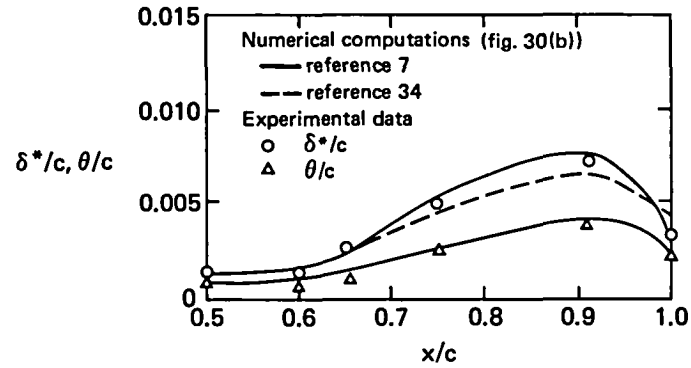

(b) Lower-surface displacement and momentum thicknesses.

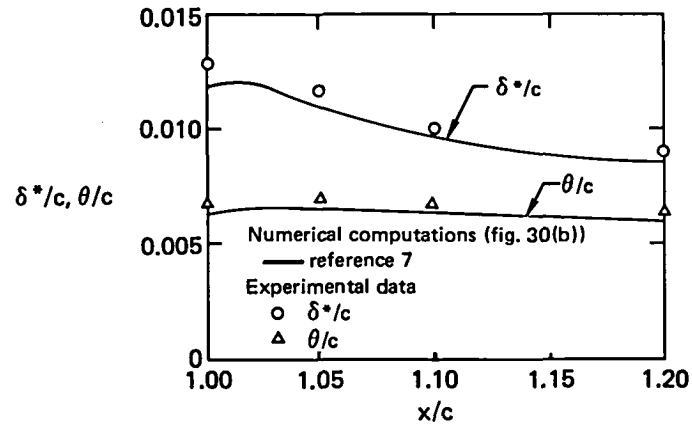

(c) Near-wake displacement and momentum thicknesses.

GP11-0232-28

Figure 31. — Comparison of calculated and measured boundary-layer and wake properties, $M_\infty = 0.6$, $Re_c = 4 \times 10^6$, $c_l = 0.61$.

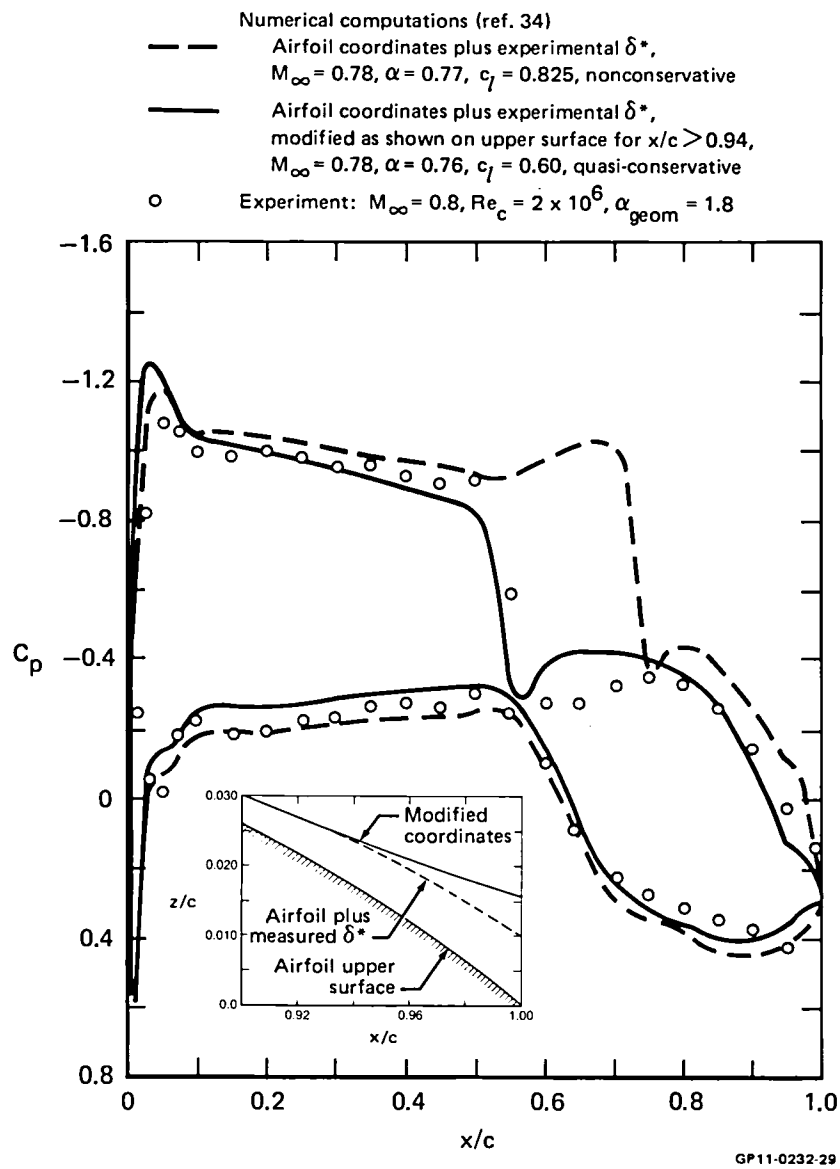

Figure 32. — Comparison of calculated and measured static-pressure distributions.

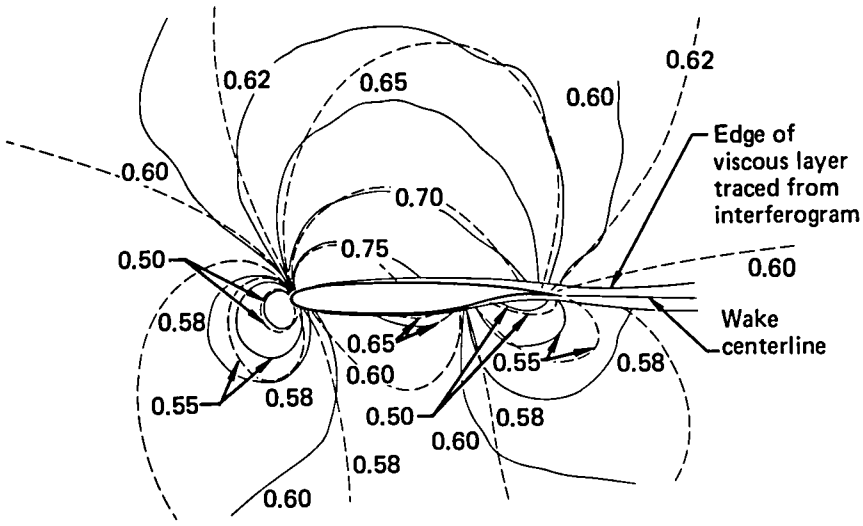

(a) $M_\infty = 0.6$, $Re_c = 4 \times 10^6$ (see fig. 30(a)).

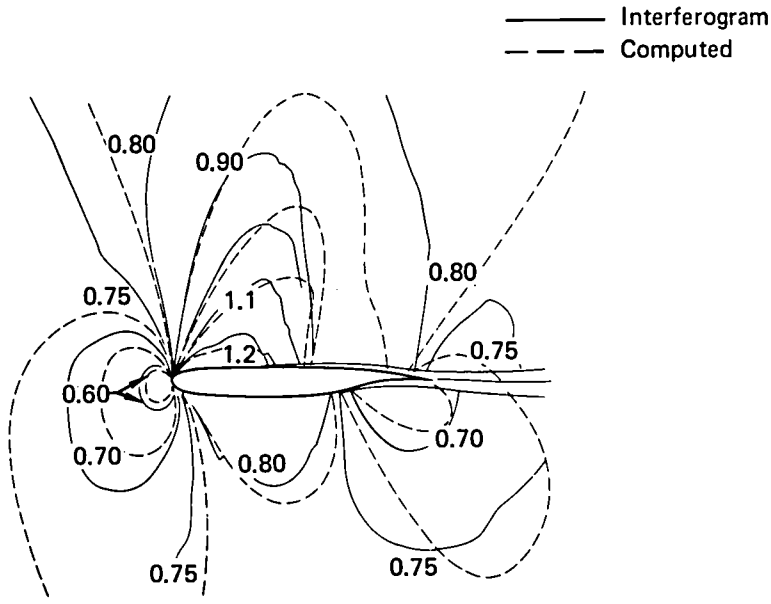

(b) Experimental $M_\infty = 0.8$, $Re_c = 2 \times 10^6$ (see fig. 32).

GP11-0232-30

Figure 33. — Comparison of Mach number contours traced from interferogram with computed contours.

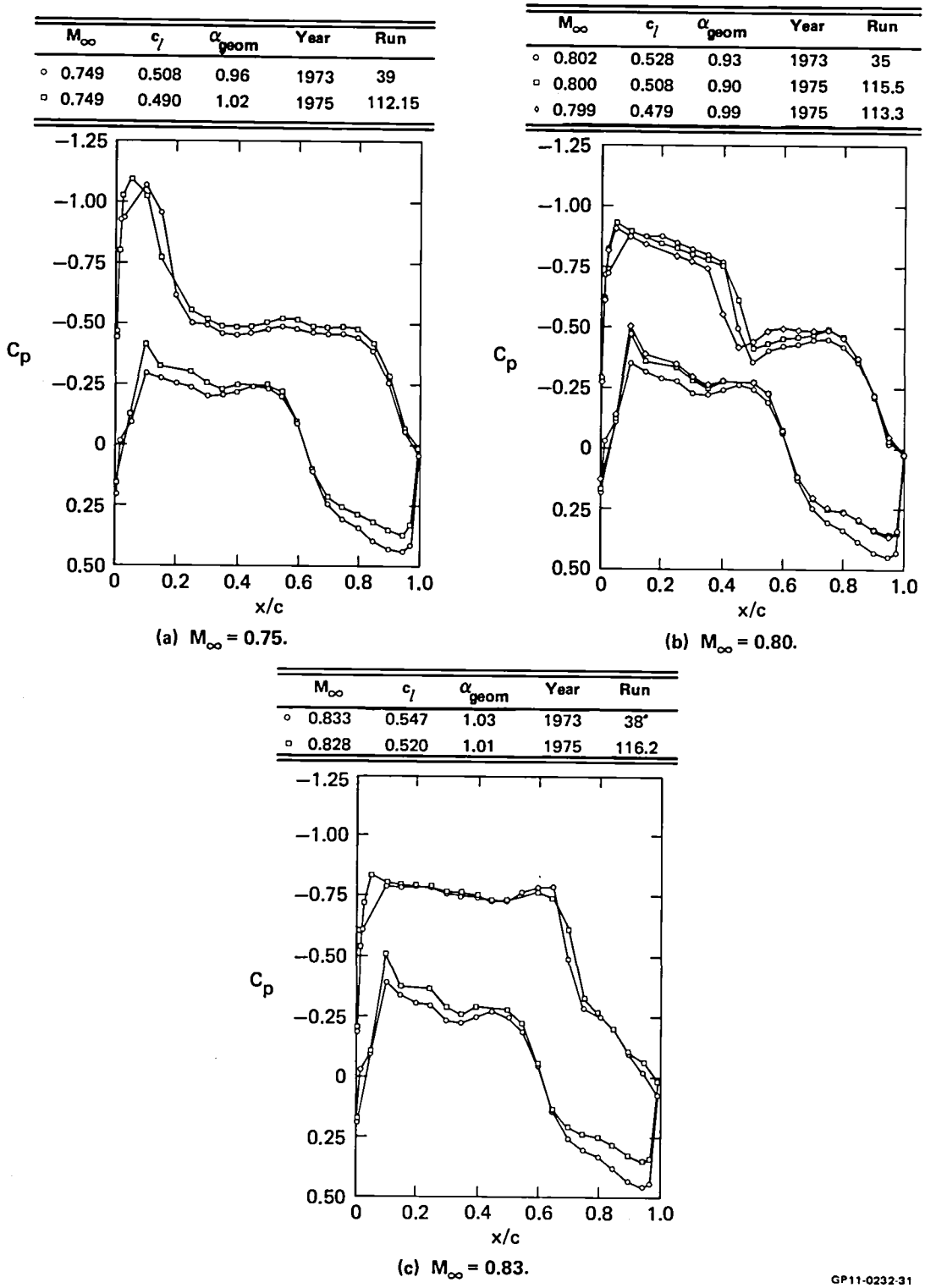

Figure 34. — Repeatability of static-pressure measurements, blunt-trailing-edge model, leading-edge boundary-layer trip, k = 0.05 mm.

Trip configuration	x/c	k (mm)
Upper	0.05	0.09
Lower	0.18	0.13

	M_∞	c_l	α_{geom}	Year	Run
○	0.600	0.512	1.03	1975	129.5
△	0.599	0.630	1.97	1975	129.6
□	0.600	0.588	1.64	1976	22.1

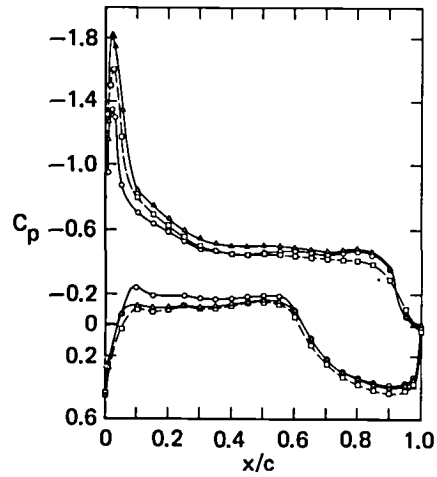

(a) $M_\infty = 0.6$, $Re_c = 2 \times 10^6$, 1975 and 1976 data.

Trip, see Fig. A-2(a)

	M_∞	c_l	α_{geom}	Year	Run
○	0.599	0.612	1.62	1977	8.2
△	0.602	0.595	1.41	1977	46.1
□	0.600	0.588	1.64	1976	22.1

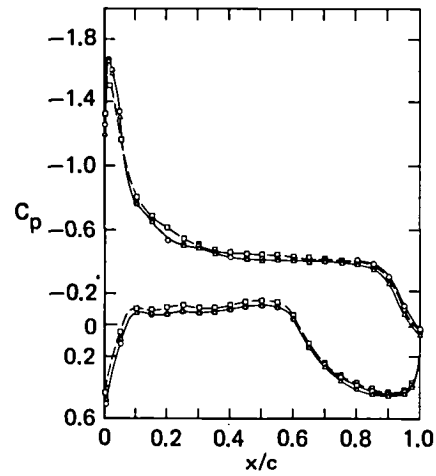

(b) $M_\infty = 0.6$, $Re_c = 2 \times 10^6$, 1976 and 1977 data.

GP11-0232-32

Figure 35. — Repeatability of static-pressure measurements, blunt-trailing-edge model, aft boundary-layer trips.

Trip configuration	x/c	k (mm)
Upper	0.35	0.13
Lower	0.18	0.13

	M_∞	c_l	α_{geom}	Year	Run
○	0.798	0.565	0.65	1977	78.2
△	0.796	0.627	0.86	1977	80.2
□	0.800	0.555	0.88	1975	121.3

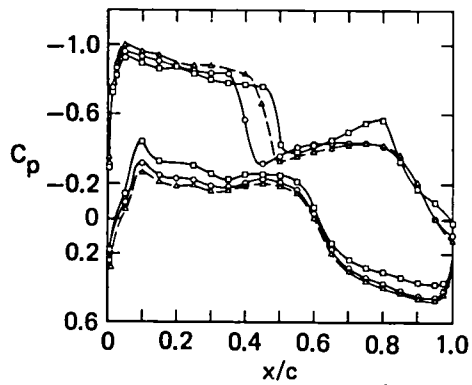

(c) $M_\infty = 0.8$, $Re_c = 2 \times 10^6$.

Trip, see fig. 35(c)					
	M_∞	c_l	α_{geom}	Year	Run
○	0.827	0.584	0.99	1975	122.4
△	0.829	0.593	0.78	1977	77.2

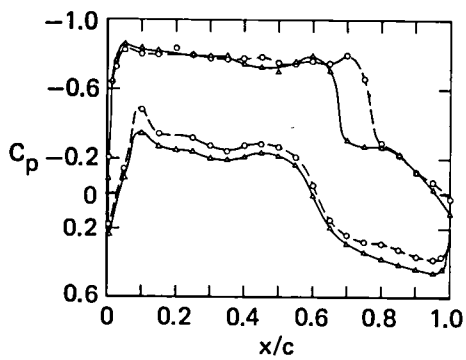

(d) $M_\infty = 0.83$, $Re_c = 2 \times 10^6$.

GP11-0232-96

Figure 35. — Concluded.

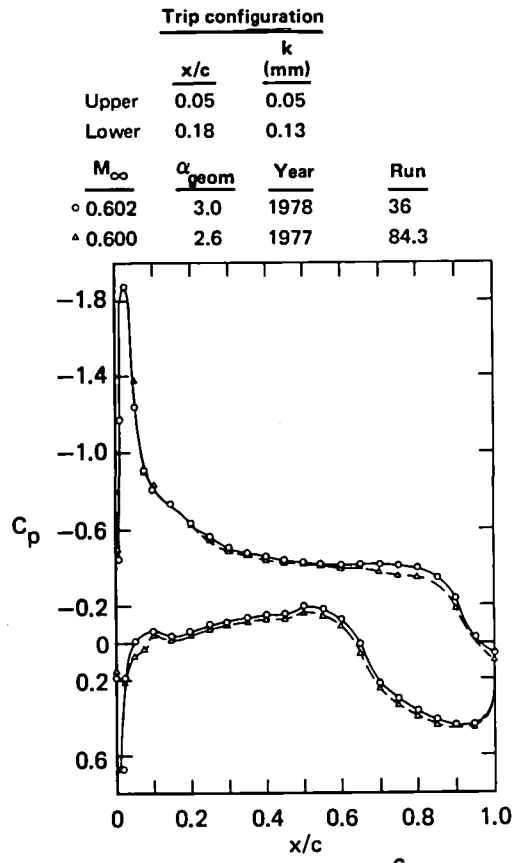

(a) $M_\infty = 0.6$, $Re_c = 4 \times 10^6$.

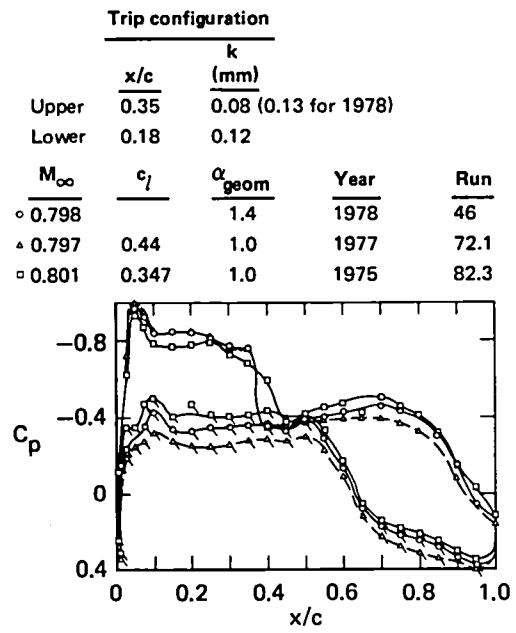

(b) $M_\infty = 0.8$, $Re_c = 3 \times 10^6$.

GP11-0232-33

Figure 36. — Repeatability of static-pressure measurements, sharp-trailing-edge model.

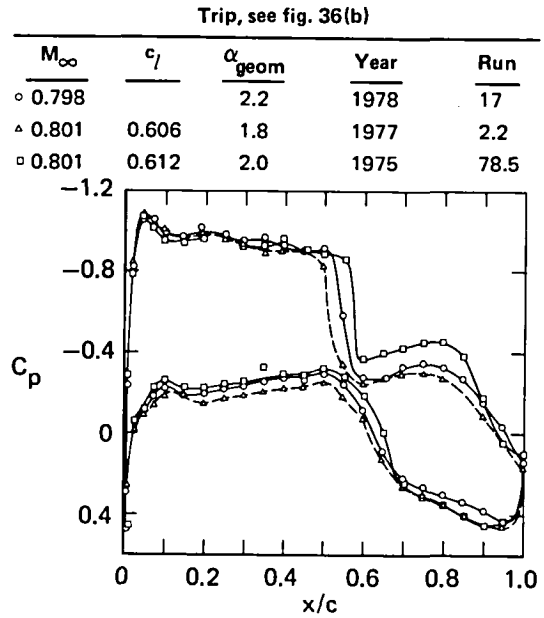

(c) $M_\infty = 0.8$, $Re_c = 2 \times 10^6$.

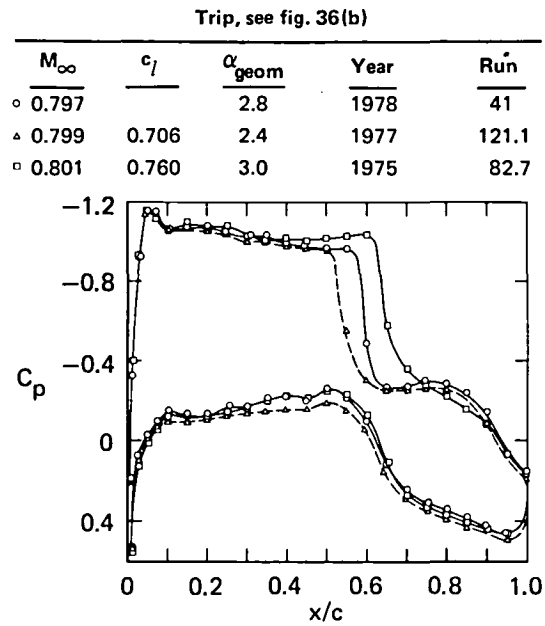

(d) $M_\infty = 0.8$, $Re_c = 3 \times 10^6$.

GP11 0232 97

Figure 36. — Concluded.

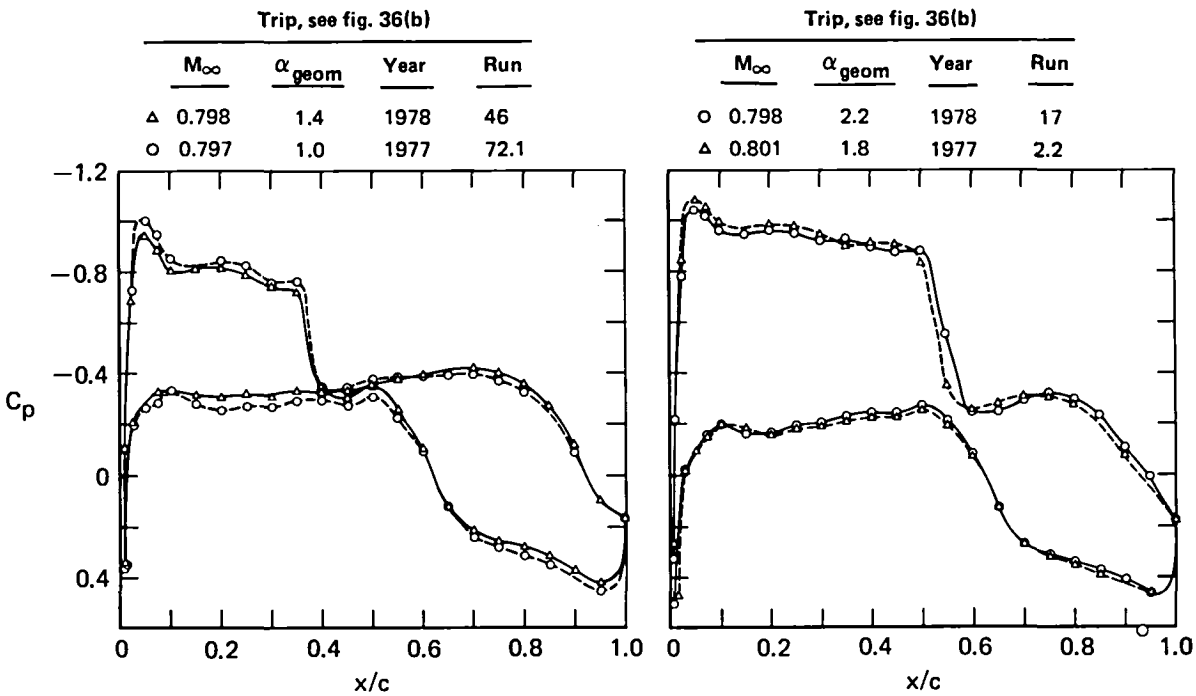

(a) $M_\infty = 0.8$, $Re_c = 3 \times 10^6$, $c_l \cong 0.44$.

(b) $M_\infty = 0.8$, $Re_c = 2 \times 10^6$, $c_l \cong 0.61$.

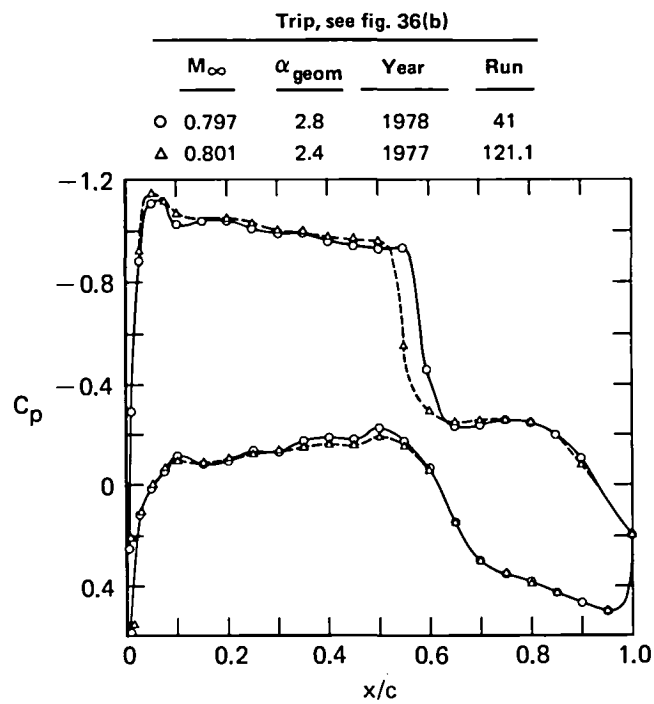

(c) $M_\infty = 0.8$, $Re_c = 3 \times 10^6$, $c_l \cong 0.71$.

GP11-0232-34

Figure 37. — Repeatability of static-pressure measurements, sharp-trailing-edge model, Cp's from 1978 shifted by 0.03.

1. Report No.	2. Government Accession No.	3. Recipient's Catalog No.
NASA TM-81336		

4. Title and Subtitle	5. Report Date
AN EXPERIMENTAL STUDY OF TRANSONIC FLOW ABOUT A SUPERCRITICAL AIRFOIL	August 1983
	6. Performing Organization Code

7. Author(s)	8. Performing Organization Report No.
Frank W. Spaid,* John A. Dahlin,† William D. Bachalo,‡ and Louis S. Stivers, Jr.§	A-8762
	10. Work Unit No.
9. Performing Organization Name and Address	T 3334 Y
*McDonnell Douglas Research Laboratories, St. Louis, Missouri; †Douglas Aircraft Company, Long Beach, California; ‡Aerometrics, Inc., Mountain View, California; §Ames Research Center, Moffett Field, California.	11. Contract or Grant No.
	13. Type of Report and Period Covered
12. Sponsoring Agency Name and Address	Technical Memorandum
National Aeronautics and Space Administration Washington, D.C. 20546	14. Sponsoring Agency Code
	505-31-41-03

15. Supplementary Notes

Point of Contact: Raymond M. Hicks, Ames Research Center, Moffett Field, California 94035, (415) 965-6396 or FTS 448-6396. Supplement available containing Data Base Information.

16. Abstract

A series of experiments was conducted on flow fields about two airfoil models whose sections are slight modifications of the original Whitcomb supercritical airfoil section. Data obtained include surface static-pressure distributions, far-wake surveys, oil-flow photographs, pitot-pressure surveys in the viscous regions, and holographic interferograms. These data were obtained for different combinations of lift coefficient and free-stream Mach number, which included both subcritical cases and flows with upper-surface shock waves. The availability of both pitot-pressure data and density data from interferograms allowed determination of flow-field properties in the vicinity of the trailing edge and in the wake without recourse to any assumptions about the local static pressure. The data show that significant static-pressure gradients normal to viscous layers exist in this region, and that they persist to approximately 10% chord downstream of the trailing edge. Comparisons are made between measured boundary-layer properties and results from boundary-layer computations that employed measured static-pressure distributions, as well as comparisons between data and results of airfoil flow-field computations.

17. Key Words (Suggested by Author(s))	18. Distribution Statement
Supercritical airfoil section Transonic airfoil flow field Pressure distributions Boundary-layer profiles Wake profiles Holographic interferograms	Unclassified - Unlimited Subject Category - 02

19. Security Classif. (of this report)	20. Security Classif. (of this page)	21. No. of Pages	22. Price*
Unclassified	Unclassified	102	A06

*For sale by the National Technical Information Service, Springfield, Virginia 22161

NASA-Langley, 1983

National Aeronautics and
Space Administration

Washington, D.C.
20546

Official Business
Penalty for Private Use, $300

THIRD-CLASS BULK RATE

Postage and Fees Paid
National Aeronautics and
Space Administration
NASA-451

U.S.MAIL

NASA

POSTMASTER: **If Undeliverable (Section 158 Postal Manual) Do Not Return**